2-P

CR 114274

AVAILABLE TO THE PUBLIC

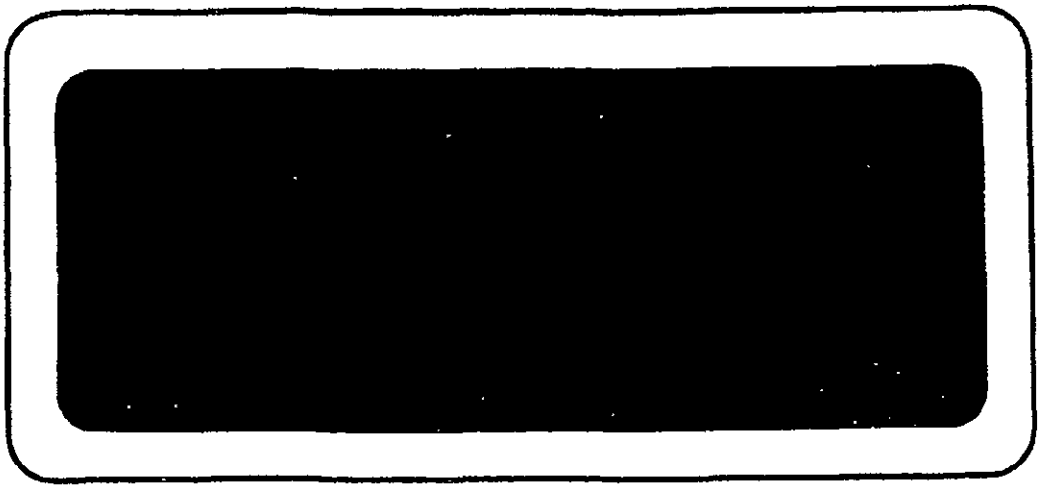

TRW®
SYSTEMS GROUP
ONE SPACE PARK • REDONDO BEACH, CALIFORNIA

HOLOGRAPHIC INSTRUMENTATION STUDIES

By Lee O. Heflinger and Robert E. Brooks

September 1970

TRW - 12122-6007-RO-00

Prepared under Contract No. NAS2-4992 by
TRW SYSTEMS GROUP
Redondo Beach, California

for

AMES RESEARCH CENTER

NATIONAL AERONAUTICS AND SPACE ADMINISTRATION

ABSTRACT

This report describes work done during the second year of a program to investigate holographic instrumentation techniques. The work describes both new methods of holographic interferometry, particularly with increased high sensitivity for the investigation of low pressure phenomena, and efforts to improve the coherence of the ruby laser. Other work which is described deals with techniques for wide angle interferometry without laser speckle, techniques of real-time and double exposure holographic schlieren, interferometry through a turbulent boundary layer, the production of holographic range contours by two frequency operation of the pulsed ruby, and the comparison of the light sensitivity of holography and photography.

CONTENTS

ILLUSTRATIONS

ILLUSTRATIONS (Continued)

1.0 INTRODUCTION

Shortly after the announcement and demonstration of two-beam holography in the early 1960's, it became apparent that the ability of the hologram to record, store, and reconstruct complex optical waves had opened up an important new class of optical instrumentation techniques. Most important of these was the common path holographic interferometry which permitted one to make interference measurements of great accuracy without the need for high quality optical components, and which also allowed the use of diffuse illumination for wide angle viewing.

The importance of these new techniques to flow field visualization was recognized by NASA-Ames and they funded TRW Systems for two years to investigate holographic instrumentation techniques. The study was broadly based, covering a large variety of possible techniques related to holographic instrumentation. The work performed during the first year has been described in a comprehensive final report[1]. The present report describes the work performed during the second year, but because of the continuity of the program, numerous references to the first year's activity are made. The two-year study has been described in a survey paper presented at the NASA-Ames Conference on Holographic Instrumentation Applications, January 13-14, 1970. A reprint of this paper is included in Appendix A of this report.

Because of the suitability of the Q-switched ruby laser for holographic recording of high speed events, emphasis throughout the program was generally directed toward ultimate use of this laser. However, both the He-Ne gas laser and the pulsed ruby laser were used to carry out the experimental work described herein. Because the coherence of the ruby laser is not equal to that of the gas laser, part of the program was directed toward means for improving the ruby laser as an illumination source for holographic instrumentation.

The report is divided into two main sections. The first deals with techniques of applying holography to fluid flow visualization. The second is concerned with coherence studies of the ruby laser and front illumination holography.

2.0 APPLICATION OF HOLOGRAPHIC INSTRUMENTATION TO FLUID FLOW VISUALIZATION

Holographic interferometry is important because it makes practical the implementation of common path interferometry. The two waves which interfere both pass through the same optical system so that phase aberrations, caused by imperfect optics, are present in both waves and therefore do not affect the resulting interferogram. Systems of high accuracy and large aperture can be constructed using relatively low cost optical elements. Equally important, holographic interferometry permits one to measure changes in a subject and allows diffuse light interferometry to be carried out on a routine basis.

An important problem in fluid flow studies is the attainment of high measurement sensitivity in order to detect and measure low pressure phenomena. A large part of this program was devoted to an investigation of hologram interferometric techniques which could take advantage of the hologram's insensitivity to imperfect optical components to give a sensitivity much greater than could be realized by conventional techniques.

Increased sensitivity has been achieved in conventional interferometry by passing the beam through the subject many times, but this technique has been limited in practice by the need for optical elements of extremely high precision. During the first year of our program, a multiple pass holographic interferometer was constructed using optics of ordinary quality and fringe multiplication of 10 times was carried out with good results.

Section 2.1 describes experiments which verify the capacity of the hologram to record phase perturbations in the subject waves as small as 1/6000 of a wavelength. The recognition of the great fidelity of the hologram recording process plus the insensitivity of the holographic interferometer to optical imperfections motivated us to search for fundamentally new approaches to obtaining great interferometric sensitivity.

A second scheme studied during the first year was high order interferometry. This made use of the fact that the phase of the reconstructed waves is proportional to the order of diffraction. The attainment of a good interference pattern depends on the non-linear addition (contact printing) of the two hologram recordings to be compared and a method for increasing the energy in the high orders of diffraction.

Another approach reported during the first year was subfringe interferometry, where the phase of the subject illumination beam (or of the reference beam) was shifted 180° between the two exposures of a double exposure hologram. In the absence of a change in the subject, the reconstructed waves cancelled one another. Very small phase changes in the subject were viewed as a brightening which could be easily detected against an otherwise dark field. Difficulties encountered in this technique were the attainment of exactly 180° phase shift and exposures of equal energy. Section 2.2 describes the four-beam, subfringe interferometer for which exposure equality and the attainment of 180° phase shift in the scene illumination is reduced to a second order requirement.

The use of diffuse illumination with the holographic interferometer permits the subject to be viewed and interference measurements to be made over a large angular range. This gives additional information and enables the researcher to obtain a more complete description of the density field associated with asymmetric flows, such as turbulent wakes.

If the flow field is symmetric, then acceptance of the scene light over a wide angular range results in averaging out of troublesome (asymmetric) phase perturbations without disturbing the symmetric flow field. Section 2.3 describes how this technique was applied to greatly reduce the effect of the turbulent boundary layer at the tunnel windows.

If the flow field which is to be studied is highly asymmetric, then it is necessary to restrict the solid angle over which the subject is viewed at any one time to avoid the averaging process described above. When diffuse subject illumination is used, the resulting interferogram is spatially

modulated in intensity by laser speckle, the size scale of which is inversely proportional to the viewing angle. This acts as spatial noise and hampers the accurate measurement of fringe brightness[2]. A scheme is described in Section 2.4 which makes use of a large number of nondiffuse beams, traversing the subject region at discrete angles and spanning a large angular range, thereby allowing the investigation of asymmetric flow fields without laser speckle. In addition, the holograms can be recorded on films of relatively low resolution, thereby decreasing the energy requirements of the illuminating laser. For lack of the required phase gratings, the scheme was not tried.

The wave storage property of the hologram can also be applied to schlieren measurement and Section 2.5 describes two schlieren techniques which are analogous to real-time and double exposure holographic interferometry. The real-time technique uses a reconstructed reference beam and permits both differential schlieren and interference patterns to be made of an irregular subject (e.g., shower glass or deformed specular surfaces). The schlieren pattern, while of interest in its own right, can also be used to unambiguously determine the sense (hill or valley) of the corresponding infinite fringe interferogram. The method works very well and has been used in practice to quantatively measure deformations of a thin metal foil.

The double exposure holographic schlieren technique is particularly applicable to ruby laser documentation of high speed events. Like the double exposure holographic interferogram, the measurements are insensitive to first order to changes in the reconstruction wavelength and geometry. The schlieren information is stored as a moire hologram pattern resulting from the two exposures. The technique depends on non-linearity in the hologram recording process and requires that the reference beam angle be changed slightly between exposures (akin to the finite fringe holographic interferogram).

2.1 TESTS DEMONSTRATING THE ABILITY OF HOLOGRAMS TO FAITHFULLY RECORD AND RECONSTRUCT WAVES WITH MINUTE PHASE PERTURBATIONS

To detect extremely small phase perturbations in the waves stored by a hologram, such as is necessary for functioning of the four-beam interferometer described in the following section (2.2), it is necessary that the hologram store and reconstruct the waves with extremely high fidelity. The experiments described below demonstrate that holograms are capable of storing phase information smaller than 1/6000 wavelength. It appears that the detection of smaller phase perturbations is limited by scattered light from the hologram and optical elements.

The experiment essentially consists of making a hologram of a subject consisting of two points, one of which is very dim compared to the other. The arrangement used is shown in Figure 2.1-1.

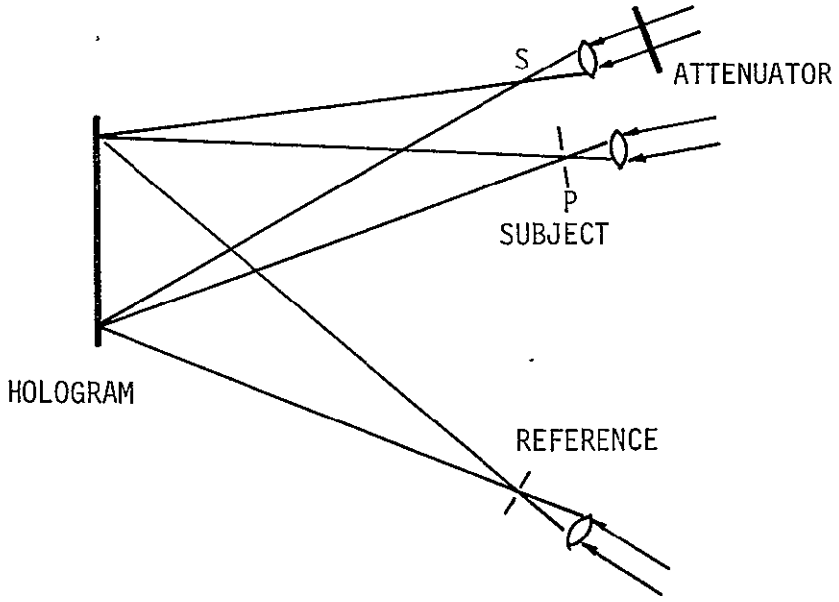

Figure 2.1-1 Arrangement Used to Measure Hologram Phase Fidelity

The subject consists of point sources P and S. The reference source and the primary subject point P are both pinhole filtered and their intensities at the hologram were adjusted to be equal. The secondary subject point S was a microscope objective without a pinhole and its intensity at the hologram ranged from 10^{-4} that of P to 10^{-7} that of P, for different holograms. All point sources were supplied from the same 15 mw helium-neon laser with equal path lengths to the hologram via each point source. The distance from the points to the hologram was about 70 centimeters, the angle from reference to P about 30 degrees, and the angle P to S about 10 degrees as viewed from the hologram.

The experimental results were as follows: Reconstructing the holograms with a point source in the same location as the reference source for the exposure, we were able to see the dim point S whenever its intensity was at least 10^{-6} that of point P. At 10^{-7} the point S was not visible to the unaided eye but the use of a small telescope, which increases the area of the hologram involved in viewing, rendered the point S visible. At 10^{-7} the point S was so faint that it was not very easily seen directly (no hologram involved) so it is not surprising that it became invisible in the hologram reconstruction, considering the inefficiency and scattering of 649F and 8E75 unbleached holograms. At 10^{-4} intensity ratio an additional image point was visible located at the position which is symmetric to S with respect to P. This additional image was considerably fainter than the direct image of point S.

The electric field at the hologram of the light wave from the primary subject P can be written as,

$$E_P = E_0 \, e^{j\alpha x} \quad , \tag{1}$$

where x is the coordinate on the hologram running in the plane of the drawing and α depends on the angle between the hologram and the direction to point P. For present purposes the sphericity of the point source waves

is unimportant and α can be considered constant.

In similar manner the wave from the secondary subject S at the hologram can be written,

$$E_s = \sqrt{I}\ E_o\, e^{j\beta x} \quad ,$$

where I is the ratio of intensity of point S to point P. A possible constant phase shift has been omitted from this formula as it is unimportant in the present connection.

The total subject field at the hologram is the sum of these and is therefore,

$$E_{\text{total subject}} = E_o\,[e^{j\alpha x} + \sqrt{I}\ e^{j\beta x}] \quad .$$

By writing the term in brackets in polar form and retaining only the first terms in a power series expansion in $\sqrt{I}$, the total subject field at the hologram can be expressed in the form,

$$\left.\begin{aligned} E_{\text{total subject}} &= E_o A e^{j\alpha x + \phi} \quad , \\ \text{where} \qquad A &= 1 + \sqrt{I}\ \cos\,(\beta - \alpha)x \\ \text{and} \qquad \phi &= \sqrt{I}\ \sin\,(\beta - \alpha)x \quad . \end{aligned}\right\} \quad (2)$$

When the point S is absent, (I = 0), this is identical to (1). For small values of I this differs from (1) by a small fluctuation in amplitude and a small fluctuation in phase, each fluctuation being periodic with the low spacial frequency $\frac{\beta - \alpha}{2\pi}$, corresponding to the small angle between the points S and P. The relative magnitude of the amplitude fluctuation is $\sqrt{I}$ and the magnitude of the phase fluctuation is $\sqrt{I}$ radians.

Thus, the total subject field at the hologram is basically a spherical wave with a tiny phase and amplitude wrinkle on it. The experiment consists of determining how small a wrinkle can be detected by the hologram. In a perfectly aligned four-beam interferometer the exposing field from the two exposures is equivalent to a single plane wave with a tiny phase only wrinkle on it.

The experimental observation that the point S is reconstructed stronger than its symmetric image in P, shows that the phase fluctuation is being detected by the hologram and at least partially reconstructed. This follows from the fact that if the hologram were to reconstruct a wave containing the amplitude fluctuation component only, the additional point symmetric to S with respect to P would appear essentially the same intensity as the image of S itself. Thus, from observation of the hologram in which $I = 10^{-6}$ it is concluded that holograms are capable of detecting properly presented phase information of 1/6000 wave, where the viewing aperture is the size of one's pupil.

The holograms made in the tests described above were also read out in a geometry like that used for the four-beam interferometer readout. This geometry is shown in the accompanying figure.

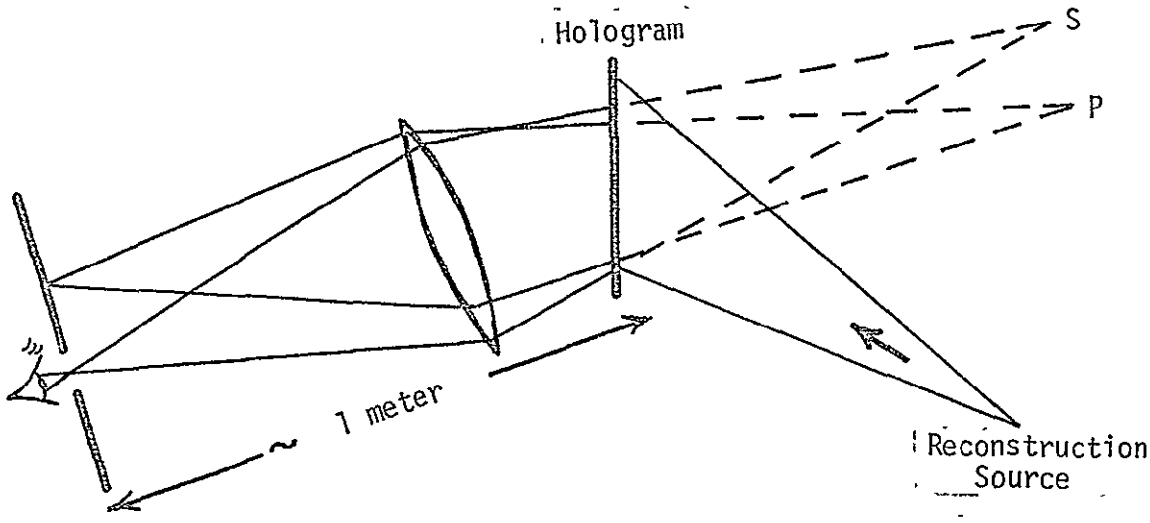

Figure 2.1-2 Hologram Readout Geometry

Here the lens forms a real image of the reconstruction of the secondary subject S at the aperture. By placing one's eye at the aperture and looking at the hologram, one sees the entire hologram illuminated. For $I = 10^{-6}$ this illumination is still in excess of the scattered light from the hologram, as is evident by moving one's eye slightly out of the real image of S so as to receive only scattered light. This readout method was not tried for the $I = 10^{-7}$ holograms.

This experiment has shown the ability of holograms to reconstruct minute phase variations of a periodic nature, which is the same form as the signal information in the four-beam interferometer. The general question of the hologram's phase accuracy under other circumstances, such as with a single point subject, is of course, not answered by the above experiment.

2.2 THE FOUR-BEAM INTERFEROMETER

The four-beam interferometer is a system which has been devised for the visualization of small aerodynamic disturbances. Its output presentation is similar to the sub-fringe interferometer, namely a dark background upon which phase perturbations show as brightenings. The principal advantage over the sub-fringe interferometer is that the system is insensitive, to first order, to errors in setting the 180 degree phase shifter and exposure equality errors.

The sub-fringe interferometer places the subject perturbation information on the hologram in the form of amplitude modulation of the basic holographic grating. It will be seen that the four-beam interferometer places the subject perturbation information on the hologram as phase modulation of the basic holographic grating at a fixed low spatial modulating frequency.

Theoretical analysis and the ultimate holographic phase sensitivity tests, described in Section 2.1, are suggestive that the system may ultimately yield sensitivities better than 1/100 of a wave.

The following sections give a description of the four-beam process, a description of the experimental assembly and tests, and an analysis of the four-beam operation showing the accuracy required of some of the adjustments.

Principle of the Four Beam Interferometer

In this section a heuristic scheme is first given which illustrates the basic process of the four beam interferometer. The heuristic scheme is then followed by a description of the actual four-beam process.

To begin with the heuristic scheme, consider a holographic recording system as shown, in which the subject is transilluminated by a parallel beam of light.

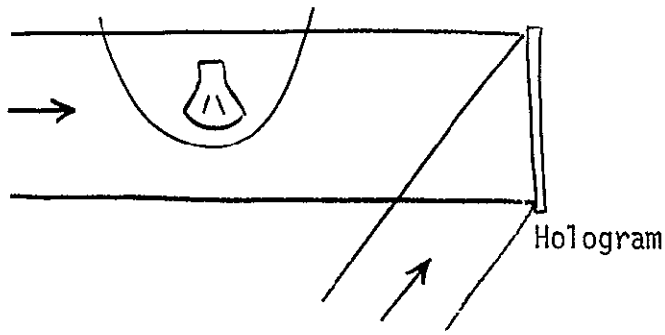

Figure 2.2-1 Transilluminated Subject

The essence of the scheme is to divide the hologram into strips, with every other strip being exposed on the first exposure when the object is absent. On the second exposure, with the object present, the complementary set of strips is exposed. In concept, but not in practice, this can be accomplished by placing a glass plate ruled with black parallel lines against the input side of the hologram. The width of each black line is equal to the space between lines. After the first exposure, the glass plate is shifted a line width so that the black lines now cover the formerly clear areas and vice versa. A second exposure with the object present then completes the formation of the hologram. Think of the strips as being a fraction of a millimeter wide, i.e., large compared to the basic fringe pattern on the hologram, but small compared to the object.

The hologram is read out as shown.

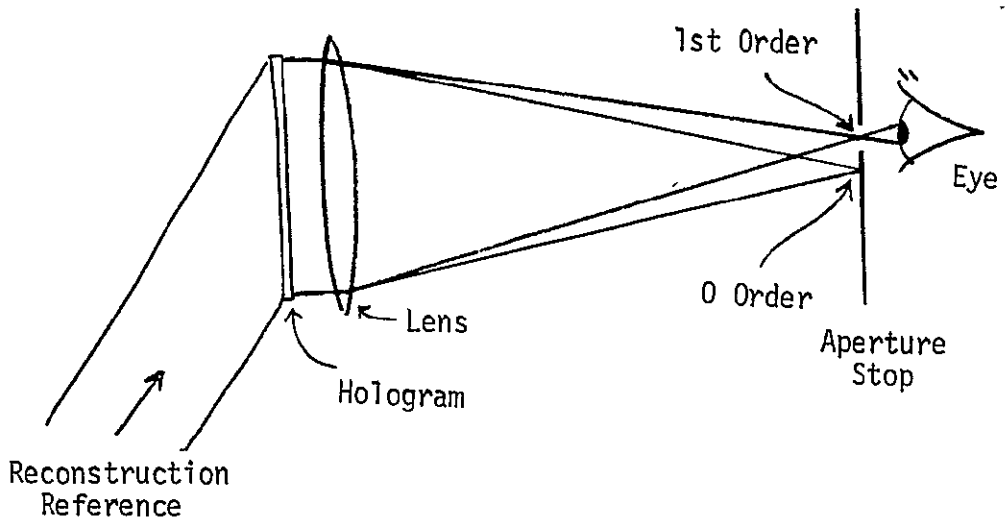

Figure 2.2-2 Hologram Readout

The hologram reconstructs the subject beam which is composed of alternate strips made from the first and second exposures. If there were no change in the phase of the light produced by the presence of the object, then the reconstructed subject beam is simply a plane parallel beam which is all focused by the lens into the zero order focus and is stopped by the aperture. However, if some portion of the object produces a small optical phase retardation, say of 1/10 of a wave, then the region of the hologram corresponding to this portion of the object will produce instead of a plane wave, a wave with a 1/10 wave phase "wrinkle" on it. This "wrinkle" stems from the retardation of phase on the second exposure which is reproduced by the strips used for the second exposure. The frequency of this wrinkle is the basic strip frequency. The situation is depicted in the sketch on the following page, where for clarity the strips are shown much coarser than would be used in practice.

Now, a wavefront with a periodic phase wrinkle on it is equivalent to a set of plane waves traveling in certain different directions. Stated another way, the wrinkled wavefront may be thought of as the output wave from a phase diffraction grating. For a sinusoidal phase wrinkle, the fraction of the power going into the first order is $[J_1(\theta/2)]^2$, where $J_1(\theta/2)$ is the Bessel function of first kind, order one, and θ is the peak-to-peak magnitude of the phase wrinkle in radians. For $\theta/2 \leq 1$ radian, $J_1(\theta/2) \cong \theta/4$, and hence the fraction of the power going into the first order $[J_1(\theta/2)]^2$ is $\theta^2/16$. For example, for a 1/10 wave shift between the two exposures, θ is $2\pi/10$ radians, giving .025 of the power into the first order.

Thus, when the observer looks at the hologram through a small aperture, centered on the first order, the hologram will appear dark where no phase change has occurred and will be bright where a phase shift has occurred, with the intensity being proportional to the square of the phase shift between exposures. The output picture thus looks like the output of a double exposure sub-fringe holographic interferogram in which a 180° phase shift was applied to the reference beam between exposures. Such a sub-fringe interferogram also has an intensity proportional to the square of the

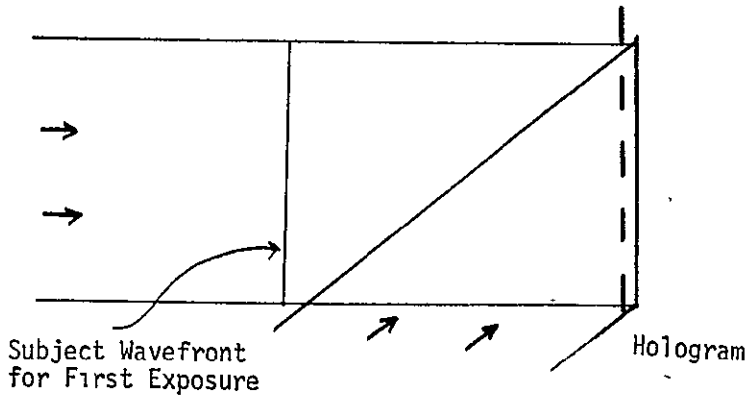

1ST EXPOSURE

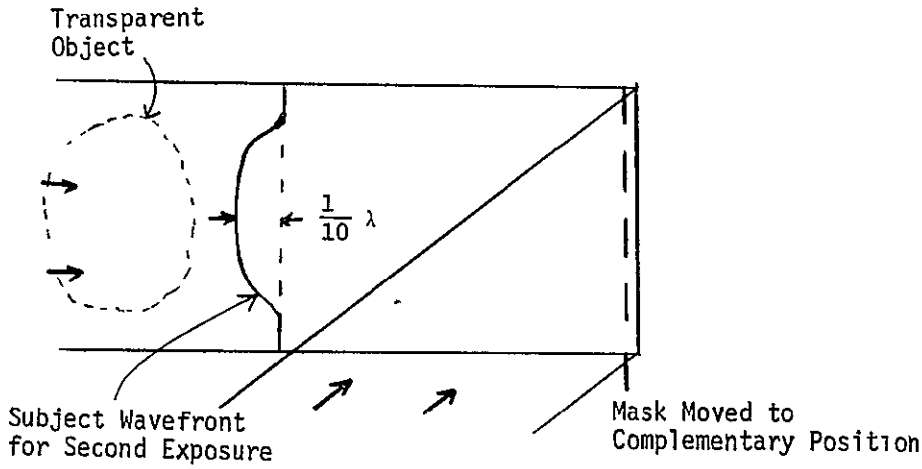

2ND EXPOSURE

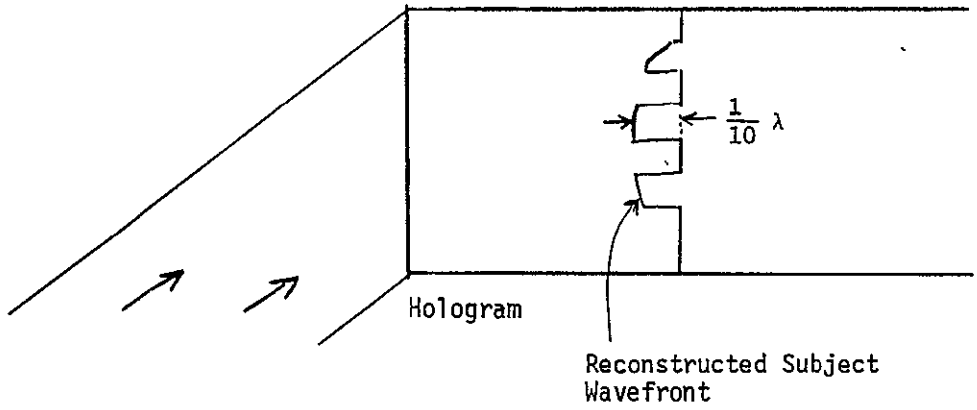

RECONSTRUCTION

Figure 2.2-3 Four-Beam Principle

differential phase shift in the subject, and in both cases the ultimate sensitivity of each technique depends upon how black the background can be made in the absence of a subject change.

As the reader has probably noted, the scheme as described thus far has little chance of success because there would almost certainly be a residual grating produced on the hologram by imperfect complementarity of the two positions of the mask. Such a residual grating diffracts light into the first order, and produces a background which is not completely dark.

The system actually used in the four-beam interferometer for producing the two complementary sets of strips is to produce the strips by interference. To accomplish this, both subject beam and reference beam are each split into two beams, the angle between the components being small and the same for both subject and reference. Figure 2.2-4 illustrates a possible configuration. The mirrors, A, B, C, and D, form two beams at a small angle. Beam splitter E divides these into subject and reference beam pairs.

The operation of the interferometer can be understood with the aid of Figure 2.2-5. The two components of the subject beam traveling at a small angle with each other are equivalent to a single wave with an amplitude which varies sinusoidally as one traverses across the beam.* The same is true for the reference wave. The interference between the subject and reference waves thus has an intensity which varies like a $\sin^2$ function for

---

* To see this, choose a coordinate system (x', y', z') with y' axis along the bisector of the two beams amd x' axis in the plane defined by the two beams. Then the electric field from the two beams is described by

$$e^{j(kx' + \ell y')} + e^{j(-kx' + \ell y')}$$

This can be rewritten as

$$(2 \cos x)\, e^{j\ell y'}$$

which can be interpreted as a wave traveling along the bisector with a slow sinusoidal variation in amplitude across the wavefront.

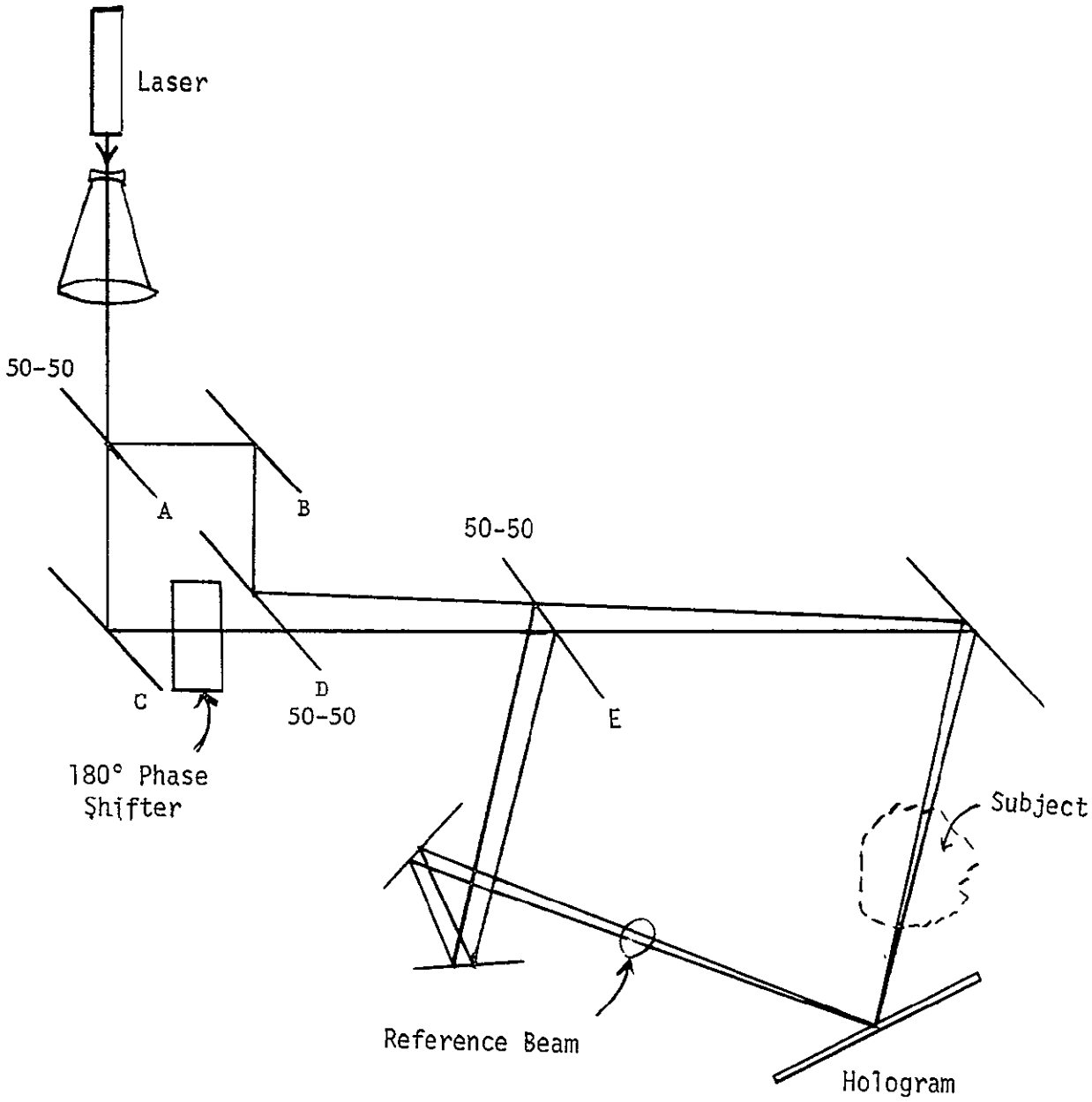

Figure 2.2-4 Four-Beam Transverse and Temporal-Matched Interferometer

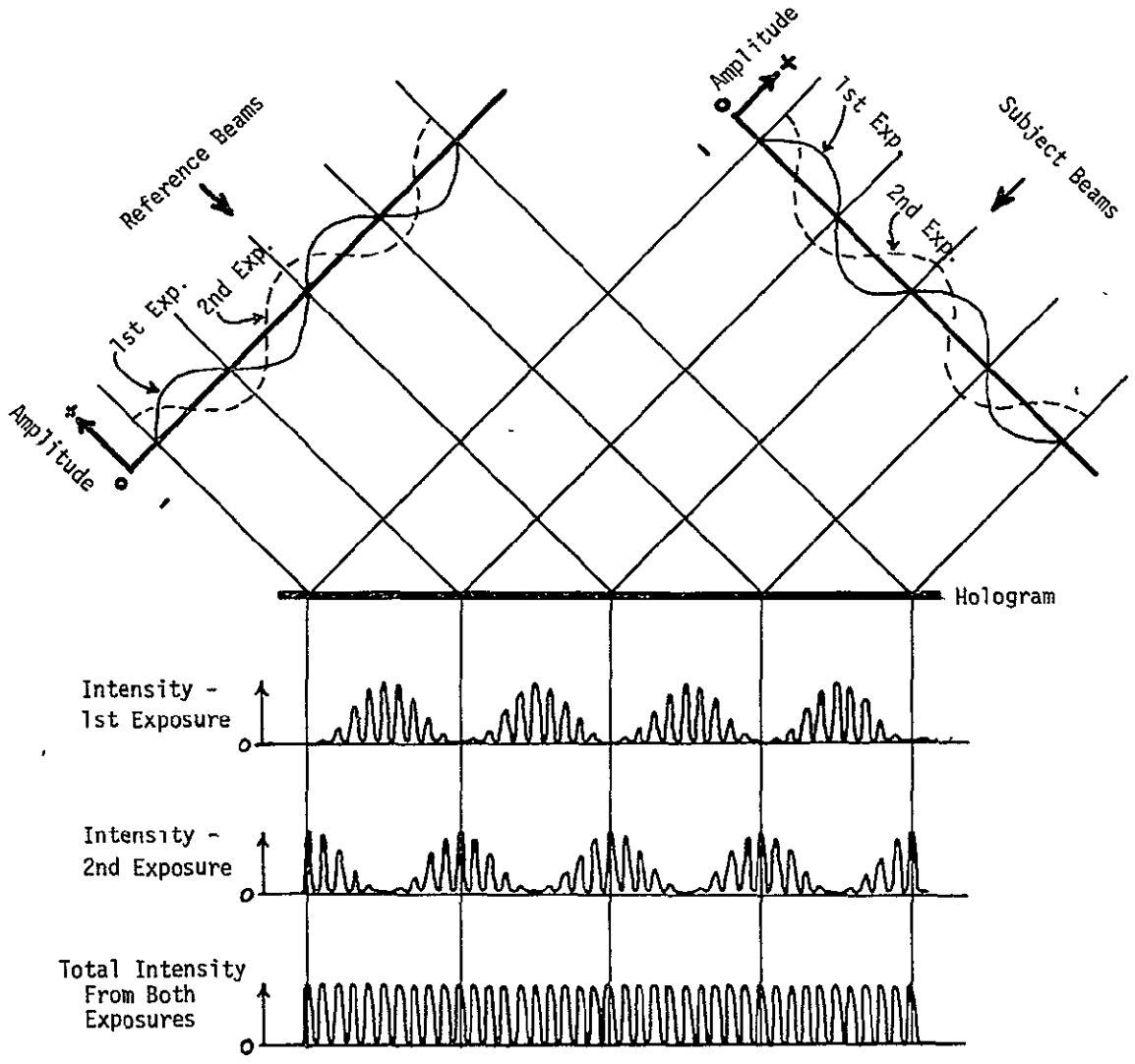

Figure 2.2-5 The Four-Beam Exposure Process in Absence of a Subject

the relatively slow variations corresponding to the fringes produced by the narrow angle between components. These slow variations correspond to the strips of the foregoing discussion. Superimposed upon these slow variations are the fine holographic fringes which correspond to the large angle between the subject beam and reference beam. In other words, the envelope of the fine fringes is the slow $\sin^2$ function.

For the second exposure, a 180° phase shift is introduced into one component of the subject beam, and the corresponding component of the reference beam. This 180° shift causes a displacement of the slow variation of intensity at the hologram so the intensity varies like a $\cos^2$ function. The phase of the fine fringe holographic component is not changed. In view of the fact that $\sin^2 + \cos^2 = 1$, the sum of the two envelope intensities is constant. Thus, the hologram produced in the absence of a change in the subject is simply a uniform grating of fine fringes which diffracts only a plane wave upon reconstruction. However, if the object introduces a small differential phase shift between the two exposures, the phase (position) of the fine fringes for the second exposure with the $\cos^2$ envelope will be shifted accordingly. Upon reconstruction, the output wave, instead of being plane, will have a small phase wrinkle on it with the amplitude of the phase wrinkle set by the differential object phase shift and period of the wrinkle set by the small angle between the components.

The reconstructed output of the hologram is viewed as in the sketch shown earlier in which the eye views the light cast into the first order.

The important question is to what extent small residual errors diffract an unacceptable background of light into the first order, in the absence of object phase shift. An analysis, outlined in the last part of this section, has been made, evaluating the significance of certain errors. The results have been surprising in that no major source problem has been uncovered. The analysis assumes that the hologram exposure is chosen to

maximize the diffracted light. Under this assumption, it is found that the subject light diffracted into the first order is (to first order analysis) not dependent upon the accuracy of the 180° phase shifter, and is not dependent upon obtaining equality of exposure for the two exposures. These results are encouraging, for the analogous phase shift and exposure equality requirements for subfringe interferometry are very demanding.

The Experimental Assembly

Figure 2.2-6 is a photograph of the experimental assembly. The unit is constructed on a metal plate which rests upon inner tubes to isolate the unit from floor vibrations. The vibration isolation achieved limits the vibration to about 1/10 of a wave or less, as estimated by visually observing the fringes produced by the interferometer. This residual vibration is too large to permit ultimate sensitivity tests with the gas laser, but such tests were not anticipated anyway, because of air currents. (For the gas laser tests, the entire unit is covered with a cardboard cover.) The unit is located in front of the pulsed laser, and it is planned to use the pulsed laser for ultimate sensitivity tests. For this, it will be necessary to modify the pulsed laser so that it will produce two Q-switched pulses separated by a few hundred microseconds. A tiny spark discharge will produce a shock or sound wave for the second exposure which will constitute the test object.

The plan of the interferometer of Figure 2.2-6 is essentially the same as described in the previous section. Namely, it consists of a Mach-Zehnder interferometer which produces two collimated beams separated by a narrow

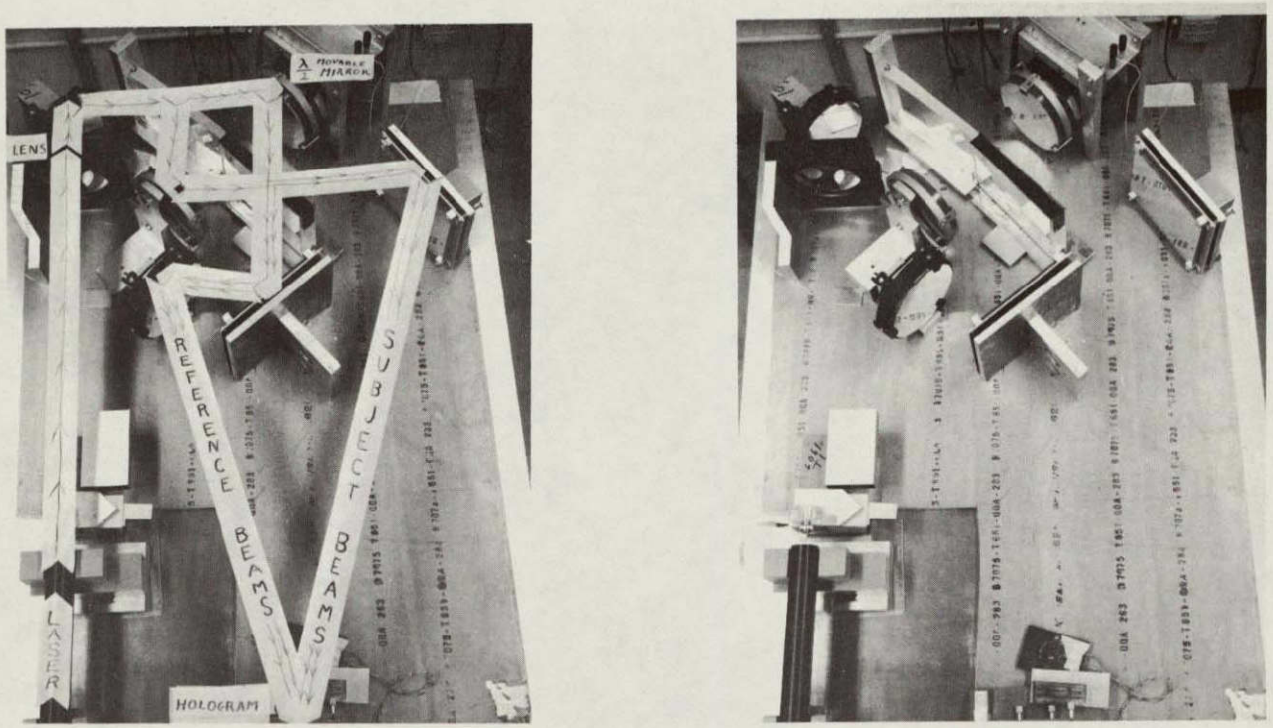

Figure 2.2-6. The four-beam interferometer experimental assembly. The heated resistor subject is near the hologram at the ends of the wires. The round mirrors are six inches in diameter.

angle, followed by a beam splitter and mirrors to produce the scene (pair of) and reference (pair of) beams for the hologram. In the arrangement pictured, one beam splitter serves the dual function of output beam splitter of the Mach-Zehnder and the scene-reference beam splitter. This conserves light, components, and space.

A microscope objective and 5" diameter 25" focal length lens expands the beam from the gas laser to 5" diameter prior to entrance into the interferometer proper. For pulsed laser operation, the microscope objective will be replaced by a simple negative lens.

To produce the 180° phase shift between exposures, one of the corner mirrors of the Mach-Zehnder is arranged so that it can be displaced normal to its surface by $\frac{1}{\sqrt{2}} \frac{\lambda}{2}$ between exposures, giving the required half-wave shift in path length. There are two modes of operation to produce the required position shift. For gas laser operation, a voltage is applied to a lead zirconate piezoelectric crystal. For the crystal used, 260 volts produces the desired half-wave path change. For pulsed laser operation, the mirror swings as a pendulum, constrained by its flexural supports so that the mirror surface does not rotate. One quarter pendulum period prior to the laser firing, the mirror pendulum is magnetically released from rest. The two Q-switched laser pulses, separated by a few hundred microseconds, occur as the mirror passes through the bottom of its swing. The pendulum's initial position is chosen so that the path change will be one-half wave, between the exposures. The mirror-pendulum has been constructed, as seen in Fig. 9-4, but has only been operated in the gas laser mode so far.

Hologram Scattering Test

One of the first tests conducted with the apparatus was to measure the low angle scattered light from the hologram. This scattered light sets a limit on the sensitivity of the technique, and we were anxious to determine if the scattering would be ruinous.

It will be recalled that in ideal operation of the four-beam technique, without any change in the subject, the hologram produced by the two exposures of the four beams, with a half wave shift of two of the beams for the second exposure, is simply a uniform grating. When reconstructed, this grating produces a single reconstructed subject beam which is focused to a point and blocked by an aperture stop. One then observes through a hole in this stop, located at the position corresponding to the first diffracted order of the subject beam. (See Figure 2.2-2) For an ideal arrangement in absence of subject, the light passing through this first order aperture is only scattered light from the zero order reconstructed beam. (The intrinsic diffracted light due to the finite aperture of the hologram is very small. We are concerned here with small angle scattering from imperfections in the emulsion which are much larger than the intrinsic diffracted light.)

To test the magnitude of this scattered light, we blocked the light passing through one side of the Mach-Zehnder arrangement and made a single exposed hologram with the remaining two beams. This hologram is essentially just a grating complete with imperfections arising from dust, imperfect mirror polish, etc. This hologram was then reconstructed with a parallel beam, and the reconstruction observed with a three inch aperture telescope feeding a photomultiplier tube. The zero order reconstructed image was slightly aberrated, as would be expected from the hologram support.* The zero order image passed easily through an aperture $.5 \times 10^{-3}$ by 1.5×10^{-3} radians which served as the selection aperture of the photomultiplier. The intensity of the zero order reconstruction was measured and then, using this same aperture size, the intensity of the scattered light in the vicinity of the zero order reconstruction was measured.

---

* Since the reconstructed image from the operating interferometer consists of a central or zero order plus other orders in its immediate vicinity, we speak of the zero order reconstructed image in this discussion. No use is made of the laser light which passes directly through the hologram and is conventionally called zero order light. That is, in this discussion, zero order does not refer to the undiffracted light passing through the hologram but refers to the principal part of the diffracted subject light.

Figure 2.2-7 gives the results. At $.5 \times 10^{-2}$ radians ($\cong \frac{1}{3}$ degree) the scattered intensity is only 10^{-4} times the zero order reconstructed intensity. This value can be interpreted as a limit on the sensitivity achievable, assuming that all other problems were conquered to the point where this scattering was setting the limit to the observable phase shifts. The fraction of the zero order reconstruction intensity cast into the first order by a subject phase shift θ is $\frac{\theta^2}{16}$. Equating this intensity to the scattered light intensity of 10^{-4} gives a phase shift θ of 4×10^{-2} radians, which is of the order of 1/100 of a wave.

This result is encouraging, especially in view of the fact that no effort was made to minimize the scattering by selection of emulsion and optimizing the processing, cleanliness, etc. Also learned from this experiment is the appropriate range for the small angles of the four beam interferometer. Values smaller than $.5 \times 10^{-2}$ radians encounter rapidly increasing amounts of scatter. A calculation of the optimum small angle based on resolution considerations alone gives smaller values for the small angle. Thus, the emulsion-scattering forces operation at somewhat larger angles, resulting in some sacrifice in resolution. With a viewing aperture the size of the photomultiplier aperture and a distance from subject to hologram of 20 cm, a subject resolution of approximately 2 mm can be expected. This corresponds to 50 resolution elements across the four inch diameter scene.

Four Beam Tests

The experimental interferometer has been operated in the double exposure four beam mode with a gas laser as source. The first observation made was that it was not possible to secure accurate registry between the coarse fringe pattern of the subject beams and the coarse fringe pattern of the reference beams. This lack of registry apparently stems from the output beam splitter, which is rather low quality. The thought then occurred that perhaps this registry was unnecessary in view of the high symmetry of the four beam configuration. A quick analysis showed that indeed this was the case.

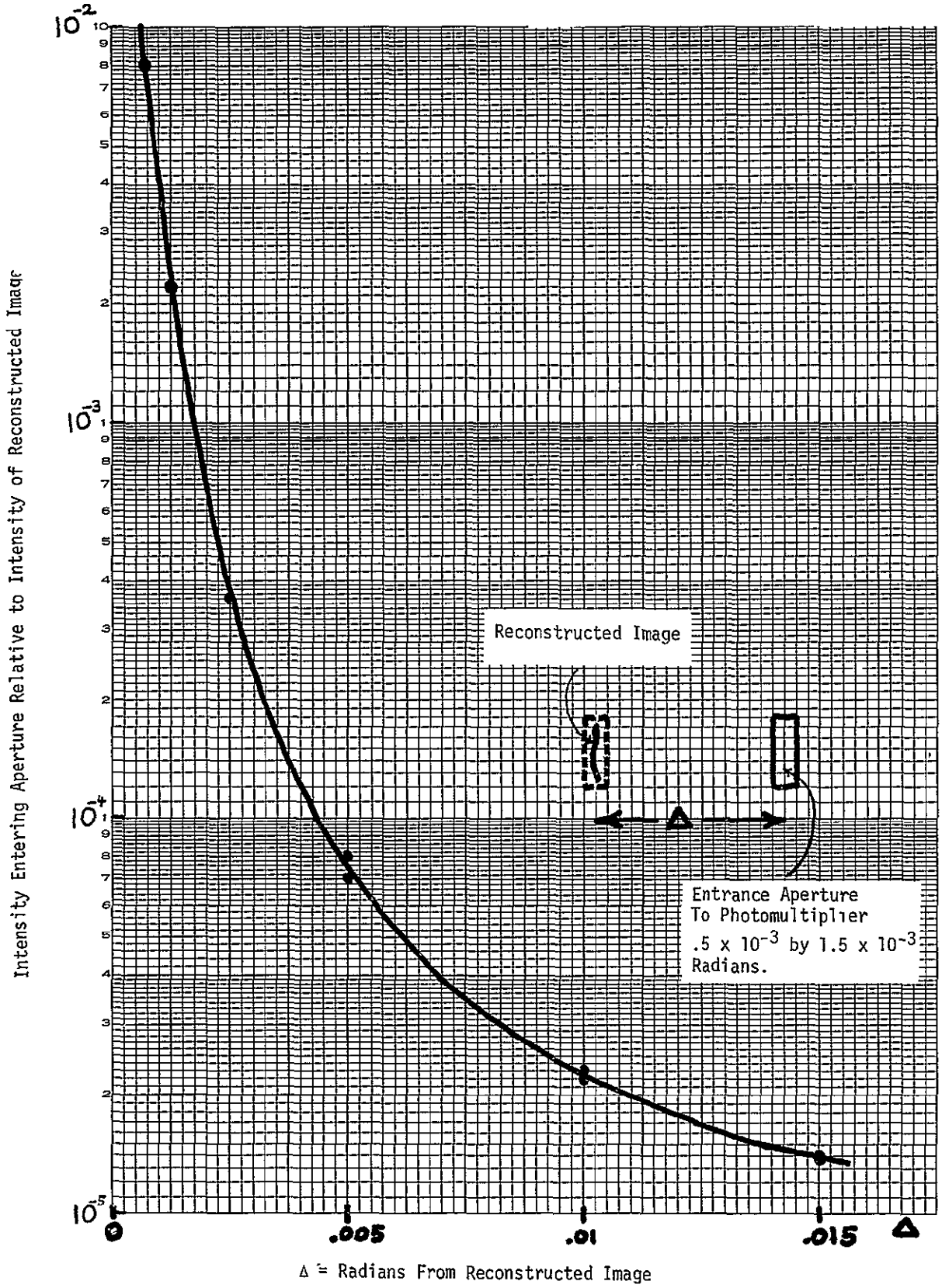

Figure 2.2-7. Graph of low-angled scattered light from a hologram made with two equal intensity collimated beams on Agfa 8E75 plate. Abscissa angle is the difference between the primary reconstructed beam direction and the photomultiplier acceptance direction.

However, a second more detailed analysis showed that there is an important penalty that must be paid for operating without registry of the coarse fringe patterns. This penalty is that the required precision of the half wave phase shift between exposures becomes very great without registry. To be specific, when the lack of registry is complete, the error in setting the half wave phase shift must be no greater than the phase shift to be detected in the subject. This requirement is the same as the phase shift requirement for subfringe interferometry. It is one of the assets of the four-beam technique that a highly accurate phase shift is not required when the coarse fringes are properly registered with each other.

The following section outlines the analysis which shows the effect of operating with the coarse fringes out of registry and estimates the precision of registry required for proper operation.

A modified arrangement of the existing components into a Michelson interferometer for production of the coarse fringes, followed by a subject-reference beam splitter, was tried with the hope that the poor quality beam splitter would do less damage in the modified configuration. Although some improvement was obtained it was still impossible to register the coarse fringes of subject and reference beams over much of the hologram simultaneously.

The gas laser tests of the four-beam technique on the modified configuration (without registry) were made with a 6 mm diameter, 15 mm long cylindrical carbon resistor as "subject". This resistor, with axis horizontal and parallel to the subject beam, was supplied with a current so that in 14 seconds its upper surface increased 10° C as measured by an attached thermocouple. At the end of the 14 second period the current was decreased to a value that just maintained the 10° C temperature rise. After 5 seconds in this maintaining state, the second exposure of 2-1/2 seconds was made. The actual subject is the heated air in the vicinity of the resistor. Some convection is evident in the results, but the flow is not turbulent. The air immediately adjacent to the surface of the resistor was calculated to

give 1/6 of a wavelength path change. A conventional finite fringe double exposed holographic interferogram, made in the same interferometer by blocking two of the beams, confirmed this value by measuring 1/3 of a wavelength at the surface of the resistor when the resistor temperature rise was doubled to 20° C as shown in Figure 3 of Appendix A. As one moves away from the resistor, the optical phase shift decreases and no quantative assessment of the magnitude has been made. Figure 2.2-8 is a photograph of the readout of one of the four-beam interferograms, where the glow surrounding the resistor shows the presence of the phase shift which is 1/6 wavelength at the resistor. Also evident in the photograph are horizontal bands which arise from imperfect registry of the coarse subject beam fringes with the coarse reference beam fringes.

Tests were made both with the coarse fringes parallel to the fine fringes and perpendicular to the fine fringes. No significant difference was observed in the results.

Tests conducted thus far are still regarded as incomplete. In particular little attention was paid to optimizing hologram efficiency which theoretically is very important. Also table vibration, air currents, and problems with the phase shifter have hindered evaluation in addition to the registry problem.

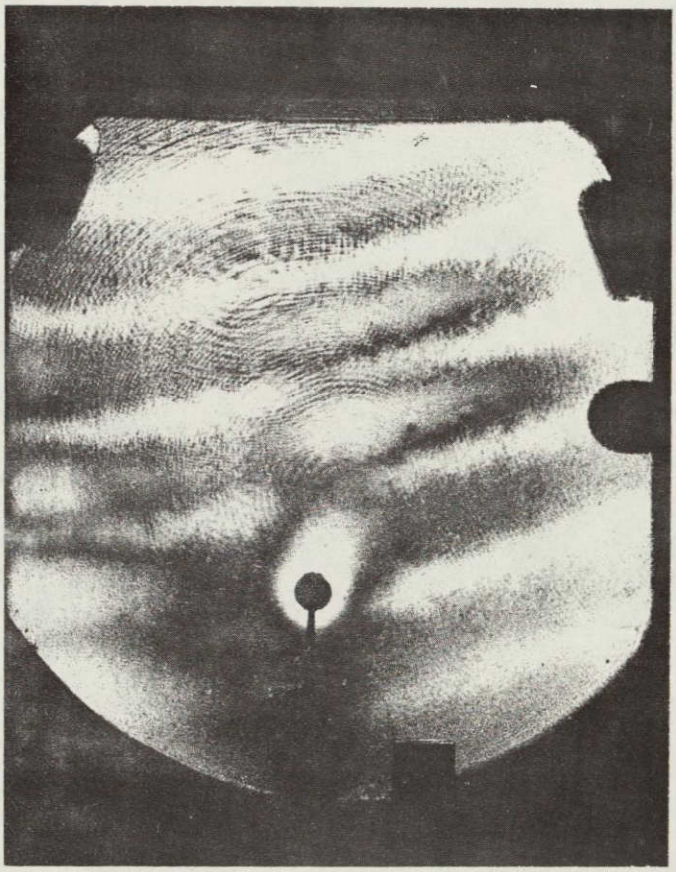

Figure 2.2-8. Readout of four-beam interferogram. Glow around resistor indicates phase shift which is 1/6 wavelength at the surface of the resistor.

Analysis of Four-Beam Interferometer

This section gives an outline of the analysis of the four-beam interferometer. The material presented here concerns itself with the effects of phase errors. A separate and similar analysis has been made for intensity errors, but is not reproduced here. Thus, for the present analysis the four beams are assumed to be of equal intensity and the two exposures of equal duration. The analysis computes the intensity as a function of position on the hologram plane resulting from the sum of the two exposures, each consisting of four beams. The intensity pattern is then interpreted in terms of the reconstructed image.

Letting x,y denote the coordinates of the hologram plane, the complex amplitudes of the electric fields of the four beams can be represented respectively by

$$\underbrace{e^{-ikx-i\frac{\ell}{2}w},\ e^{-ikx+i\frac{\ell}{2}w}}_{\text{SUBJECT PAIR}},\qquad \underbrace{e^{ikx-i\frac{\ell}{2}w-i\frac{\phi}{2}},\ e^{ikx+i\frac{\ell}{2}w+i\frac{\phi}{2}}}_{\text{REFERENCE PAIR}},$$

where the optical frequency factor $e^{i\omega t}$ has been suppressed, as is customary. The coefficient k depends upon the angle of incidence, and is given by $\frac{2\pi}{\lambda}$ sin (angle of incidence). For simplicity, the hologram has been oriented to make equal angles with the subject and reference beams, the arrangement also used in the experiment. The coefficient ℓ, which is small compared to k, corresponds to the small angle between the beams of each pair. The value of ℓ is approximately $\frac{2\pi}{\lambda}$ times the small angle. The variable w can be replaced by x to represent the case when the coarse fringes are parallel to the fine fringes, or can be replaced by y to represent the case when the coarse fringes are perpendicular to the fine fringes. The variable ϕ is included to cover the case where the coarse fringes formed by the reference pair are out of phase (by ϕ radians) with the coarse fringes of the subject pair. Computation of the intensities formed by the reference pair only and the subject pair only gives, respectively,

$2[1 + \cos(\ell w + \phi)]$ and $2(1 + \cos \ell w)$, which represent the coarse fringes. It is appropriate to think of ϕ as either fixed or as very slowly varying as one moves across the plate, due to the lack of registry of the coarse fringes stemming from imperfect optics.

The complex amplitude of the first exposure is obtained by taking the sum of the amplitudes given above for the individual beams. Thus

$$A_1 = e^{-ikx-i\frac{\ell}{2}w} + e^{-ikx+i\frac{\ell}{2}w} + e^{ikx-i\frac{\ell}{2}w-i\frac{\phi}{2}} + e^{ikx+i\frac{\ell}{2}w+i\frac{\phi}{2}} \quad .$$

The intensity at the hologram for the first exposure is given by

$$I_1 = A_1 A_1^* \quad ,$$

where A_1^* denotes the complex conjugate of A_1.

For the second exposure, two additional phase changes are introduced; namely, the subject phase shift θ which shifts the phase of the two subject beams and the phase shift ψ which shifts the phase of the right hand (or upper) beam of each pair. The ψ phase shift has the target value of π (i.e., 180°) and its function is to displace all the coarse fringes by 180° so that the sum of the first and second exposures result in a uniform fine fringe grating except where the subject has introduced a phase shift. The subject phase shift θ varies slowly with x and y, corresponding to the structure in the subject. The ψ phase shift may change slightly with x and y if the phase shifter is not perfect.

Introducing these phase shifts into the second exposure, the complex amplitude of the light at the hologram is

$$A_2 = e^{-ikx-i\frac{\ell}{2}w+i\theta} + e^{-ikx+i\frac{\ell}{2}w+i\theta+i\psi} + e^{ikx-i\frac{\ell}{2}w-i\frac{\phi}{2}} + e^{ikx+i\frac{\ell}{2}w+i\frac{\phi}{2}+i\psi} \quad .$$

The intensity at the hologram for the second exposure is $I_2 = A_2 A_2^*$. Thus the total exposing intensity for both exposures is

$$I_1 + I_2 = A_1 A_1^* + A_2 A_2^* \quad .$$

This multiplication can be carried out using a sort of matrix notation to reduce the mess. The thirty-two complex terms can be paired into twelve cosine functions and a constant. At this point in the analysis, advantage is taken of the fact that θ is small and ψ is almost equal to π. Let $\psi = \pi+\beta$, so that β is small, representing the imperfections of the phase shift. Expanding in powers of θ and β, omitting terms of higher order than the first, and utilizing some trigonometric sum formulae, the intensity may be written:

$$\begin{aligned}\frac{I_1 + I_2}{8} = 1 &+ \cos\frac{\phi}{2}\left[\cos 2kx + \frac{\theta}{2}\sin 2kx\right] \\ &- \frac{\theta}{4}\left[\sin\left(2kx + \ell w + \frac{\phi}{2}\right) + \sin\left(2kx - \ell w - \frac{\phi}{2}\right)\right] \\ &+ \frac{\beta}{4}\left[\sin \ell w + \sin(\ell w + \phi)\right] \\ &+ \frac{\beta}{4}\left[\sin\left(2kx + \ell w + \frac{\phi}{2}\right) - \sin\left(2kx - \ell w - \frac{\phi}{2}\right)\right] \quad .\end{aligned} \tag{1}$$

The consequences of this intensity pattern on the reconstruction readout are most easily understood by examining the two extreme cases $\phi = 0$, where the coarse fringes of subject and reference beams match, and $\phi = \pi$, where the coarse fringes of the subject beam interlace those of the reference beam.

For the case $\phi = 0$, the intensity given by formula (1) becomes

$$\begin{aligned}\frac{I_1 + I_2}{8} = 1 &+ \cos 2kx \\ &+ \frac{\theta}{2}(1 - \cos \ell w)\sin 2kx \\ &+ \frac{\beta}{2}\sin \ell w \\ &+ \frac{\beta}{2}(\sin \ell w)\cos 2kx \quad .\end{aligned}$$

Since θ and β are both small, the terms $1 + \cos 2kx$ are the dominant part of this expression. These terms represent the basic grating or carrier frequency: the other terms represent small perturbations. The θ contribution is at 90 degrees to the basic carrier, and hence represents a phase modulation of the carrier. On the other hand, the β contribution is in phase with the carrier, and hence represents an amplitude modulation. Now the exposure of the hologram is chosen so as to maximize the diffraction efficiency of the grating. Therefore, small increases or decreases of the exposing grating intensity (i.e., amplitude modulation) do not significantly change the diffraction efficiency of the grating produced. In other words, amplitude modulation of the grating changes the line widths of the grating lines. But since the operating point is chosen at the maximum diffraction point, both increases and decreases in line width cause only a slight second order decrease in diffracted light out. Thus for operation at the maximum efficiency point, the β contribution does not produce any first order effect on the diffracted light.

Such is not the case for the θ variations however, for the θ contribution modulates the phase of the basic grating. That is, the θ variation shifts the position of the basic grating lines. This phase modulation can be made evident by rewriting the above expression in the form,

$$\frac{I_1 + I_2}{8} = 1 + \cos\left(2kx - \frac{\theta}{2} + \frac{\theta}{2}\cos \ell w\right) + \frac{\beta}{2}\sin \ell w + \frac{\beta}{2}(\sin \ell w)\cos 2kx \quad ,$$

where again only first order terms in θ have been retained. From this form, one observes that the phase of the basic grating oscillates with a phase excursion of $\frac{\theta}{2}$ at the coarse fringe frequency.

The result is that in this case where $\phi = 0$, the subject phase shifts (θ variations) manifest themselves by producing a phase wrinkle, with the coarse fringe frequency, on the output diffracted light. The error β, in setting of the 180° phase shift, does not produce any first order change in the diffracted light when the exposure is chosen to maximize the diffracted light.

The above expression also gives the magnitude of the phase wrinkle on the diffracted subject light. This diffracted subject light can then be resolved into zero order subject light and sideband orders by means of a Bessel function expansion. When this is done, it is found that the ratio of the intensity of one of the first order sidebands to the intensity of the zero order subject light is $\frac{\theta^2}{16}$, where again θ is assumed small.

Shifting attention now to the case $\phi = \pi$, where the coarse fringes of the subject beam interlace those of the reference beam, a different behaviour is found. Formula (1) evaluated for $\phi = \pi$ gives

$$\frac{I_1 + I_2}{8} = 1 - \frac{\theta}{4}[\cos(2kx + \ell w) - \cos(2kx - \ell w)] + \frac{\beta}{4}[\cos(2kx + \ell w) + \cos(2kx - \ell w)] \quad .$$

In this case, the carrier or basic grating has disappeared, giving a uniform grey exposure for $\theta = \beta = 0$. The presence of subject phase shift does give rise to the desired sideband components so that the readout process does indeed reveal the presence of subject phase variations as with the $\phi = 0$ case. However, the above expression also reveals that errors in the 180° phase shift, rendering β different from zero, also give outputs in the same manner as do subject phase shifts. Thus, for useful results, the 180° phase shift must be set to zero with the same accuracy as the subject phase variations one desires to observe. This is a stringent requirement in practice which makes operation with the $\phi = 0$ case preferable, with its absence of this stringent requirement. Operation of the four-beam interferometer in the $\phi = \pi$ case resembles the operation of the two-beam sub-fringe interferometer in several respects.

The case $\phi = 0$ of coarse fringe registry is insensitive to errors β in setting of the 180° phase shifter. The case $\phi = \pi$ of complete misregistry surpresses the basic grating with the result that errors β in setting of the 180° phase shifter produce an undesirable readout. It is thus important to

examine the case of arbitrary ϕ in order to evaluate the precision required in registering the coarse fringes which will retain the insensitivity of the $\phi = 0$ case.

Formula (1) for the intensity incident upon the hologram can be written in the form:

$$\frac{I_1 + I_2}{8} = 1 + (\cos \tfrac{\phi}{2}) \cos 2kx$$
$$+ \tfrac{\theta}{2} \left[\cos \tfrac{\phi}{2} - \cos (\ell w + \tfrac{\phi}{2})\right] \sin 2kx$$
$$+ \tfrac{\beta}{4} \left[\sin \ell w + \sin (\ell w + \phi)\right]$$
$$+ \tfrac{\beta}{2} \left[\sin (\ell w + \tfrac{\phi}{2})\right] \cos 2kx \quad .$$

The term cos 2kx appearing on the top line of this formula represents the carrier or basic grating. Its coefficient, cos $\frac{\phi}{2}$, is non-zero except for $\phi = \pm\pi$, the case examined previously. The second line represents the phase modulation of the grating by the subject phase shift θ, inasmuch as it has the multiplier sin 2kx which is at 90° to the basic carrier. The coefficient of this second term is proportional to θ and oscillates at the coarse fringe frequency, with the magnitude of the oscillation being independent of ϕ. Thus, the subject always produces the same amount of phase modulation independent of ϕ.

The third line contains only terms of the coarse fringe frequency and hence does not influence the readout, which uses a sideband of the basic carrier.

The fourth line has the multiplier cos 2kx which is in phase with the basic carrier. Thus, this term represents amplitude modulation of the basic carrier, the modulation frequency being the coarse fringe frequency and the depth of modulation being proportional to β, the 180° phase shift error. Note that the magnitude of the oscillations of the coefficient in the fourth term are independent of ϕ, as was the case with the second line.

Consequently, the change in behavior with ϕ comes about only from the cos $\frac{\phi}{2}$

term which alters the strength of the basic carrier. Whenever this carrier is reasonably strong so that the other terms represent small phase and amplitude modulations of the carrier it should be possible to suppress the amplitude modulation contribution to the readout by choosing the exposure to optimize the diffraction efficiency

Thus, the precision required in setting the coarse fringe registry, ϕ, is not high. For example for $|\phi| < 90°$ the carrier is greater than 70% of its maximum strength so that for $|\beta| < 10°$ ($|\beta| < \frac{1}{6}$ radian) the percentage amplitude modulation is less than 12%. By exposing for maximum diffraction efficiency, so that both increases and decreases in amplitude cause only second order decreases in reconstructed amplitude, the fundamental component of the amplitude modulation should be reduced by at least one order of magnitude giving less than 1.2% amplitude modulation in the reconstruction. This amount of residual amplitude modulation casts the same intensity into the readout as a subject phase shift θ of .024 radians or 4/1000 of a wavelength.

This example also illustrates that the ultimate phase sensitivity is approximately equal to the accuracy of the 180° phase shifter, β, divided by the suppression ratio of the amplitude modulation created by operating at the peak of diffraction efficiency.

Although the precision $|\phi| < 90°$ seems extremely tolerant it should be remembered that this precision of registry of the coarse fringes must be maintained for all the coarse fringes simultaneously, i.e. over the entire hologram. Thus, this is not a particularly lax requirement and it is fortunate that the tolerance on ϕ is as large as it is.

2.3 INTERFEROMETRY THROUGH A TURBULENT BOUNDARY LAYER

Holographic interferograms of aerodynamic type subjects, made with a diffuse source of light behind the subject, contain more information than conventional interferograms in which a single parallel beam of light traverses the subject. The increased information content stems from the fact that the diffuse source of light passes light through the subject from many different directions. Each of these directions contains the information about the integral of the density change along that direction. It is conceptually possible to use the information obtained by viewing the holographic interferogram from many different directions to compute the three-dimensional density distribution within the subject, even in the absence of subject symmetry. In reality such a three-dimensional analysis appears difficult and to the author's knowledge has not yet been performed.

What we report on here is a far more modest scheme in which the large information content of a diffusely illuminated holographic interferogram is utilized to permit accurate interpretation of symmetric flows in the presence of boundary layer turbulence on the windows of the test chamber. Such a subject viewed in the presence of boundary layer turbulence with a conventional parallel beam interferometer will have the subject fringes displaced by the boundary layer density fluctuations. The technique reported on here is simply to view the subject from a sufficient number of viewing directions so that the boundary layer effects are averaged out. However, due to the symmetry of the subject, the subject contributions to the fringe pattern do not change for the different viewing directions. Thus, the resulting picture reveals the fringe pattern of the subject undistorted by the boundary layer. The limit on the magnitude of the boundary layer fluctuations permitted is set by the tolerable decrease in contrast of the subject fringes.

In practice, the viewing of the subject from a variety of directions is easily accomplished by using a wide aperture lens as shown in the figure.

This essentially amounts to focusing a wide aperture copy camera upon the subject of the holographic image.

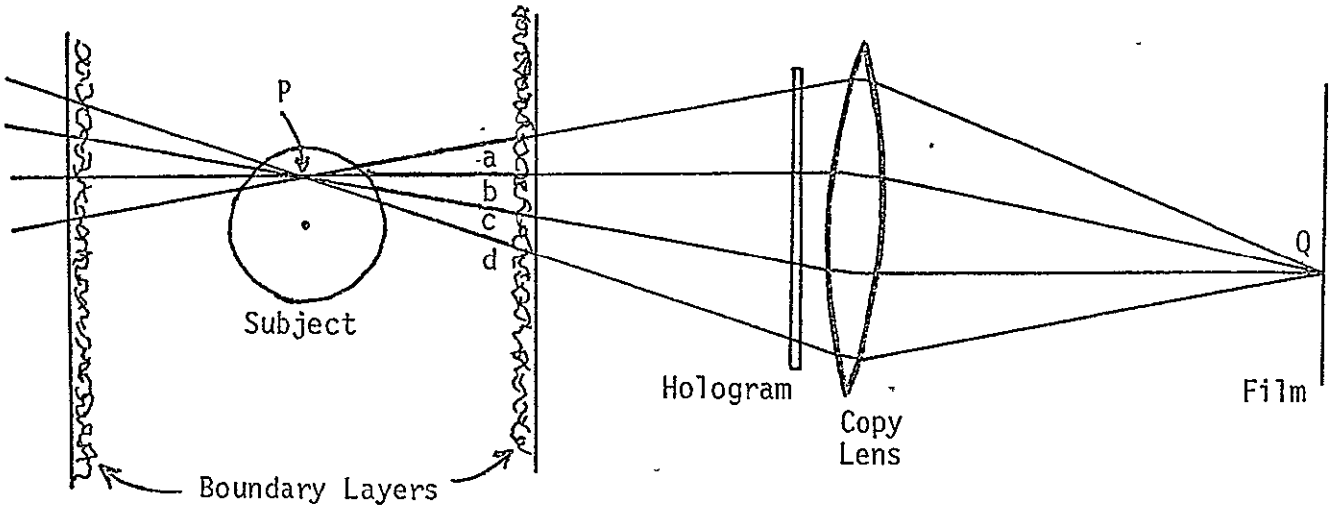

Figure 2.3-1 Wide Aperture Hologram Viewing

Here the point Q on the film receives many rays passing through point P in the mid-plane of the symmetric subject. Sample rays a, b, c, and d are shown. These rays traverse the subject at different directions but because of the subject symmetry they all experience essentially the same phase shift due to the subject perturbation between exposures. Let ϕ denote this subject phase shift. The phase shift ϕ depends of course on the location of the point P in the mid-plane of the subject.

When these rays traverse the boundary layer each will suffer a phase shift dependent upon the change in the boundary layer path between exposures. Since the boundary layers are not at the focal plane and since the size scale of the boundary layer turbulence is small compared to the diameter of the light cone at the boundary layer, the rays a, b, c, and d will each suffer different boundary layer phase shifts. Let θ denote the phase shift due to the boundary layer. For each point P, θ is a function of the ray direction.

As a simple model of the random boundary layer phase shifts we assume a Gaussian distribution. Specifically, we assume that the fractional boundary layer area in which the phase shift lies between θ and $\theta + \Delta\theta$ is,

$$\frac{1}{\sigma\sqrt{2\pi}} e^{-[\theta^2/2\sigma^2]} \Delta\theta \quad , \tag{1}$$

where σ is the RMS magnitude of the phase fluctuation.

The intensity observed along any given ray depends on the sum of the subject and boundary layer phase shifts and is proportional to $\cos^2\left(\frac{\phi + \theta}{2}\right)$. Because of the ground glass diffuser the intensities all add incoherently for the different rays. Thus, the total intensity at Q observed through the given subject point P for the full aperture is

$$I(\phi) = \frac{1}{\Omega_\tau} \int \cos^2\left(\frac{\phi + \theta}{2}\right) d\Omega \quad ,$$

where the integral is taken over the solid angle Ω_τ accepted by the viewing aperture.

When the viewing aperture encompasses sufficient boundary layer area so that essentially a complete sampling of the boundary layer phase shift is obtained, this integral may be rewritten, using (1) above, in the form

$$I(\phi) = \frac{1}{\sigma\sqrt{2\pi}} \int_{-\infty}^{\infty} e^{-[\theta^2/2\sigma^2]} \cos^2\left(\frac{\phi + \theta}{2}\right) d\theta \quad .$$

Using the trigonometric identities,

$$\cos^2\left(\frac{\phi + \theta}{2}\right) = \frac{1}{2}\left[1 + \cos(\phi + \theta)\right] = \frac{1}{2}(1 + \cos\phi\cos\theta - \sin\phi\sin\theta) \quad ,$$

the integral reduces to standard forms (7.4.1 and 7.4.6 of N.B.S. Handbook of Mathematical Functions) yielding,

$$I(\phi) = \frac{1}{2}(1 + e^{-\sigma^2/2} \cos \phi) \quad .$$

Notice that for no turbulence, $\sigma = 0$, the intensity is $I(\phi) = \frac{1}{2}(1 + \cos \phi)$, and thus the fringe position is unaffected by the turbulence. The fringe visibility,

$$V \equiv \frac{I_{max} - I_{min}}{I_{max} + I_{min}} \quad ,$$

is readily obtained from the foregoing formula and is

$$V = e^{-\sigma^2/2} \quad .$$

This formula shows that as σ, the RMS fluctuation of the boundary layer phase shift, increases, the visibility of the subject fringes decreases. For $\sigma = 0$, of course, $V = 1$, and for $\sigma = 2.15$ radians one has $V = 0.1$ which is still a useable value. However, for $\sigma = \pi$ radians the visibility is down to .007 and for larger phase shifts the visibility becomes vanishingly small.

Other statistical models for the boundary layer phase shift give similar results. Namely, for peak to peak boundary layer phase shifts less than a wavelength, the subject fringes remain visible but for peak to peak phase shifts greater than one wavelength the subject fringes are not expected to be visible.

An experiment was performed to test the technique of viewing through turbulence. A candle flame was used as subject. Care was taken to remove drafts so that the candle flame was laminar and axially symmetric. A "turbulent boundary layer" was made by blowing the output of a laboratory heat gun through a channel consisting of two plexiglass sheets separated by one inch. This channel was about 9 inches from the candle, between the candle and hologram. From the channel to the hologram was about 6 inches,

just sufficient for unobstructed access of the reference beam. Diffuse illumination was used in one of the standard pulsed laser holocameras.

The boundary layer heat flow was present on both exposures but the candle was lit only for the second pulse.

Figure 2.3-2a shows a copy of the holographic image, focused upon the candle flame. This picture shows very little evidence of the turbulent boundary layer. In order to achieve a maximum aperture for this copy it was made by placing the copy film in the projected real image from the hologram. In this way the effective f number was about f/4, a larger aperture than permitted by our stock of lenses. A quasi cw ruby laser was used for this reconstruction to minimize wavelength shift aberrations.

Figure 2.3-2c shows the same hologram under the same conditions except the copy film is placed in the real image of the boundary layer. The subject is now so completely out of focus as to be undetectable. The boundary layer turbulence is slightly visible because it is sufficiently thin so that its path variations are somewhat independent of direction.

Figure 2.3-2b shows another attempt to view the boundary layer. This picture was made with a conventional camera at f/45 focused upon the candle flame. Because of the small aperture, averaging over the boundary layer is very incomplete, allowing the boundary layer phase shifts to show in the interferogram. We have been unable to produce a copy from this hologram which accurately reproduces the view one would obtain from a collimated beam Mach-Zehnder interferometer. Such a view would make the boundary layer even more evident than in the f/45 picture.

The contrast in the candle flame fringes, Figure 2.3-2a, is so high as to indicate that greater boundary layer turbulence could be permitted. Moreover, if the scale size of the turbulence were closer to the flame fringe spacing the confusion of the subject fringes by the boundary layer would be greater, resulting in a greater benefit from using the averaging technique.

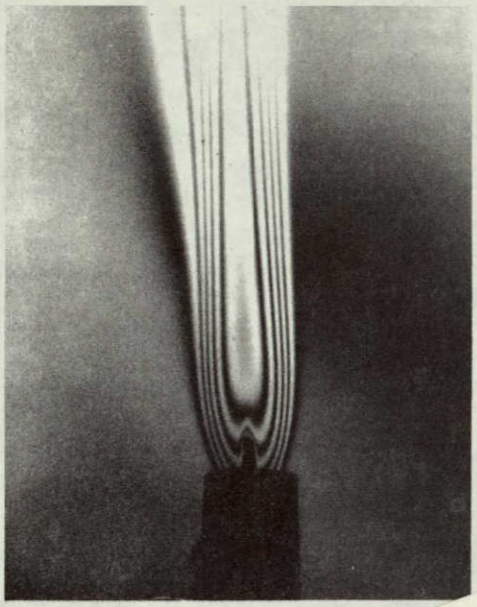

a

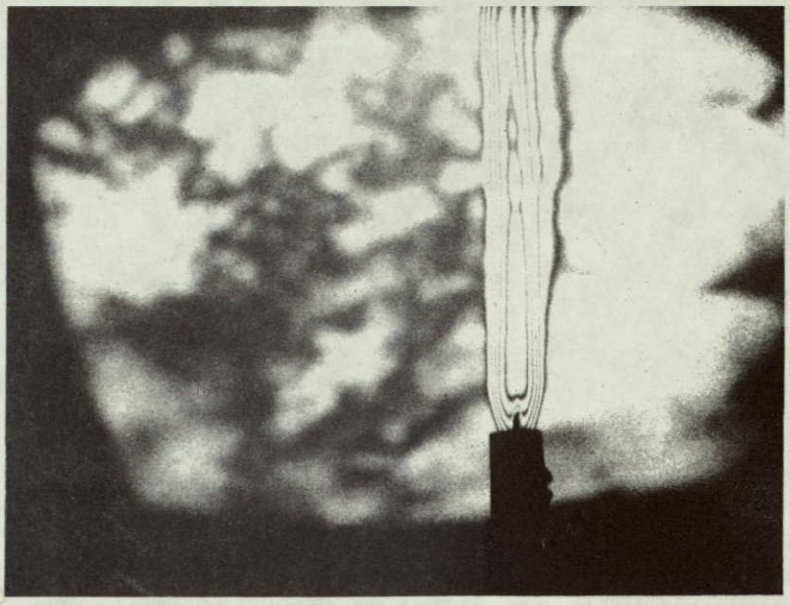

b

c

Figure 2.3-2. Interferograms of candle flame through turbulent boundary layer. (a) Viewed with a large angular aperture. (b) Viewed with small angular aperture showing the effect of the boundary layer. (c) Interferogram of boundary layer turbulence from the same hologram as (a), but made by placing the copy film in the projected real image at the location of the boundary layer. The effective angular aperture is thus so wide that the candle flame is not apparent.

To conclude the evaluation of the technique we mention two limitations. The first is the requirement for subject symmetry and has already been mentioned. Figure 2.3-3 shows what happens when a non-symmetric subject is viewed with a wide aperture. This turbulent candle flame was photographed with the same real image ($\simeq$ f/4) technique of Figure 2.3-2a. There was no boundary layer. It will be observed that the wide aperture has averaged out the subject fringes in some regions almost to invisibility. This occurs because the subject phase shift changes rapidly with viewing direction in certain regions.

The second limitation is the requirement for stability in the system. If a hologram is made in which a small motion of some component occurs between exposures the hologram will usually have a background of fringes. Such a hologram is often still useful visually for the subject fringe component can often be distinguished from the background. However, if the averaging technique is used on such a hologram the subject fringe contrast will drop to unacceptable values if the motion was sufficient to cause more than one wave of phase variation over directions accepted by the averaging aperture. The pictures illustrated were made from a hologram which was essentially free of extraneous motion. Several other holograms were not useful, due to motions of the heated plexiglas, causing background fringes.

Figure 2.3-3. Wide aperture view of interferogram of a non-symmetrical subject, showing obliteration of fringes.

2.4 WIDE ANGLE HOLOGRAPHIC INTERFEROMETRY WITHOUT LASER SPECKLE

Introduction

One of the more dramatic features of the hologram is that it allows the recorded image to be viewed over a wide angular range. This can be used to advantage with holographic interferometry to obtain a number of different interferograms corresponding to beams passing through the subject in different directions. In the past this has been accomplished by illuminating the subject with diffuse light.[3]

The main objection to the use of diffuse light is that the spatially random phase imparted to the illumination waves by the diffuser gives rise to an image which is modulated by a granular intensity pattern called laser speckle or laser granularity.[4] The speckle pattern, acting as a source of spatial noise, hampers accurate measurement of the interference pattern, particularly for low visibility fringes.[2] Furthermore, the size scale of the speckle pattern becomes larger, and hence a greater annoyance, as the angular viewing aperture decreases. This is incompatible with the desire for a restricted angular viewing aperture so as to clearly define the direction of the light through the subject and to increase the depth of field so that the fringes will focus on the subject.

The following describes a technique which permits the subject to be viewed over a wide angular range by illuminating the subject with a number of collimated beams (plane waves) at discrete, but precisely known, angular directions. The problem of laser speckle is avoided entirely. A collimated beam of laser light is conveniently split into a number of discrete beams by means of a diffraction grating which produces many orders of diffraction in accurately defined directions. Figure 2.4-1 shows an arrangement for splitting the laser beam into three beams. A separate hologram is produced using each of the three beams. (To avoid cluttering the diagram, the three reference beams are not shown). Although this arrangement might prove practical when just a very few viewing directions are needed, as the number of beams is increased the complexity of making many holograms becomes great.

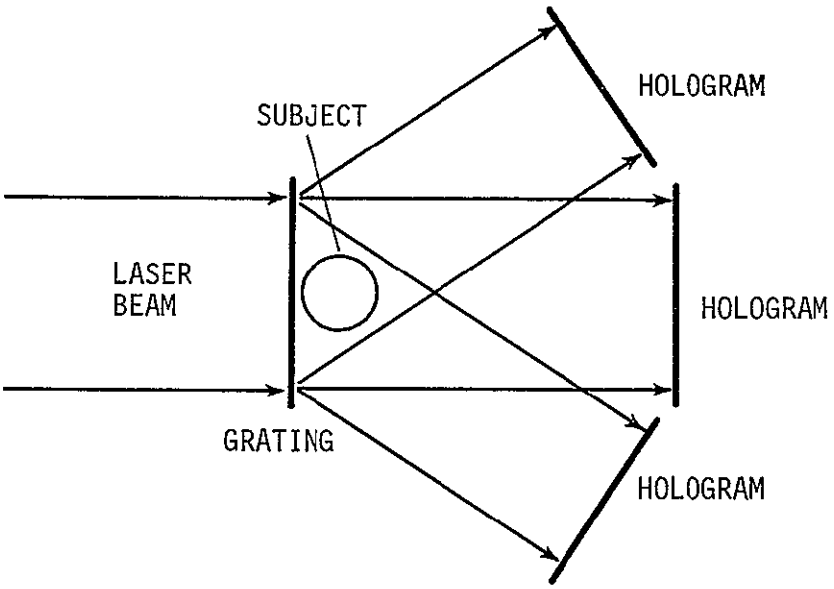

Figure 2.4-1 Multiple-Hologram, Wide Angle Interferometer

The remainder of the discussion is devoted to describing a simple means for recording all the subject beams on a single hologram. The means by which the angularly dispersed beams are gathered together for compact recording is to let them fall on a second diffraction grating after they have traversed the subject region. Upon striking the second grating, each subject beam generates a number of diffracted orders, only one of which is needed to convey the interferometric information about the subject beam. If the grating constants of the two gratings are slightly different, we will show that beams emerging from the second grating which convey information about all the subject beams, are only slightly separated in angle and can be conveniently recorded on a single hologram. Because of the small angle separating adjacent recorded beams, the angle to the reference beam can likewise be quite small permitting the hologram recording to be made on film of high sensitivity (low resolution requirement).

Fig. 2.4-2 shows a possible arrangement of the double grating holographic interferometer. The angular range of the subject beams (65°) the same as Fig. 2.4-1. To avoid cluttering the diagram, only one of the diffracted orders

from each subject beam at the second grating is shown passing through the lens. The unwanted beams are conveniently blocked by an aperture in the focal plane of the lens.

In the discussion that follows, we will consider only plane diffraction gratings by which the light is angularly dispersed in the plane of the paper. The techniques can be extended to two-dimensions by the use of diffraction "grids" or crossed gratings which additionally disperse the beams out of the plane of the paper.

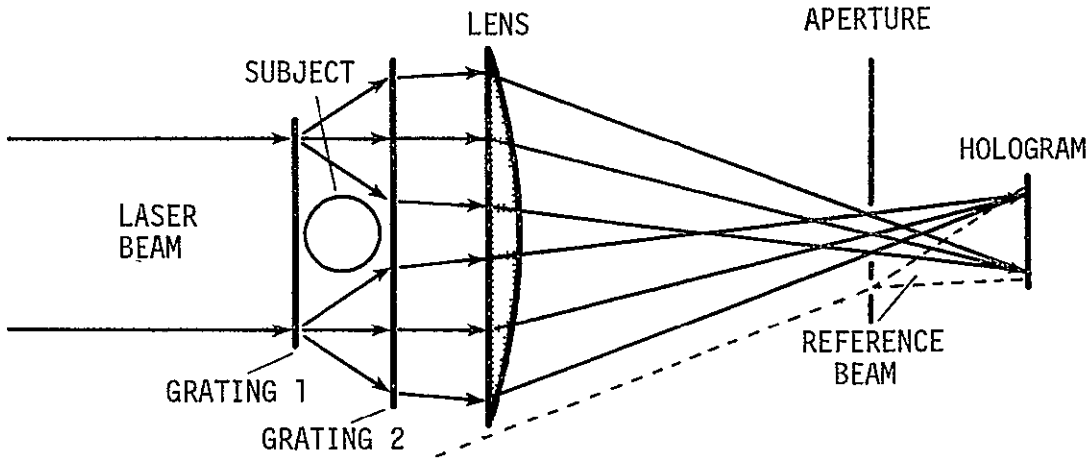

Figure 2.4-2 Double Grating Holographic Interferometer

Analysis

For a collimated beam of wavelength λ incident normal to the first grating, the diffraction angles, θ_1, are given as,

$$\sin \theta_1 = m\lambda/d_1, \qquad m = 0, \pm 1, \pm 2, \ldots \ldots \ldots$$

where d_1 is the grating constant and m is the order number. The beams diffracted from the first grating pass through the subject area and the choice of the ratio λ/d_1 determines the angles between adjacent beams. For small angles, the angular separation is approximately constant. As the diffraction angles becomes larger, the separation becomes smaller due to the

nonlinearity of the sine function.

When the beams from the first grating are incident on the second grating (assumed parallel to the first), the diffraction angles θ_2 from the second grating are given as,

$$\sin \theta_1 + \sin \theta_2 = n\lambda/d_2, \qquad n = 0, \pm 1, \pm 2, \ldots\ldots\ldots$$

The two preceeding equations can be combined to give the more compact expression for the diffraction angles θ_2 as,

$$\sin \theta_2 = \frac{\lambda}{d_1}\left[n \frac{d_1}{d_2} - m \right].$$

Note that this expression has the same form as the diffraction from the first grating if we consider the expression in the brackets, $[nd_1/d_2 - m]$ as an "effective" or compound order number. The compound order depends on the two integers m and n, but takes on fractional values which are multiples of the quantity $(d_1/d_2 - 1)$. Thus, regardless of the angular separation of the diffracted beams from the first grating, the angular separation of the beams from the second grating can be as closely spaced as desired by a suitable choice of the ratio of the grating constants. The practical limitation on the minimum angular spacing of adjacent beams at the hologram is the angular spreading of the subject beams by phase changes in the subject, aberrations in the interferometer optics, and need for subject resolution.

In order to make the analysis of the system more meaningful it is instructive to look at a simple example. For this purpose we shall choose the ratio $d_1/d_2 = 1.1$ and plot a matrix of the values of the compound order number as a function of the orders m and n as they span the range from -5 to +5. The matrix is shown on the following page in Figure 2.4-3.

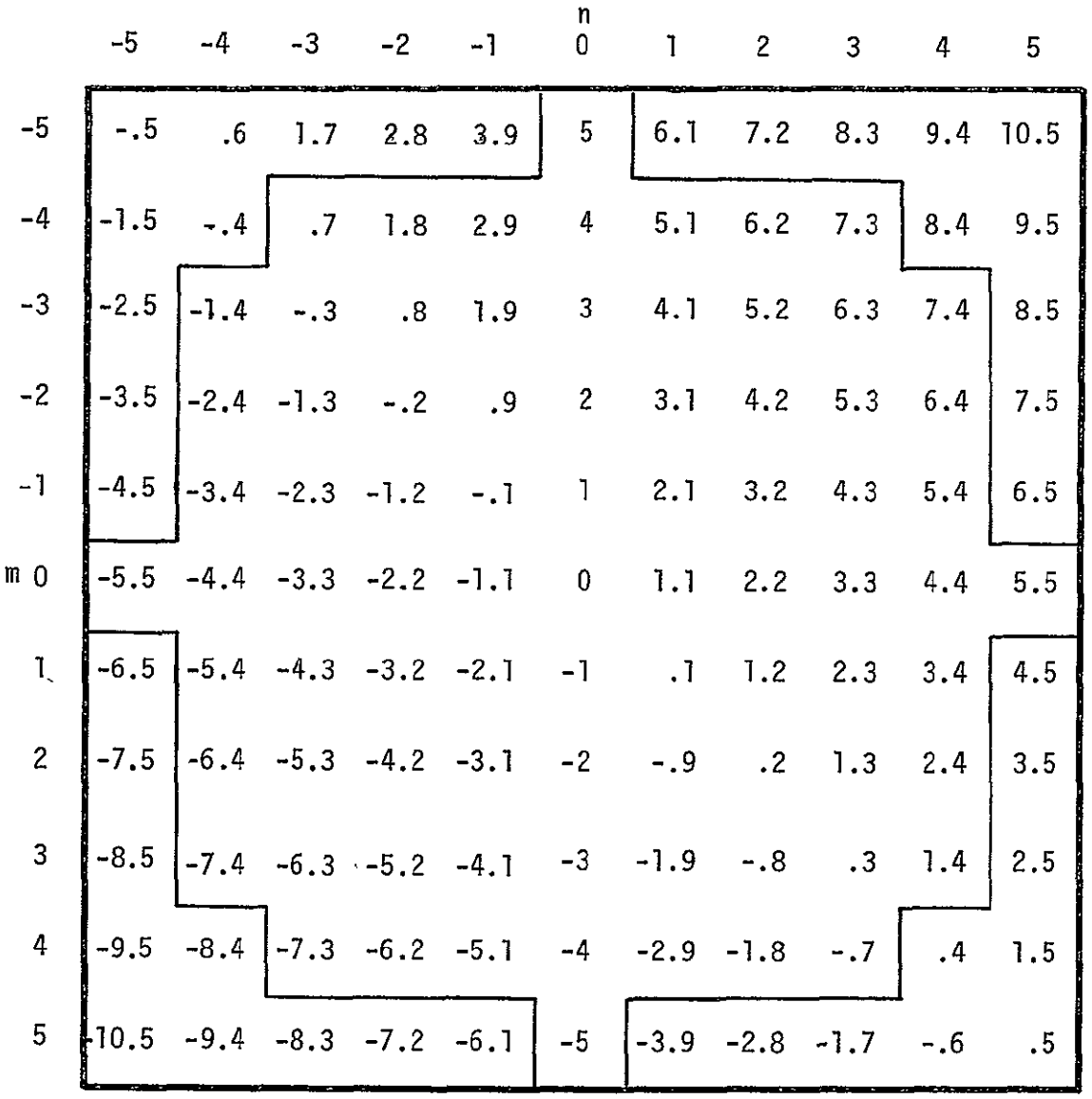

m \ n	-5	-4	-3	-2	-1	0	1	2	3	4	5
-5	-.5	.6	1.7	2.8	3.9	5	6.1	7.2	8.3	9.4	10.5
-4	-1.5	-.4	.7	1.8	2.9	4	5.1	6.2	7.3	8.4	9.5
-3	-2.5	-1.4	-.3	.8	1.9	3	4.1	5.2	6.3	7.4	8.5
-2	-3.5	-2.4	-1.3	-.2	.9	2	3.1	4.2	5.3	6.4	7.5
-1	-4.5	-3.4	-2.3	-1.2	-.1	1	2.1	3.2	4.3	5.4	6.5
0	-5.5	-4.4	-3.3	-2.2	-1.1	0	1.1	2.2	3.3	4.4	5.5
1	-6.5	-5.4	-4.3	-3.2	-2.1	-1	.1	1.2	2.3	3.4	4.5
2	-7.5	-6.4	-5.3	-4.2	-3.1	-2	-.9	.2	1.3	2.4	3.5
3	-8.5	-7.4	-6.3	-5.2	-4.1	-3	-1.9	-.8	.3	1.4	2.5
4	-9.5	-8.4	-7.3	-6.2	-5.1	-4	-2.9	-1.8	-.7	.4	1.5
5	-10.5	-9.4	-8.3	-7.2	-6.1	-5	-3.9	-2.8	-1.7	-.6	.5

Figure 2.4-3 Two-dimensional Array of Compound Orders, $[nd_1/d_2 - m]$

There is nothing to limit the size of the matrix to the range of m and n values that we have chosen. However, in general the energy in the diffracted orders decreases as the magnitude of m and n become large, so that there is a practical limitation to the range of m and n values. For the choice of the ratio $d_1/d_2 = 1.1$ and the matrix size shown, there is no degeneracy or overlap of compound orders. Matrix diagonals (upper left to lower right) correspond to angularly adjacent beams from the second grating which span the angular range of the subject.

Energy Distribution Among the Compound Orders

The diffraction gratings used in the system can be either amplitude gratings, phase gratings, or a combination. Because of the absorption of energy by all but pure phase gratings, we shall consider this type for the remainder of the discussion. Let the first grating be a simple sinusoidal phase grating with the spatial phase modulation expressed as,

$$\phi(x) = A \sin 2\pi x/d_1,$$

where A is the amplitude of the phase excursion which varies in the x direction. Such a grating can be produced by recording the interference pattern from two coherent collimated beams of light intersecting at an angle $\theta = \arcsin \lambda/d_1$ (one beam is assumed normally incident) on a sheet of photosensitive material which induces a change in refractive index or thickness linearly proportional to the exposure. Promising materials for producing phase gratings are bleached photographic emulsions, dichromated gelatin, or photopolymers.

For a unit amplitude plane wave incident on the first grating the amplitude of the mth order of diffraction from the simple sinusoidal grating is given as the mth order Bessel function of A, $J_m(A)$. The graph shown in Figure 2.4-4 shows the Bessel functions for integer valued arguments, (A is integer valued) and variable order p = n. This gives a good idea of how the amplitude falls off for large values of m and n.

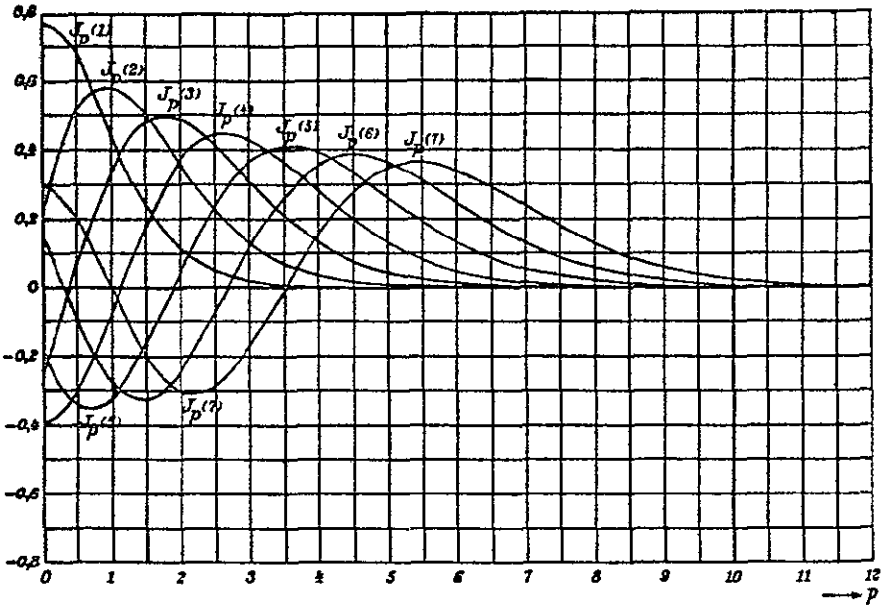

Figure 2.4-4 Bessel Functions of Constant Argument and Variable Order[4]

If the mth order beam from the first grating is incident on the second grating whose spatial phase modulation is described as,

$$\phi_2(x) = B \sin 2\, x/d_2,$$

then the amplitude of the light in the nth diffracted order from the second grating is $J_m(A)\, J_n(B)$ and the intensity of the light in the (m,n)th order is proportional to the square of the amplitude, $[J_m(A)\, J_n(B)]^2$. Figure 2.4-5 shows the relative intensities of the (m,n) order beams from the two gratings where we have for the sake of continuing our example, taken A = B = 3. The beams with significant relative intensity, taken as greater than or equal to 0.1% are enclosed within the internal boundary drawn on the matrix diagram of Figure 2.4-3. Note the absence of order overlap on Figure 2.4-5.

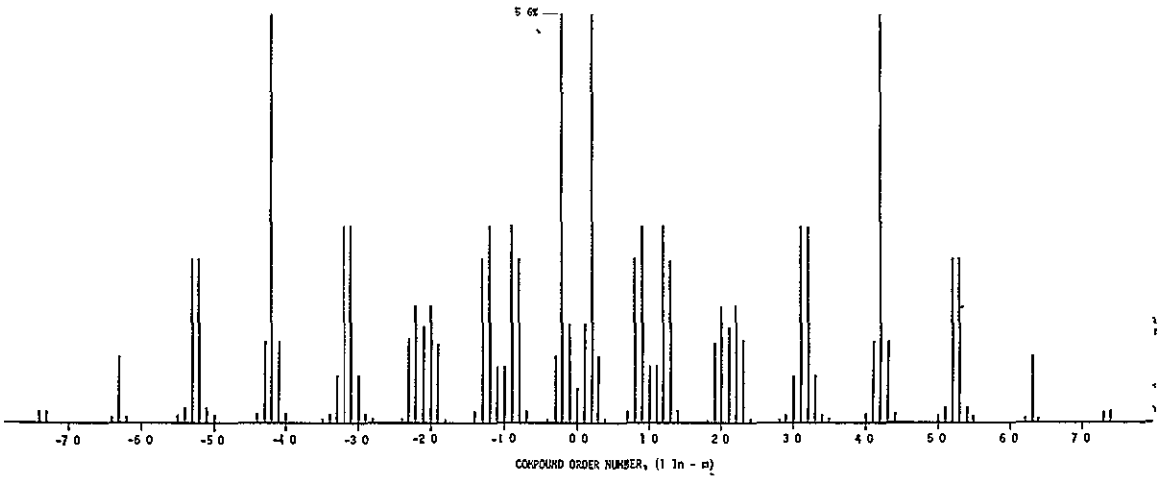

Figure 2.4-5. Relative intensity of the compound orders for two sinusoidal phase gratings, $[J_m(3)\ J_n(3)]^2$.

We would like to design our system so that the energy in the diagonal (m,n) orders which we record on the hologram have approximately equal energy over the desired angular range and then drop to zero so as to avoid any possibility of order overlap. The following design choices are available:

1. We can choose the values of A and B, and hence control to some extent the distribution of the light into the m and n orders at each grating, although this presumes that we can control A and B during the manufacture of the grating. The larger A and B are, the more orders that exist with significant energy. By choosing d_1/d_2 to be small, we can have a large number of orders without overlap. With A = B = 3 in our example, we obtain about 6 to 8 subject beams with significant energy and without order overlap.

2. Any of the matrix diagonals provide a set of angularly adjacent (m,n) orders which represent each of the subject beams. When we choose the main diagonal (passing through the compound order 0.0) we obtain maximum energy on the hologram (in our example the main diagonal

orders, contained 20.2% of the total energy). As we go off the main diagonal the energy content drops, but we can perhaps obtain a more even distribution of the energy among the recorded beams. In our example, the diagonal passing through compound order ±2.0 gave 5 beams of roughly equal energy containing approximately 6.8% of the total energy (see Figure 2.4-5).

3. By making the gratings so that they are not simple sinusoidal gratings (e.g. nonlinear exposure versus phase relationship), higher spatial frequency harmonics will result and this will change the entire distribution of energy among the orders.

4. By tilting the gratings with respect to one another and to the incoming laser beam we gain additional design flexibility. In addition we can rotate the gratings with respect to one another (rulings no longer parallel) to facilitate separation of the orders.

2.5 HOLOGRAPHIC SCHLIEREN

Real-Time Holographic Schlieren

In the usual case of holographic wavefront reconstruction, the reference waves illuminate the hologram and the recorded subject waves issue forth for viewing. It is quite possible to interchange these roles by illuminating the hologram with the subject waves, whereupon the recording reference waves issue forth. This interchange in the roles of the subject and reference waves forms the basis for a real-time schlieren system capable of good performance even though the subject beam may suffer phase aberrations due to imperfect (but fixed) optical elements.

Figure 2.5-1 shows how the schlieren system can be used for flow field visualization where the chamber windows may be of poor quality.

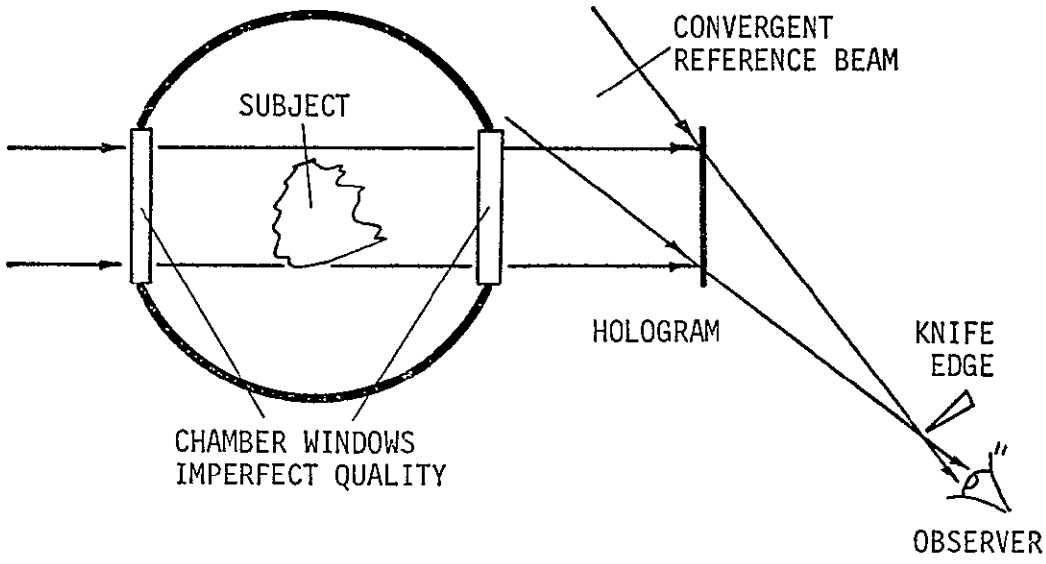

Figure 2.5-1 Real-Time Holographic Schlieren for Flow Field Visualization Through Imperfect Chamber Windows

The hologram is recorded using a convergent reference beam and with the flow field in its initial (e.g., unperturbed) state. After development of the hologram, it is accurately repositioned in the system. For viewing, only the subject beam illuminates the hologram. The convergent reference beam is reconstructed and comes to a sharp focus. If the subject is now perturbed, phase perturbations on the subject waves are directly transferred to the reconstructed reference beam and it no longer comes to a perfect focus. The schlieren focus can then be probed with the knife edge and the phase perturbations of the reference beam, which correspond to the subject perturbations, can be viewed. Because the phase aberrations of the imperfect chamber windows and collimating optics were present during the hologram recording, they do not affect the schlieren pattern.

In the preceeding example, the observer does not view the subject, as is the usual case in schlieren viewing, but rather the brightness distribution of the reference beam at the plane of the hologram. Accurate measurements requires that ray deviations due to phase perturbations of the subject beam (including chamber optics) are not great, so that a one-to-one correspondence can be made between the reference and subject rays. The arrangement is practical where the subject waves are nominally plane (or spherical), a situation commonly encountered in high sensitivity schlieren systems.

If the ray deviations of the subject beam are large, the real-time holographic schlieren system can still be used if a relay lens is used to focus the subject (assumed to be the major source of severe perturbations) upon the hologram to restore (with image inversion) the one-to-one correspondence between subject and reference rays. Figure 2.5-2 shows the use of the schlieren system with a reflecting subject. In this configuration schlieren can even be performed on diffuse subjects. This is an important technique, for the schlieren presentation shows strain directly rather than displacement as shown by the interferometric techniques. Since strain is more directly related to safety and failure analysis, the schlieren-strain presentation is of considerable application value.

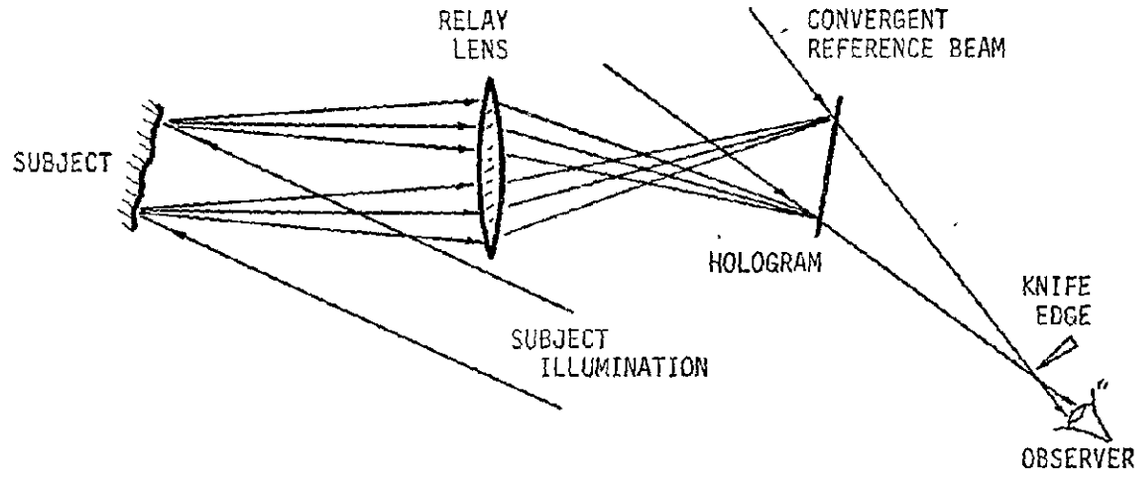

Figure 2.5-2 Real-Time Holographic Schlieren of a Reflecting Subject. The Relay Lens Insures One-to-One Correspondence Between Subject and Reference Rays.

In addition to making schlieren measurements, the arrangements shown in Figures 2.5-1 and 2.5-2 can also provide interference measurements if during readout the unperturbed convergent reference beam is observed simultaneously with the reconstructed reference beam. A theoretical development and description of experimental results of the real-time schlieren/interferometry technique is described in the paper, Phase Visualization Using a Reconstructed Reference Beam, reprinted in Appendix B.

Double Exposure Schlieren

Although the real-time schlieren technique has important applications, measurement accuracy depends on a recording reference beam which is free of aberrations. In addition, it suffers many of the limitations of real-time holographic interferometry; the same wavelength must be used for recording and playback and the hologram must be accurately located in the recording apparatus. These restrictions make it difficult to use with high speed ballistic phenomena where it is desirable to use a pulsed ruby laser for recording.

Extension of the technique such that it is useful with the pulsed ruby laser has resulted in the method of double exposure holographic schlieren which is now described. Two hologram recordings are made on the same hologram plate (although recordings on two separate plates which are subsequently paired is also possible). The first recording is of the subject in its unperturbed state (e.g., before firing a projectile), and the second recording is of the subject in its perturbed state (in the presence of the projectile and its shock envelope). Besides the introduction or perturbation of the subject, nothing else in the system is changed except to introduce a slight change in the angle of the hologram reference beam. The reference beam is changed enough to produce a finite fringe interferogram of the subject change when the hologram is viewed in the conventional way. If the hologram recording material is non-linear, careful examination of the hologram reveals a moire beat pattern which corresponds to the difference between the two hologram exposures, and hence the phase changes induced by the change in the subject. When the hologram is illuminated by a playback reference beam, the moire pattern serves to diffract light at a small angle about the reconstructing reference beam. Phase changes in the subject are therefore directly transferred to these diffracted beams, and they may be examined by schlieren techniques to observe the changes in the subject.

Figure 2.5-3 shows a simple illustration of the scheme. The unperturbed and perturbed subject (shown by solid and dotted lines, respectively) is located between the recording plate and the illumination source. Although a lens can be used after the hologram (on reconstruction) to focus the reference beam to a point, for simplicity a convergent reference beam is shown. The solid beam indicates the reference beam used with the first exposure (unperturbed subject) and a dotted beam indicates the beam used with the second exposure. A slight angle thus exists between the two reference beams.

For viewing, the hologram is illuminated by the reference beam and the subject beam is reconstructed in the usual way; however, this beam is not of interest. What is of interest is the light about the reconstruction reference beam which is diffracted by the moire pattern on the plate. The angle between these diffracted orders is equal to $\Delta\theta$, the angle between the reference beam during the recording (assuming the same reconstruction wavelength and geometry, and ignoring the phase perturbations due to the subject change).

To make a schlieren observation of the subject change, one of the diffracted orders is selected and observed using a knife edge or mask at its nominal focus. If a first order diffracted beam is used, then the phase change induced is equal to the phase change in the subject. If a higher order diffracted beam is used, then the phase change in the beam is multiplied by the order of diffraction. Figure 2.5-3c shows the zero order and some higher orders of diffraction.

Advantages of the double-exposure technique are that all the information about changes in the subject is stored on the hologram plate after the two exposures are made. It is not necessary to preserve the subject during the viewing step, or to return the hologram to the recording apparatus. Although best results are obtained if the recording and reconstruction geometry and wavelengths are similar, this is not a necessary condition. Most important, the recording reference beam need not be free of

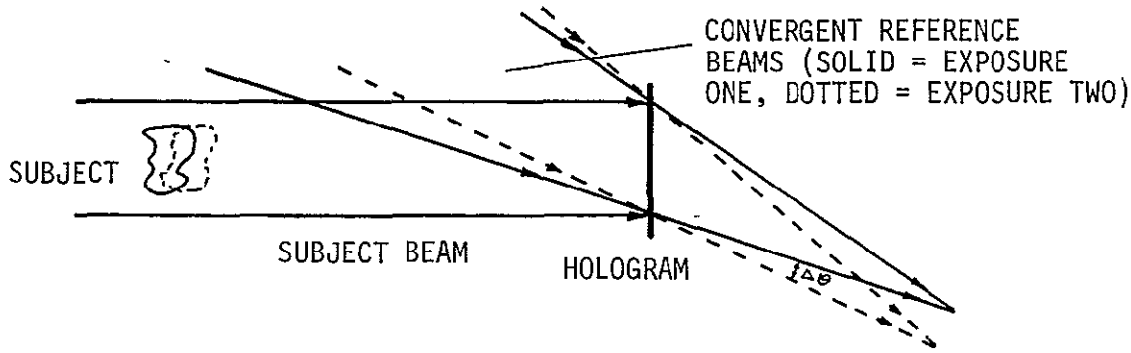

(a) Record the Hologram. $\Delta\theta$ = Change in Reference Beam Angle Between Exposures.

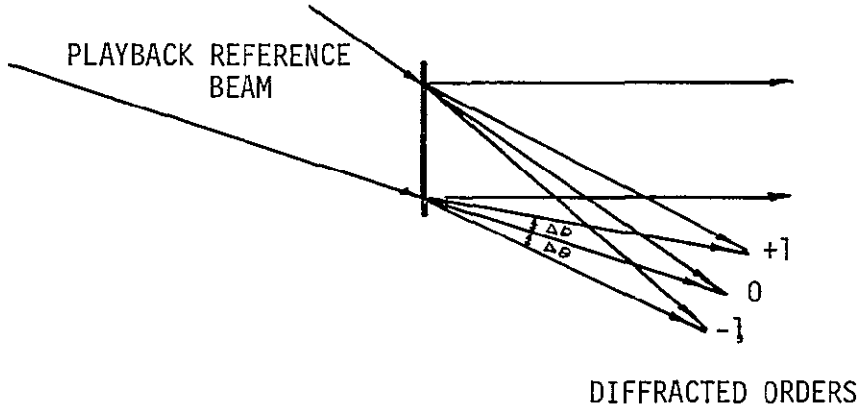

(b) Playback of the Hologram

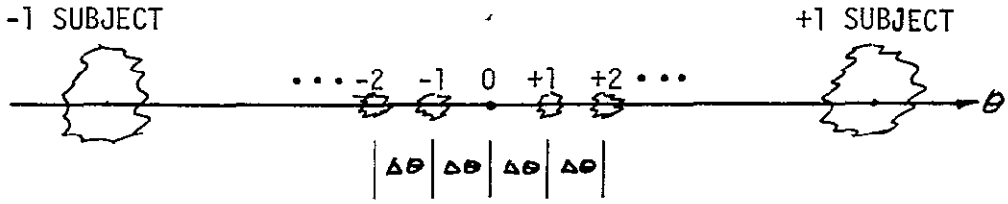

(c) Angular Distribution of the Reconstructed Beams

Figure 2.5-3

Recording and Playback of the Hologram for Double Exposure Holographic Schlieren.

aberrations to obtain an accurate measurement, although aberrations in the reconstruction reference beam directly affect the accuracy of the measurements. Therefore, it is quite feasible to make the hologram using a pulsed ruby laser which is usually phase-aberrated, and to carry out the reconstruction with a low power gas laser whose wavelength may be different, but which provides a reconstruction beam free of phase aberrations.

Analysis

For simplicity, assume that the scene and reference beams which fall on the hologram are nominally collimated. As such, they will form a hologram which is nominally a plane diffraction grating (at least over the small portion of the hologram which we shall consider at a given time). The angles are all to be measured relative to the normal to the hologram plate (assumed flat) with positive angles counterclockwise. The grating spacing for the first exposure is given as

$$S_1 = \frac{\lambda}{\sin \alpha_1 - \sin \theta_1}$$

where α_1 is the angle of the subject beam and θ_1 is the angle of the reference, and λ is the recording wavelength. Similarly, the grating spacing of the second exposure is given as

$$S_2 = \frac{\lambda}{\sin \alpha_2 - \sin \theta_2} \quad .$$

If a non-linear recording material is used to record the two hologram patterns, a moire beat pattern, corresponding to the intermodulation between the two recordings, is present on the hologram. Since $1/S_1$ is the fringe frequency of the first exposure and $1/S_2$ is the fringe frequency of the second exposure, the moire beat frequency is equal to the difference between the two fringe frequencies and is given as

$$\frac{1}{S^*} = \frac{1}{S_2} - \frac{1}{S_1} \quad .$$

If θ_R is the angle of the reconstruction reference beam, and β is the angle of the light diffracted by the moire pattern, the moire spacing can be written as

$$S^* = \frac{N\lambda'}{\sin \beta - \sin \theta_R}$$

which, when combined with the preceding equation, gives

$$\frac{1}{S^*} = \frac{\sin \beta - \sin \theta_R}{N\lambda'} = \frac{\sin \alpha_2 - \sin \theta_2}{\lambda} - \frac{\sin \alpha_1 - \sin \theta_1}{\lambda} \quad . \qquad (1)$$

Here N is the order of diffraction by the moire pattern and λ' is the reconstruction wavelength. Multiplying through by the optical wavelength and regrouping, Equation (1) can be rewritten as

$$\frac{\lambda}{\lambda' N} (\sin \beta - \sin \theta_R) = (\sin \alpha_2 - \sin \alpha_1) - (\sin \theta_2 - \sin \theta_1) \quad .$$

Taking advantage of the fact that $\beta - \theta_R$, $\alpha_2 - \alpha_1$ are each small quantities, we may expand each of the differences between the sines in a power series, retaining only the first terms, giving

$$\frac{\lambda}{\lambda' N} (\beta - \theta_R) \cos \theta_R = (\alpha_2 - \alpha_1) \cos \alpha_1 - (\theta_2 - \theta_1) \cos \theta_1 \quad .$$

Thus

$$\beta - \theta_R = \frac{\lambda'}{\lambda} N \left[(\alpha_2 - \alpha_1) \frac{\cos \alpha_1}{\cos \theta_R} - (\theta_2 - \theta_1) \frac{\cos \theta_1}{\cos \theta_R}\right] \quad .$$

This equation gives the angular deviation of the reconstructed beam from the reconstruction reference beam. The cosine terms are essentially constant, and in the case tested are effectively unity because of the small angles used.

The angular deviation of the reconstruction is proportional to the order of diffraction. Its magnitude is the sum of two terms, $\theta_2 - \theta_1$, which is the change in the reference beam between exposures and $\alpha_2 - \alpha_1$, the angular deviation due to the change in the subject. It is the latter term which is of importance to us because it is the one responsible for the schlieren pattern, and the one which conveys to us information about the subject change. Of importance is the fact that greater sensitivity may be possible from the observation of high orders of diffraction.

Experimental Results

Two tests have been made of the double exposure schlieren technique. The first tests, mentioned in the survey article in Appendix A, were made with the narrow angle configuration of Figure 16 using a birthday candle as subject. The rather poor result is pictured in Figure 17 of Appendix A.

Subsequent to the survey paper, a second wide angle test was made, using the test setup for the four-beam interferometer shown in Figure 2.2-6 For the double exposure schlieren tests, two of the beams were blocked, leaving only a subject and reference beam separated by a wide angle. The reference beam was offset 2° between the exposures.

The subject was a pair of resistors in a tank filled with silicone oil. The tank windows were made of thin 3/32 inch unselected window glass, which placed some reliance on the self compensation aspect of the double exposure schlieren technique. A first 1/2 second exposure was made, then

the resistors were slightly heated for 30 seconds. After another 20 second equilibration period, the second 1/2 second exposure was made.

Figure 2.5-4 shows photos made of the readout. The upper two photos have the knife edge in slightly different positions, as evidenced by the increased darkening on the left side of the resistors in the right picture. Inserting the knife edge still further blocks out the main field and leaves light only from the right side of the resistors, where it has been deflected by the heating. This is shown in the lower left figure.

For comparison, an infinite fringe double exposure holographic interferogram was made under the same heating conditions. The lower photo of Figure 2.5-4 shows this interferogram.

For this subject, the interferogram is a superior presentation; but for other subjects, e.g., subjects with sharp gradients such as shocks, the schlieren presentation may be superior.

Agfa 10E70 plate was used; tests with both light and heavy exposures showed that all had an adequate non-linlear characteristic to create the desired readout at 2° from the direct reconstruction beam. Operation at 1/2 degree offset encountered excessive low angle scattered light from the direct illumination beam. The readout was performed in a different assembly from that used to make the holograms.

These tests demonstrate the correctness of the basic principle involved in the double exposure schlieren process, and the ability to do schlieren through imperfect optics with a separate readout assembly.

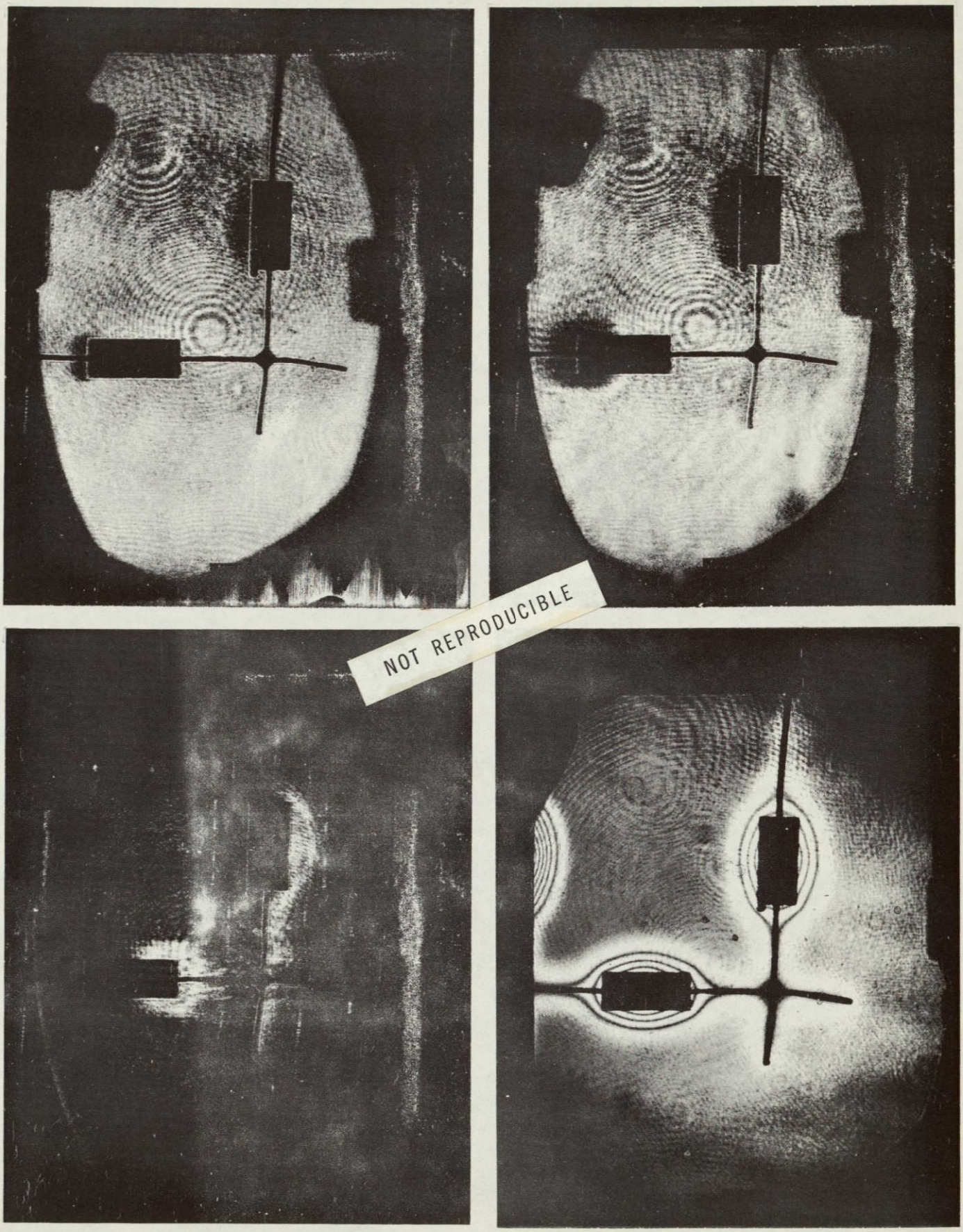

Figure 2.5-4. Double exposure schlieren of heated 8mm diameter resistors in silicone oil. Three different knife edge positions are shown in upper and lower left pictures. Lower right photo is a double exposure holographic interferogram under the same heating conditions.

3.0 COHERENCE STUDIES AND FRONT LIGHTED HOLOGRAPHY

Of great importance for the development of holographic instrumentation techniques is the improvement of laser performance so that the techniques are not limited by the laser. Because fluid flow measurements often involve the recording of high speed phenomena, the emphasis in this program has been on techniques which could use the Q-switched ruby laser as an illumination source. The ruby laser, presently the most suitable pulsed laser, is often restricted in its usefulness in holographic applications because of its limited coherence. A portion of the program, therefore, was directed toward improving the coherence of the ruby laser.

Many of the coherence matching schemes which have been so successfully employed when making holograms of rear illuminated subjects cannot be applied when making holograms of front illuminated subjects. Front illuminated holography makes much greater demands on the laser coherence, and the hologram of a front illuminated subject serves well as a diagnostic tool for measuring the laser coherence.

In the course of making front lighted holograms using a ruby laser with a mode selecting output reflector consisting of a dielectric slab (sapphire or quartz), the laser could be made to operate simultaneously at two frequencies. This resulted in a coherence function which is periodic, and a hologram made with such a laser would exhibit contour fringes superimposed on the image. Section 3.1 describes the experimental program which was carried out to study the coherence of the ruby laser, and Appendix C is a technical paper devoted to the exploitation of the two-frequency ruby laser for holographic contouring.

It is often convenient to reconstruct with a He-Ne gas laser the holograms which have been recorded with a ruby laser. The resulting image is generally accompanied by aberrations which result from the change in optical wavelength, and is of limited usefulness when good image resolution is needed. Section 3.2 describes how the recording and reconstruction geometries should be related in order to minimize image aberrations.

3.1 PULSED LASER COHERENCE STUDIES AND FRONT-LIGHTED HOLOGRAPHY

An instrumentation tool of considerable utility is the ability to make pulsed laser holographic interferograms of large front-lighted scenes. It is with this goal in mind that we have conducted a variety of experiments with the pulsed ruby laser, exploring its coherence and its ability to make front-lighted holograms and holographic interferograms. It was in the course of these experiments that the contouring technique described in Appendix C was discovered. In this section, a few examples of front-lighted holograms will be given with some comments concerning the nature of the coherence as manifested by the holograms.*

Figure 3.1-1 illustrates the performance from a very basic laser configuration. The end reflectors of the laser oscillator cavity were both single surface dielectric reflectors, so the cavity has little influence on longitudinal mode selection. In the holographic image at the path match position, the reconstruction is very bright. The width of this band is about one centimeter, which is the coherence length of the laser under these conditions. It would not have been surprising to find the holographic image absent except along this path match band. Such is not the case, however, as is evidenced by the dim reconstruction throughout the remainder of the scene. The origin of this residue of coherence throughout the scene is uncertain, but probably stems from residual reflections off the ends of the ruby and other components within the oscillator cavity.

The oscillator cavity was long, 3.35 meters, and restricted by a 7.5 mm aperture to the best portion of the ruby. Under these conditions, as will be illustrated later, the transverse coherence is essentially complete.

---

* The relation between the reconstructed intensity of a holographic image and the spectral content of the exposing laser is given in Appendix D. This relation is very important to the contouring of Appendix C and is also relevant to the studies described in this section.

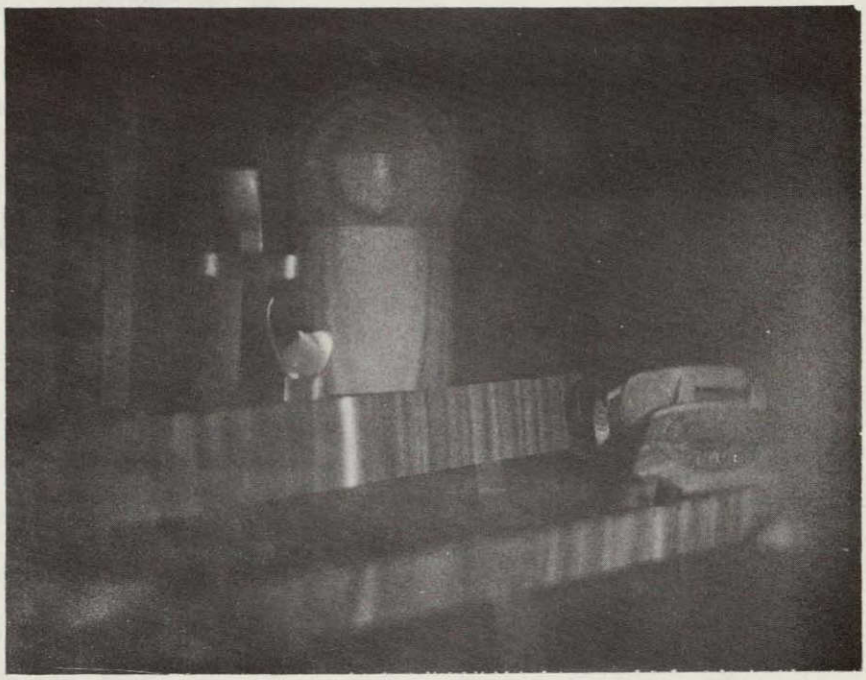

Figure 3.1-1. Photo of holographic image made with a dielectric reflector on the output end of laser cavity. Not Q-switched.

It should be noted that the limited coherence evidenced in Figure 3.1-1 is entirely adequate for transmission or silhouette-illuminated objects of arbitrary depth, when the proper path-matched arrangements are used. Many excellent holograms have been made under these conditions[5].

Figure 3.1-2 shows the effect of a simple increase in oscillator cavity complexity. For these pictures, the output reflector was a two-surface reflector consisting of a parallel slab of uncoated sapphire of 5.7 mm optical thickness. The reflectivity of such a slab varies periodically with frequency and two adjacent peaks of reflectivity will just barely fit within the lasing line width as determined from the preceding picture, Figure 3.1-1. As the line position is a function of temperature which was not controlled accurately, usually only one peak lies under the line, with the result shown in Figure 3.1-2. The band of good coherence is widened in this case because the reflectivity decreases for frequencies away from the frequency of peak reflectivity, thus restricting the lasing to a region narrower than that permitted by the dielectric reflector.

On an occasional shot, the line profile would straddle equally two adjacent peaks of reflectivity, permitting lasing at two separated frequencies. These occasional shots would produce two frequency contours as illustrated in the right photo of Figure 20 in Appendix A.

In producing holograms of the type shown, it is clear what to expect if one were to optically delay a portion of the reference beam light. Namely, for this portion of delayed reference light there would be a new path match position in the scene separated from the original path match position by the distance required to give a subject light delay equal to the inserted reference delay. Thus, the holographic image would show bright reconstructions at both path match positions.

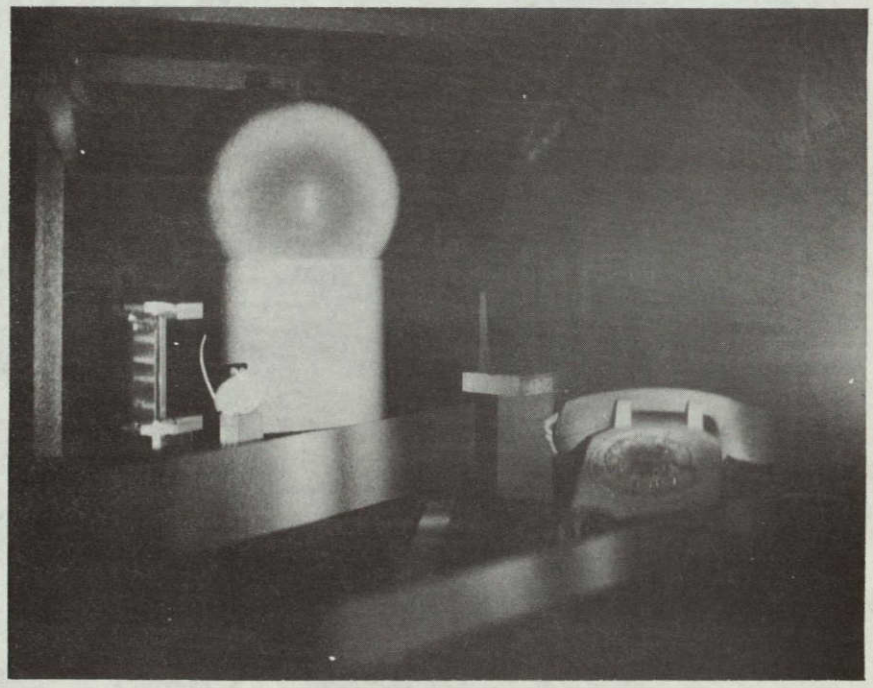

Figure 3.1-2. Typical shots with 5.7 mm optical path sapphire resonant reflector, which show no contours. Neither is Q-switched.

An easy way of introducing such a delay for a portion of the light is to insert an additional partial reflector within the laser cavity. This is not as simple as an actual external delay, but the effect is still there. In one experiment with the laser operating in a manner that produced a band of good coherence 5 cm wide at the path match position, a thin (0.5 mm) uncoated slab of sapphire was inserted into the cavity at a distance of 50 cm from one end of the cavity. As expected, holograms produced with this new configuration had a bright band in the reconstructed image 50 cm from the path match position of quality equal to the bright band at the path match position.

Figure 3.1-3 Upper is an elaboration of this idea in which three quartz reflectors were placed at random positions within the cavity at one time. The length over which a bright reconstruction occurs is enhanced. The foreground cardboard strip is about 1 meter in front of the ball. The contours apparently arise from the optical thickness, 23 mm, of the quartz reflectors, but the contours are not periodic or suitable for measurement.

By arranging two of the 23 mm thick quartz reflectors as the output reflector of the cavity, separated from each other by 23 mm, periodic contours are obtained. Figure 20, Left, of Appendix A was made with this configuration, as was Figure 3.1-3 Lower. An interesting aspect of Fig. 3.1-3 Lower is that it shows the difficulty of holding still within a fraction of a wave, even for a millisecond. The dark patch on the lower part of the neck and the upper shoulder fail to reconstruct because of motion.

The basic laser cavity itself creates additional structure to the coherence that extends for long distances. As an example, Figure 3.1-4 shows two photos from the same hologram. In the upper one, the copy camera was focused on the mouse at the path match position. In the lower one, the copy camera was focused on the "TRW" at the left edge. The TRW sign was made of glass-beaded reflective strip and had a path mismatch of 33 meters between scene beam and reference beam. The bright square above the TRW (also beaded)

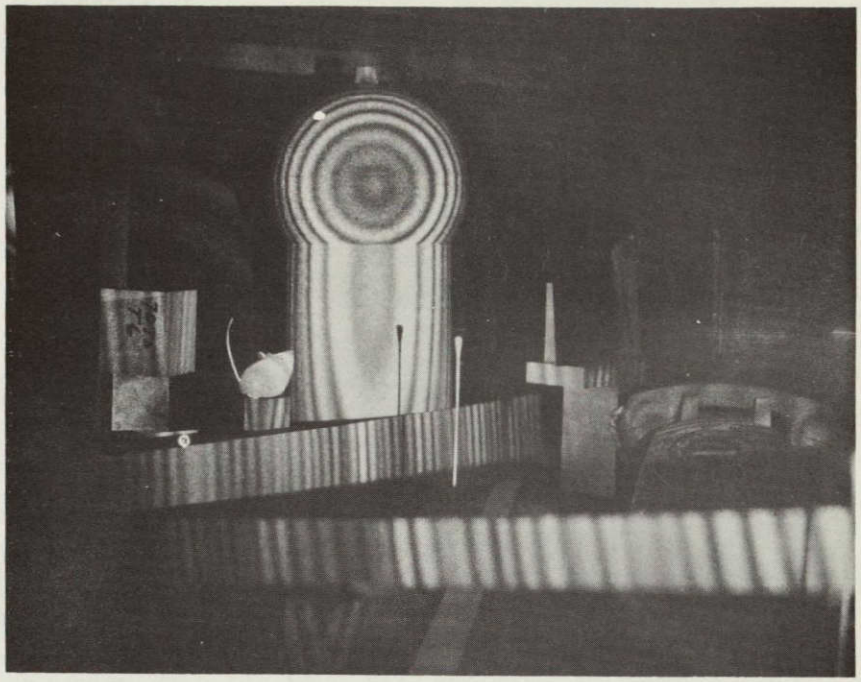

Figure 3.1-3 Upper, Q-switched shot with several reflectors within cavity showing extension of coherence and uncontrolled contours.

Lower, Headache No. 10, showing inability of a person to hold still for the 1 ms of the regular lase pulse. 23 mm contours.

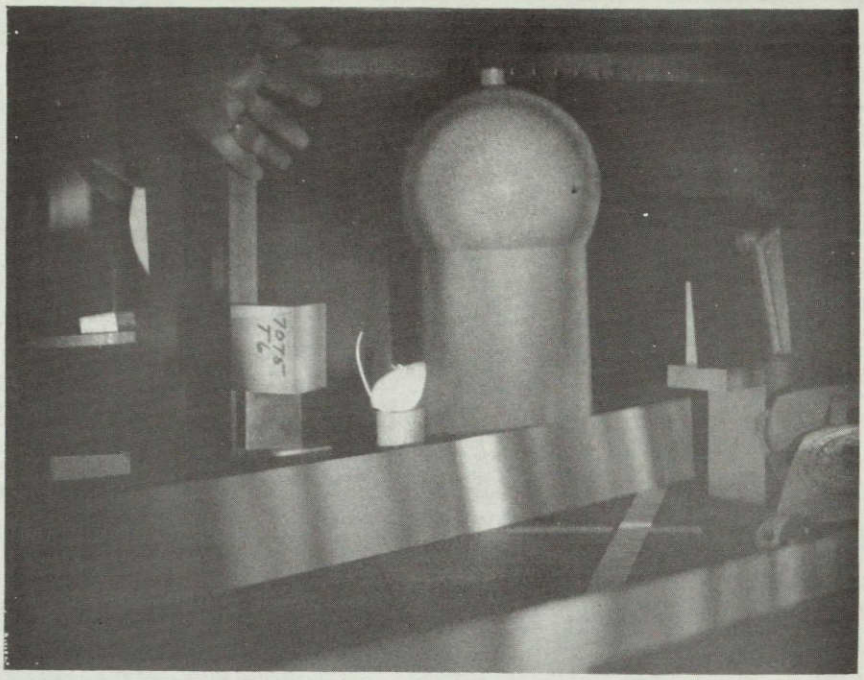

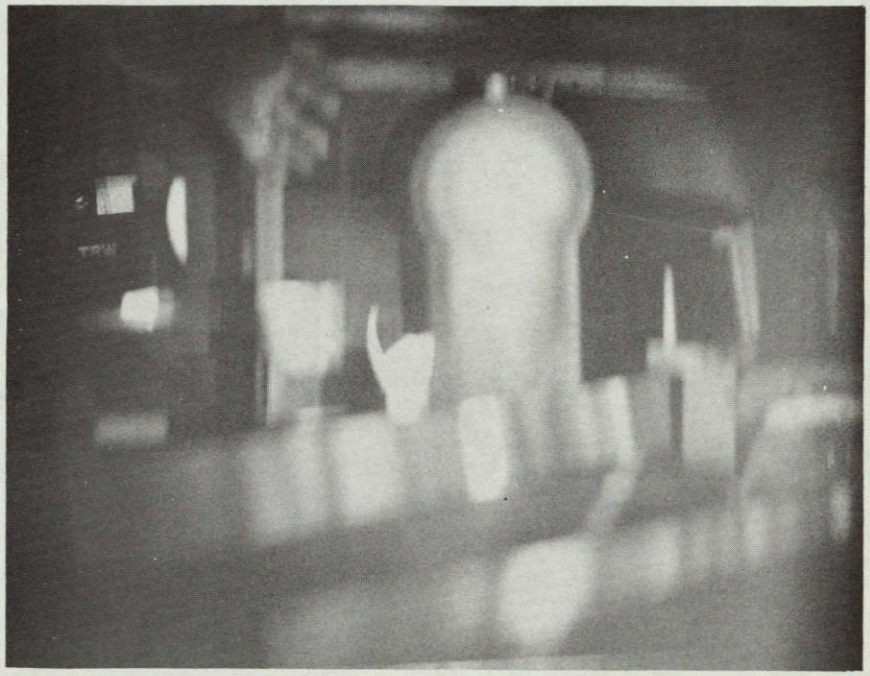

Figure 3.1-4 Two photos from the same Q-switched hologram. Upper, copy camera focused near. Lower, copy camera focused on reflective TRW sign at 33 meters path mismatch.

has a path mismatch of 15 meters. The cavity length was approximately 3.35 meters, and the 33 meter path mismatch was not adjusted to a multiple of the cavity length. The foregoing pictures and this picture in particular emphasize that a measure of the coherence at a certain path mismatch distance is inadequate to describe the complex variations of coherence that occur with pulsed lasers.

A simple technique for achieving highly coherent output from a pulsed ruby laser is to use cryptocyanine dye as a Q switch. Figure 3.1-5 illustrates operation with the dye cell Q switch which shows uniform coherence over the .75 meter deep sloping card. For such operation, it is essential that the dye concentration be carefully adjusted so that only one Q-switched pulse is produced.

Figure 3.1-6 shows dye cell operation in which two Q switched pulses were emitted, separated by about 100 microseconds. The holographic image on the left shows horizontal bands which are range contours created by the two different frequencies selected by the dye on the separate pulses. Recall that it is immaterial whether the two frequencies occur simultaneously or sequentially for multifrequency contour production. The simultaneous photographic image on the right does not show the horizontal bands because the photograph is unaffected by coherence. (Figure 3.1-6 was made without a diffuser in the subject beam so that the structure of the beam profile is visible in both pictures. The diagonal structure visible in both pictures is a property of the beam and probably arises from optical imperfections in the amplifier rod.)

Figure 23 of Appendix A shows interferograms, each made with two single dye cell pulses separated by three minute intervals. In Figure 23a the two frequencies selected by the dye were in adjacent peaks of the reflectivity of the resonant reflector, giving an average spacing the same as the contour interval of Figure 20, Right, of Appendix A. In Figure 23b the dye cell selected frequencies within the same reflectivity peak, but it is not possible to tell whether the frequencies were identical. This frequency shifting between dye cell pulses renders the interpretation of the interferograms difficult.

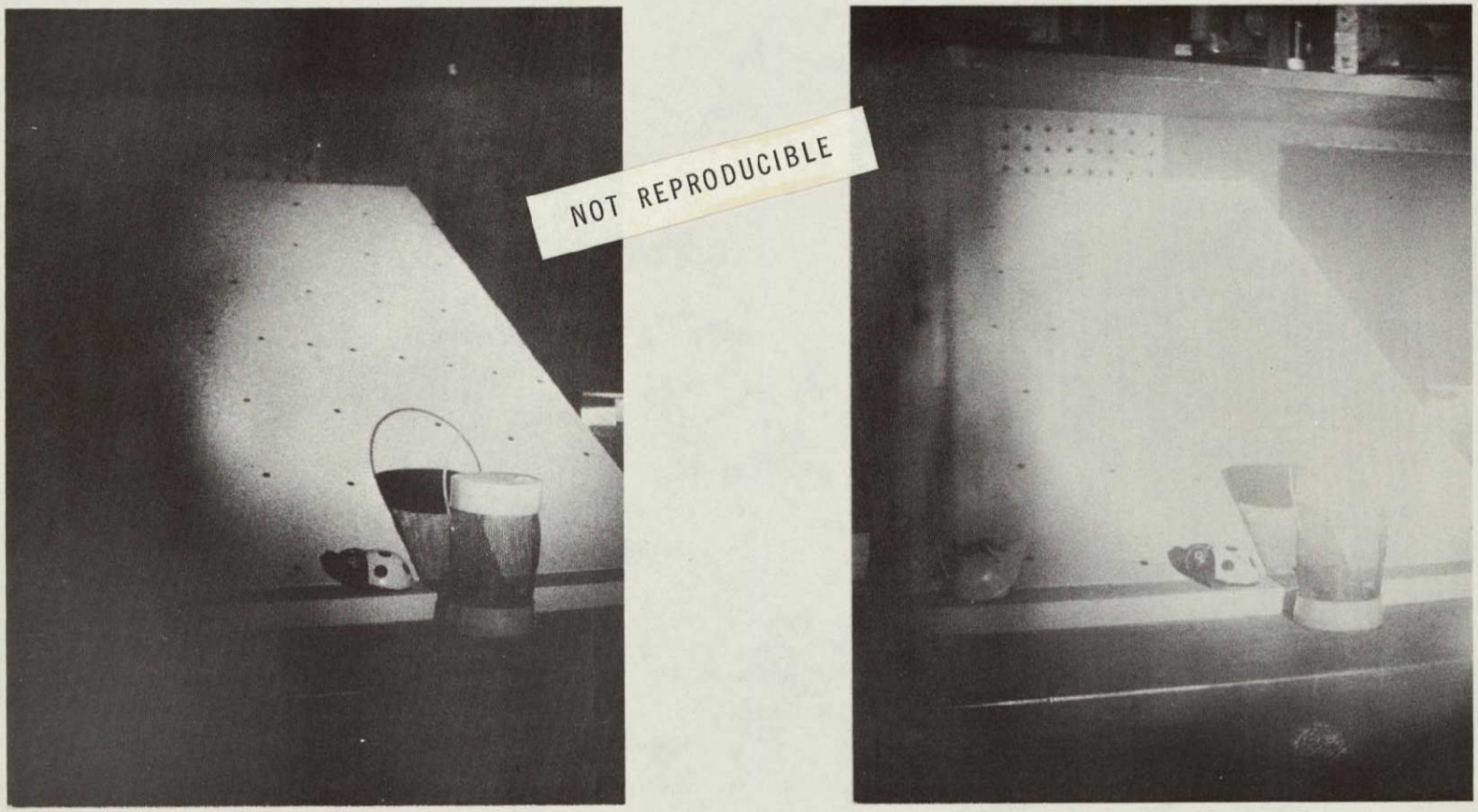

Figure 3.1-5 Photographs of a holographic image made with a single pulse from a cryptocyanine dye cell Q-switched ruby laser. The uniformity of reconstruction intensity as a function of range distance on the slanted cardboard demonstrates the temporal coherence produced by the dye cell. In the right photograph, the copy camera was overexposed in order to show the wide dynamic range of the holographic image, which recorded items on the shelf, etc., even though they were not in the principal beam.

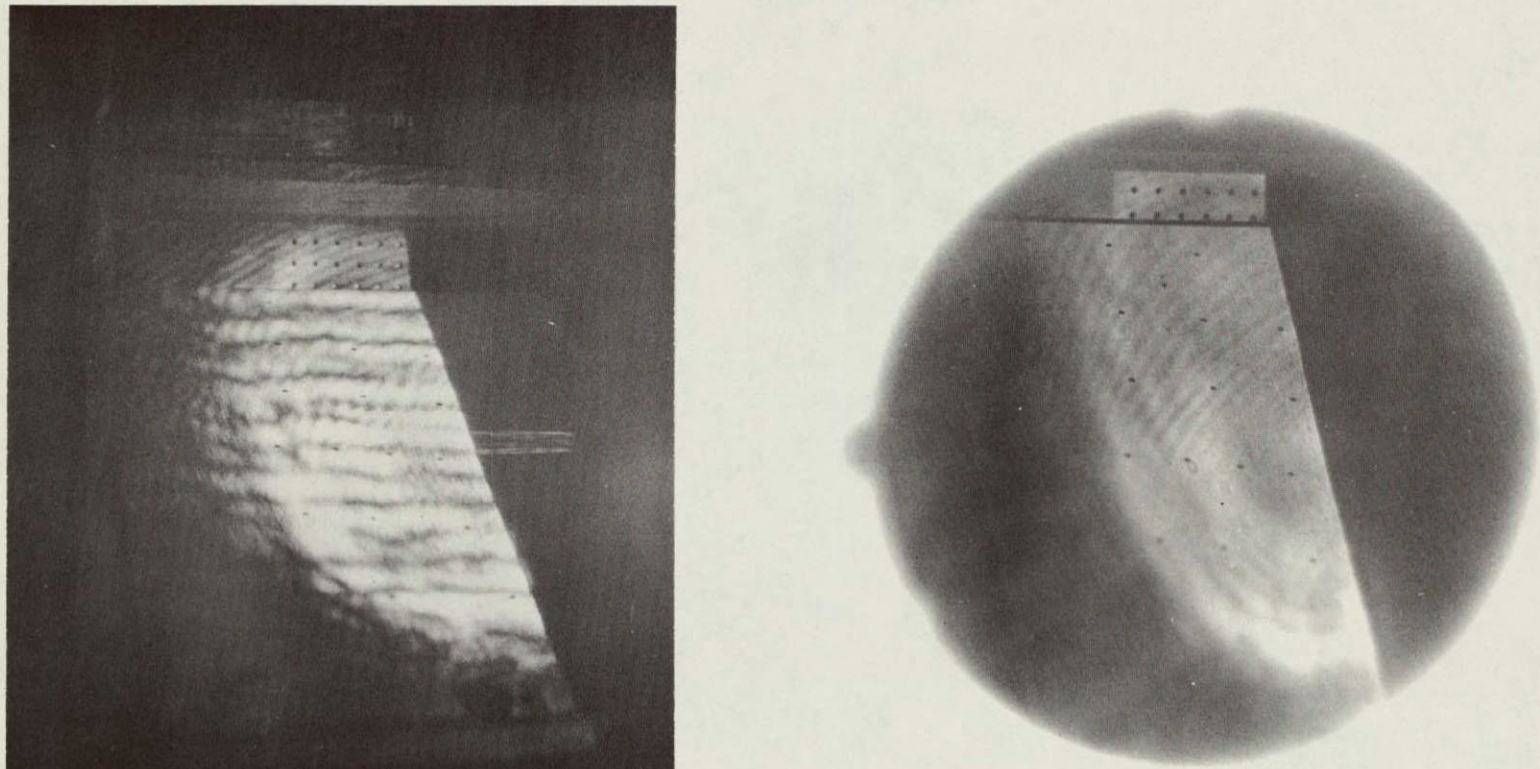

Figure 3.1-6. Simultaneous holographic image (left) and conventional photographic image (right) of laser output beam in which two Q-switched pulses were emitted, separated by about 100 microseconds. The range contours in the holographic image, which are absent in the photographic image, demonstrate that the optical frequency was different for the two pulses. Hologram, type 8E75 plate. Photograph, type 103F plate with f/2.5, 7 inch lens.

Figure 3.1-7, made with dye cell operation, illustrates that the transverse coherence is also complete. In this figure, the laser beam was diverged onto the card without a diffuser, and the reference beam was taken from the center 5% (area) of the laser beam. If, for example, one side of the beam had been incoherent with the center, then that side would have failed to reconstruct in the hologram while the simultaneous photograph would have shown light there. Thus, the absence of differences between the photograph and hologram show essentially complete transverse coherence.

While the holographic image is the ultimate tool for evaluating the coherence of a pulsed laser, the production and reconstruction of holograms is time consuming. We have found that a simple Michelson interferometer for producing fringes on polaroid film is quite useful for the rapid exploration of the effect of laser parameters on fringe quality.

The configuration is shown in Figure 3.1-8 Upper. The mirrors are 2.5 cm x 3 cm in size and are advertised as $\lambda/4$ diagonals for use in reflecting telescopes. The beam splitter is advertised as a $\lambda/4$ Herschel wedge, also for use as a diagonal in reflecting telescopes when viewing the sun. One face of the diagonal has been dielectric-coated for 50% reflectivity. The coating increases the light output of the interferometer by about a factor of three over that obtainable from the uncoated surface. Elements are held in place to the metal base block with double-backed tape. Path lengths of the two arms are made as nearly equal as possible with a millimeter rule.

The interferometer is placed directly in the output beam of the pulsed laser which has a diameter of about 1.5 cm. So far, no mirror damage has occurred. The output of the interferometer is diverged by a -20 cm focal length negative lens.

The interferometer is used as follows: After adjustment with a gas laser so as to produce fringes of about 1/2 cm spacing at a distance of 15 feet from the negative lens, a Polaroid camera back is held up in the beam in the darkened room as the laser is pulsed. After the 10 second development, the Polaroid film then reveals the fringe contrast produced by the laser.

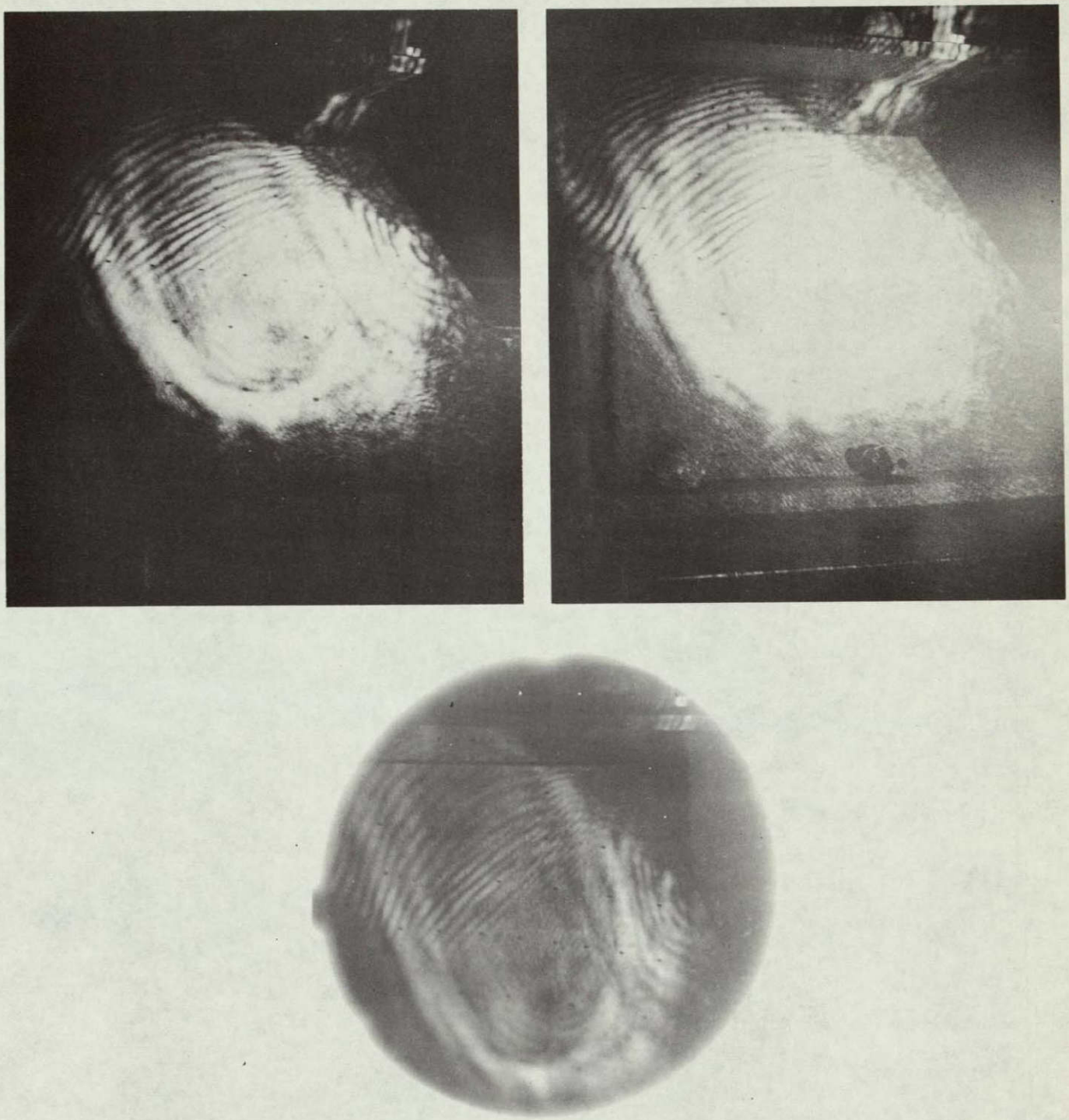

Figure 3.1-7 Simultaneous holographic images (upper), and a conventional photograph (lower) of the laser output beam diverged onto the cardboard with a negative lens. The identical patterns in hologram and photograph demonstrate the complete transverse coherence of the laser output. The structure arises primarily from imperfect amplifier rods. Upper copies are from the same hologram with different exposures of the copy camera. [A slightly different viewing angle of the photograph obscures the streak under the shelf visible in the upper part of the holographic images.] Hologram, type 8E75 plate. Photograph, type 103F plate, f/2.5, 7 inch focal length lens.

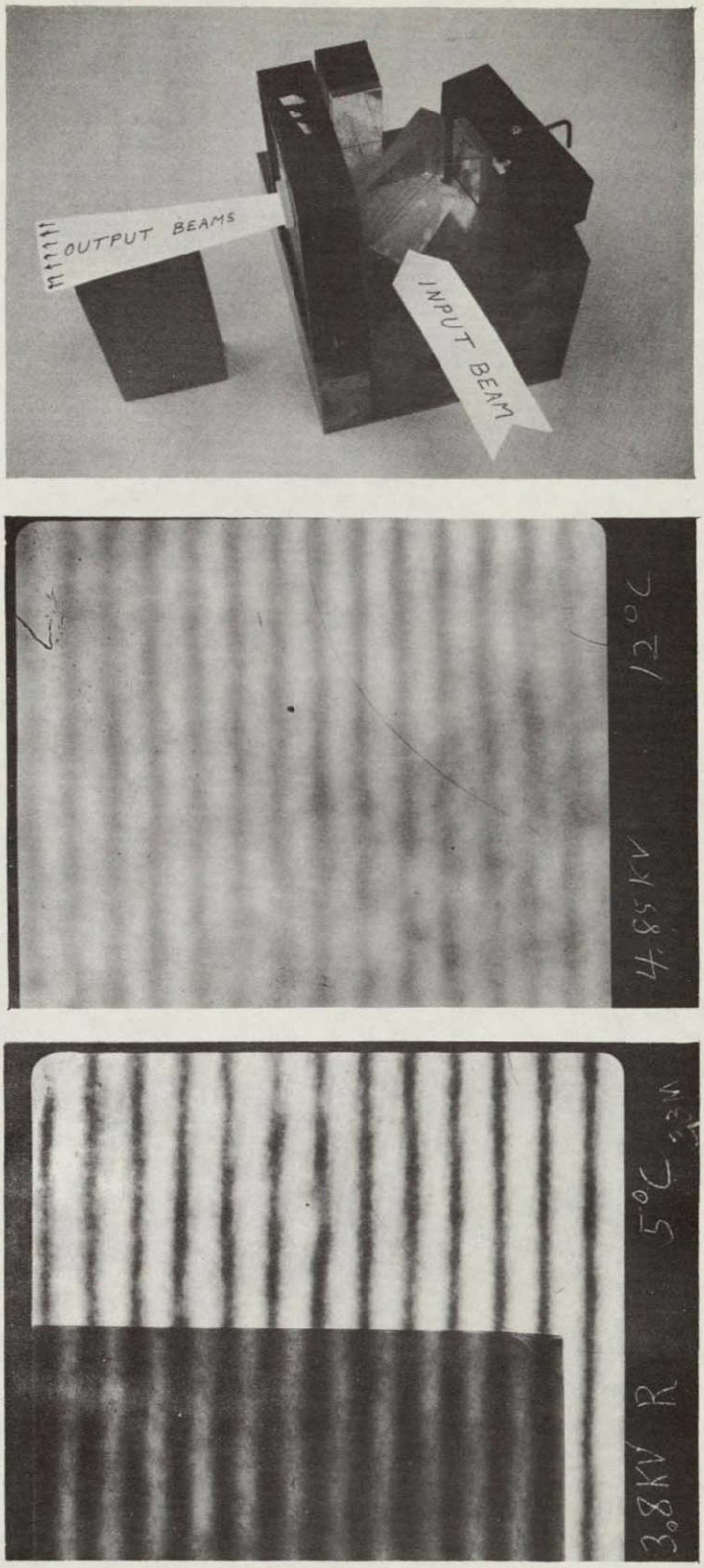

Figure 3.1-8 Upper, simple Michelson interferometer used as rapid evaluato of laser performance.

Middle and Lower, fringes produced with the instrument showin poor fringe contrast and improved fringe contrast after param optimization.

Polaroid 3000 speed film is used with a deep red filter over the input face to keep out stray light (pump light, etc.). A neutral density wratten filter over a portion of the input helps in giving greater exposure latitude and in estimating the fringe contrast obtained.

We have found this quite useful for the rapid exploration of the effect of the various laser parameters. For example, after being plagued with dingy low quality holograms for some time, we ran through a sequence of shots with the Polaroid-Michelson monitor, varying the rod temperature and the bank voltage. We quickly found the conditions which maximized the contrast of the Polaroid fringes. Then, upon taking an actual hologram with these conditions, we were delighted to find a bright high quality hologram.

The Polaroid-Michelson, of course, does not give information about the coherence length from the laser, but apparently through its transverse mismatch or residual path length errors, it has enough correlation with the fringe quality of the holograms themselves to be useful as a rapid evaluator. Poor fringe quality on the Polaroid means that the hologram quality will be poor. The converse does not seem to be a logical requirement, but so far it has worked that way: i.e., good Polaroid fringes are accompanied by good holograms.

Figure 3.1-8, Middle, shows poor quality Polaroid fringes before parameter optimizations, and Figure 3.1-8, Lower, shows the improved quality after parameter optimization. The wratten filter over the lower portion of Figure 3.1-8, Lower, is N.D. 0.7, giving an attenuation of 5, which permits an estimate of fringe visibility to be made.

3.2 REDUCTION OF IMAGE ABERRATIONS FROM HOLOGRAMS RECORDED WITH A RUBY LASER AND PLAYED BACK WITH A HELIUM-NEON LASER

It is well known and can easily be shown that a hologram image will theoretically be free of aberrations if the reference beam location and wavelength is exactly the same for both recording and reconstruction. However, in practice it is often desirable to use a different laser having a different wavelength for reconstruction. The most common example is the use of the c.w. He-Ne laser to reconstruct holograms recorded with a pulsed ruby laser. The wavelength ratio for He-Ne/ruby is 0.911 and for krypton/ruby is 0.932.

The purpose of this discussion is to point out that the aberrations induced by a change in wavelength can be eliminated (to the extent of third-order aberration analysis) by the proper location of the recording and reconstruction reference sources. A third-order analysis of hologram aberrations has been made by Champagne[6]. Based on his results, optimum recording and reconstruction geometries have been determined which, for a given object point, reduce the spherical aberration, coma, and astigmatism terms to zero.

Let $\mu = \frac{\lambda_c}{\lambda_r}$ be the ratio of the reconstruction to the recording wavelength, and let the subscripts o, r, and c refer to the object, recording reference, and reconstruction reference. Let R denote the radial distance from the center of the hologram to the object, reference, or image point, and α the angle to the hologram normal, which lies in the plane of the object and reference,

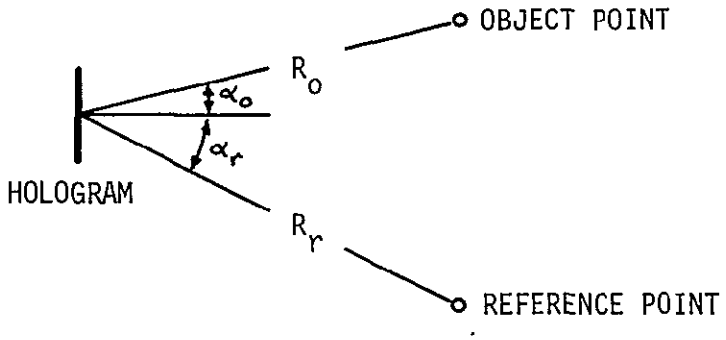

Figure 3.2-1 Hologram Recording Geometry

For a given object point, spherical aberration and coma are eliminated when $R_o = R_r = R_c$. In addition, astigmatism is eliminated when the reconstruction angle α_c satisfies

$$\sin \alpha_c = \sin \alpha_r + \frac{1 - \mu}{2} (\sin \alpha_o - \sin \alpha_r)$$

Note that $\frac{1 - \mu}{2}$ is only .045 for He-Ne/ruby so that the aberration-free reconstruction reference angle differs only slightly from the recording reference angle. In practice, the above formula need not be used, for the proper angle can easily be found by rocking the plate and observing the image. Thus, the conditions for aberration-free imaging are obtained by placing the object at the same distance as the recording and reconstruction reference sources and slightly tilting the reconstruction reference angle from the recording reference angle.

Although complete elimination of aberrations is achieved only for object points lying on the arc of radius R_r (choosing the appropriate angle α_c), small changes in the object location cause only small aberrations, and in practice there will exist a volume throughout which high resolution imaging can be achieved. This is important where a relatively small volume at a relatively long distance from the hologram must be sharply imaged.

Qualitative tests of this aberration reduction geometry have been made using a pulsed ruby laser for making the holograms and a He-Ne laser for reconstruction. Visual observations of the virtual image with long working distance magnifiers (telescopes) were convincing that the geometry offers a real improvement over similar holograms made in which no attention was paid to the above rules.

3.3 A COMPARISON OF HOLOGRAPHY AND PHOTOGRAPHY ON THE BASIS OF REQUIRED SUBJECT ILLUMINATION ENERGY

Of great importance in the practical application of holographic instrumentation techniques is the energy required of the illumination laser to obtain an acceptable hologram. This is particularly important at the present time, for the state-of-the-art of coherent lasers restricts us in a practical and economic sense to pulsed lasers with energy per pulse of the order of a few joules and with c.w. gas lasers to a few watts.

A useful way of measuring the sensitivity of the holographic process is to compare it to photography on the basis of the energy required to illuminate the subject. Our attention was first drawn to this comparison by the difficulty we had in getting conventional photographs with the same laser illumination that was producing excellent holograms. Obtaining sufficient exposure of the photograph was difficult even though an f/2.5 lens and high speed 103F film was used. This was surprising in view of the slowness of holographic emulsions and the reputation holography has of being a slow process. The holograms made with the same illumination were showing detail even in areas only dimly lit by stray illumination. In Figure 3.1-5 an attempt to show these dim regions has been made by over-exposing the camera copying the holographic image.

Goodman[7] has analyzed the relation between holographic sensitivity and photographic sensitivity in the case of diffraciton-limited imaging where the apertures of hologram and camera are equal. His basis of comparison is the number of photons required per resolution element. He finds a factor of 10 or more in favor of holography.

Our surprise here was to learn that the sensitivity of holography is comparable to that of photography in some rather conventional configurations in which holography with slow plates is compared to cameras with high speed films. The circumstance with which the present comparison is concerned is direct holography (not lens assisted) of table top or larger scenes and the comparison is on the basis of the light energy which must

be supplied to the subject for holography and photography. Resolution is not considered, it being assumed that visual inspection of the holographic image or photograph is the end use.

Photography and holography scale in different ways, and thus there is some difficulty in comparing the two. However, some comparision of the two systems under conventional conditions can be seen from simple formulas, to be derived presently, for the light energy E which must be supplied to the object in order to obtain a photograph or hologram.*

The physical arrangement is as follows:

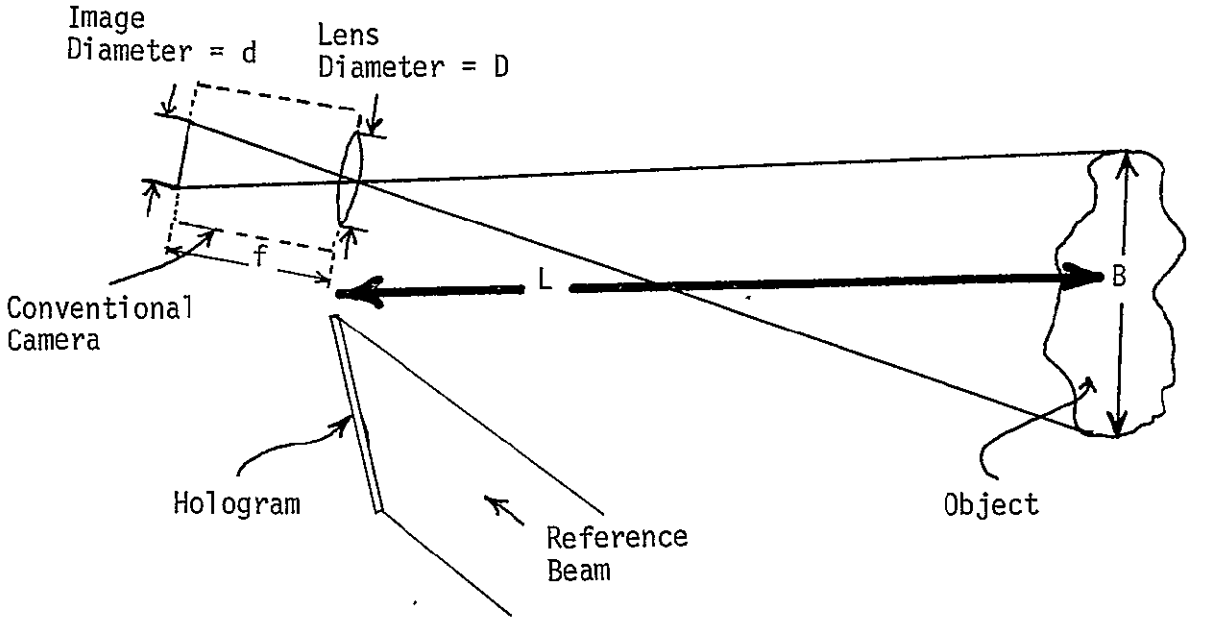

Figure 3.3-1 Holography-Photography Comparison Arrangement

* This discussion is only concerned with subject illumination energy. For scenes that are large compared to the hologram size, the reference energy is insignificant compared to the subject illumination energy.

For present purposes it is sufficient to assume that the object reflects all the incident energy uniformly into a hemisphere. Thus, the subject light energy density at the camera or hologram is $E/2\pi L^2$, and the fraction of the energy passing through the lens is $\left(E/2\pi L^2\right) \cdot \left(\frac{\pi}{4} D^2\right)$. This energy all lands in the image of diameter d and thus the <u>average</u> energy density in this image is

$$= \frac{E}{2\pi L^2} \left(\frac{\pi/4\ D^2}{\pi/4\ d^2}\right) \quad .$$

Equating this energy density to the film sensitivity S gives the following formula for the energy required to illuminate the subject in the case of photography.

$$E_{\text{photography}} = 2\pi L^2 \left(\frac{d}{D}\right)^2 S_{\text{photography}} \qquad (1)$$

An equivalent formulation of the expression (1), somewhat closer to conventional photographic thinking, is obtained by expressing the image diameter d in terms of the object diameter B through the relation $d = \frac{f}{L} B$, where f is the focal length of the camera lens. This substitution yields the following expression for the energy required to illuminate the subject:

$$E_{\text{photography}} = 2\pi B^2 \left(\frac{f}{D}\right)^2 S_{\text{photography}} \quad . \qquad (2)$$

Here $\frac{f}{D}$ is the usual f/number of the lens and the required energy is seen to be independent of distance to the object, as is familiar.

In the case of the hologram, the total energy density at the hologram is equal to the subject light energy density $E/2\pi L^2$ at the hologram plus the reference light energy density. This total is $\left(E/2\pi L^2\right)(1 + \sigma)$ where σ is the ratio of reference light to subject light. Equating this energy density to the holographic plate sensitivity gives the following

formula for the energy required to illuminate the subject in the case of holography:

$$E_{\text{holography}} = 2\pi L^2 \frac{1}{1+\sigma} S_{\text{holography}} \quad . \tag{3}$$

A comparison of photography to holography can be made by dividing Equation (2) by Equation (3) giving the ratio of energies required to illuminate the subject as:

$$\frac{E_{\text{photography}}}{E_{\text{holography}}} = \left(\frac{B}{L}\right)^2 \left(\frac{f}{D}\right)^2 (1+\sigma) \frac{S_{\text{photography}}}{S_{\text{holography}}} \quad .$$

The quantity $\left(\frac{B}{L}\right)^2$ is essentially the solid angle Ω subtended by the subject. Thus, the above formula may be written

$$\frac{E_{\text{photography}}}{E_{\text{holography}}} = (\text{f - number})^2 \, [\Omega(1+\sigma)] \frac{S_{\text{photography}}}{S_{\text{holography}}} \quad . \tag{4}$$

Three sets of experiments have been made which may be compared with this formula. The first, done while making Figures 3.1-6, 3.1-7, and similar pictures, used 103F film for the camera and 8E75 for the hologram. The lens was an f/2.5, 7 inch focal length and the pulsed laser was used. The scene reference ratio σ was 5. The energy actually required to illuminate the subject for photography was found to be 50 times that predicted by formula (4) when the manufacturer's film sensitivity data (given in Appendix E) is used. Because the ruby 6943Å line falls on the shoulder of the sensitivity curve it is suspected that the manufacturer's data may be inaccurate.

A second experiment was performed by decreasing the object size B by a factor of 7 so that a photograph could be obtained with 8E75 plate, the same as used for the hologram. The object in this case was just the

bright spot of the laser beam, diverged to about three inches diameter, incident on the card. This experiment gave agreement with formula (4) within a factor of 2. It should be noted, however, that in this case the hologram continued to show the full card by scattered light while the photograph showed nothing other than the directly illuminated spot. It is this large dynamic range that gives the hologram its superiority.

The third and most extensive set of experiments was done with a 15 mw helium-neon gas laser. The same type plates were used for both hologram and camera, were from the same box and developed in the same developer for the same length of time. Agfa type 8E70 and 10E70 were used. A number of comparisons were made with σ from 3 to 10. For many of the tests, the subject was a corroded copper teakettle, 9" in diameter, 18 inches from the hologram. For other tests, a 3" diameter white circular card was used. With the same subject illumination, the camera exposures were 40 times as long as the hologram exposures, so this introduced the possibility of reciprocity failure in the emulsion. Consequently, for holography the subject and reference beams were attenuated by 40 times so that hologram and camera exposures were the same duration. With all these refinements, good agreement was obtained with formula (4).

One aspect made clear by these tests is that one needs to expose for considerably higher densities when using photography as compared to holography. Formula (4), on the other hand, assumes equal densities. The holograms perform well with rather low density exposures. At comparable densities, the photographs are very poor and have almost no dynamic range. To obtain photographic images that are in some sense comparable to the holographic images, required at least a factor of three increase in illumination to increase the density of the photographic negatives into the useful range.

To utilize formula (4) for comparison purposes it is necessary to know the useful range of σ. To determine the useful range of the factor $(1 + \sigma)$, a sequence of gas laser holograms was made with reference beam to

subject light ratios σ from 1000:1 down to 1:1. The subject was the copper teakettle which had a rather dull diffuse appearing finish.

Reconstruction of the holograms made with ratios 1:1, 2.5:1, 5:1, and 10:1 were all superb, with side by side comparison required to detect slight differences.* At 100:1 ratio the reconstruction was still good and would definitely be classified as in the useful range. At 1000:1 the brighter parts of the teakettle were reconstructed, but the dimmer parts were lost in the scattered light from the hologram. The 1000:1 hologram would not be considered useful under most circumstances.**

Thus, in an attempt to give a numerical limit for the useful range of σ, one can somewhat conservatively choose $\sigma = 100$ as defining the useful limit for the scene tested. For this scene Ω had the value 1/4, so that the product $\Omega(1 + \sigma) \tilde{=} \Omega\sigma = 25$ at the limit of the useful range.

It is worthwhile to note that this useful limit of 25 for the product $\Omega(1 + \sigma)$ can be expected to be somewhat independent of object size. This follows, since the useful range of σ depends upon the size of the subject in the hologram. For example, if the light in the 1000:1 case had all originated at some tiny subject subtending only a small visual angle, it would easily have risen well above the hologram noise level. More specifically, if the subject solid viewing angle Ω is decreased by a factor of two, its apparent brightness increases by a factor of two for the same

---

* The reference mirror had a slight "lemon peel" finish which produces a small fluctuation of intensity in the reference beam. This may have contributed to the broadness of the region of "superb" reconstructions.

** A simple and very useful photometer for measuring low light levels can be made by using a silicon solar cell feeding a microvoltmeter (such as HP 425 A). A resistor is placed across the solar cell to keep the voltage below .1 volt to insure linearity. (Linearity can easily be checked with neutral density filters.) For the experiments described here, 600 microvolts across 1000 ohms corresponded to a 6 second exposure of 8E75.

subject illumination energy. This leads to the conclusion that the hologram noise level actually sets a bound on the product $\Omega \cdot \sigma$, for which the experiments have given the value of 25 as the observed useful limit.

Applying this limit of 25 for the product $\Omega(1 + \sigma)$, we see that formula (4) states that photography using an f/2 lens and the same emulsion as used for holography requires 100 times as much energy to illuminate the subject as does holography. This will result in equal densities for the photograph and the hologram. As mentioned before, at least a factor of three increase in energy for the photograph is required to increase the photographic density into the useful range. Thus, 300 times as much energy is required to illuminate the subject for photography with an f/2 lens as is required for holography, when the same emulsion is used.

Now from the plot in Appendix E we find that conventional high speed films such as TRI-X are about 300 times as sensitive as 10E70 and 10E75 holographic plates. Thus we conclude that the required subject illumination energy for holography is of the same order of magnitude as that required for photography, even though high speed films and f/2 lenses are used, provided the holographic scene-reference ratio is properly chosen.

For the more customary cases in pictorial holography where the scene-reference ratio is chosen to optimize the hologram quality, the subject illumination energy required for photography with an f/8 lens and high speed film is seen to be comparable to that required for holography.

We therefore conclude that the common conception of holography as a "slow" process is incorrect, and that even in the conventional case of non-diffraction-limited pictorial presentations, holography is definitely competitive with photography from the standpoint of light economics, in spite of the higher speed of photographic films.

4.0 CONCLUSIONS AND RECOMMENDATIONS

The fact that the hologram is capable of faithfully recording minute phase perturbations and that the fixed phase errors of the system can be cancelled has lead us to speculate that it should be possible to construct holographic interferometers which measure phase very much more accurately than has been previously possible. Although our aims were not fully realized, our expectations are undiminished and we are confident that further work in this area would result in improved performance of the interferometers described in this report as well as entirely new ones.

Of the schemes tried in the course of this program, the holographic multipass interferometer has yielded the best results. Good interferograms were obtained with a fringe multiplication of 10 using angular selection to discriminate in favor of the desired output beam. A hybrid system using both angular and coherence selection would appear to extend the technique to fringe multiplication of about 100, but with low light efficiency. Unfortunately, the multipass technique is hampered by reduced image resolution (due to beam walking which accompanies angular selection). The subject beam also suffers a long optical delay from the many passes it makes through the subject so that the method does not seem well suited to large, high-speed aerodynamic events.

The high order interferometer described in the first year's report depends for its success on a highly non-linear recording material and upon the production of very clean, high quality fringes by the interferometer. Such fringe quality is not easily obtained in large practical pulsed laser systems. Experimental results with gas lasers were marginally successful and it does not now seem prudent to persue this specific approach any further.

The subfringe holographic interferometer, which is simply a conventional holographic interferometer with a 180° phase shift of one of the beams between exposures, constitutes a particularly simple system providing useful qualitative presentation in the 1/10 wave region. When used with a

parallel subject beam, the system even has the convenience advantage that the holograms may be viewed with regular office lights. The control of this simple system to produce 1/100 wave sensitivity appears difficult. However, the readily compatible combination of multipass and subfringe methods is promising for obtaining 1/100 wave sensitivity.

The four-beam holographic interferometer offers the potential for detecting extremely small phase shifts. As with the subfringe interferometer, its presentation is principly qualitative with phase variations appearing as brightness variations. The full potential of the method has not yet been adequately explored and it is expected that greatly improved experimental results can be obtained with further effort.

Wide angle diffuse light interferometry is a simple, yet effective approach to obtaining more complete information about asymmetric flow fields. Work is needed to increase the angular range of the recording (presently about 60°) without undue system complication and to provide simple means for inverting the data to obtain the density distribution of the flow field.

Several methods for creating a finite fringe diffuse light interferogram in the plane of the subject have been developed and work very well. These permit fringe interpolation to 1/10 or 1/20 wave where laser speckle. is not a serious problem.

Where laser speckle may be a problem, the use of the wide angle, nondiffuse interferometer (Section 2.4) is an alternative, particularly if laser energy is at a premium. The problem facing the implementation of this system is the fabrication of phase gratings of a size comparable to the subject cross-sectional area and of uniformly high quality. A promising approach toward fabrication of the phase gratings is by recording an interference grid on a photoresist coated glass plate. Much remains to be done with this approach and it is deserving of further activity.

Real-time holographic schlieren (Section 2.5) has already proven to be quite valuable and is simple to carry out. The double exposure schlieren system has been demonstrated experimentally and the results are

typical of unrefined laser schlieren systems in which extraneous interferences clutter the presentations. The technique is especially valuable for the study of high-speed phenomena where differential measurements are desired and should be studied further to explore the limits of its performance.

A promising area which should be explored is the holographic schlieren system for use on diffuse objects. Experiments are necessary here to determine the techniques applicability to realistic engineering objects. Specifically, it needs to be determined whether the technique will tolerate the usual brightness variations which occur over the surface of a part to be tested. The technique's direct presentation of strain rather than displacement is of great practical importance.

There can be no doubt about the usefulness of the Q-switched ruby laser as an illumination source for holography, and also no doubt about the need to improve its coherence, beam uniformity, reliability, and simplicity of apparatus and its operation. Improved coherence makes possible front lighted holograms of great depth (limited ultimately by the pulse length and pulse energy) and does away with the need for constraining and complicated holographic camera arrangements. For double exposure holographic interferograms of front lighted subjects of large depth, there is the additional requirement that the laser operate at the same frequency for both pulses to avoid range contours which interfere with the interpretation of the interference fringes. The need for improved performance of the ruby laser is widely recognized as it affects not only holographic instrumentation techniques, but much of the future of holography and coherent optical applications.

Out of this program has come a greater understanding of the special problems associated with the use of the ruby laser for holography and of the techniques to improve its performance. A continuation of this work is a task of considerable importance

One of the most important results of the coherence studies has been the discovery of the pulsed ruby, two frequency contouring technique

(Appendix C). The present experiments have demonstrated contouring with 1 cm and longer contour intervals. Preliminary experiments have indicated how the technique can be extended to produce pulsed ruby contours down to about 1/2 mm. A promising application for this technique is the testing of parabolic antennas. By dusting the antenna with a powder of retroreflective glass beads even large antennas could be done with lasers of a joule output. By testing from the center of curvature (not the focus) the range contours show only departures from the sphere of best fit, simplying the data handling.

Acknowledgement

The authors wish to acknowledge the contribution of R. F. Wuerker in this program. Not only has he been of continuous value in discussions throughout the program but specifically the research of Sections 2.3 and 3.1 were performed jointly with Dr. Wuerker. Dr. Wuerker's participation in the work described in Sections 2.3 and 3.1 was supported by Air Force Contract F33615-68-C-1119.

HOLOGRAPHIC INSTRUMENTATION STUDIES

L. O. Heflinger
R. E. Brooks
Physical Electronics Laboratory
TRW Systems Group

ABSTRACT

This program* is an investigation of holographic techniques applicable to NASA's instrumentation needs. A number of interferometric and schlieren systems have been devised, analyzed, and tested in the quest for a system sensitive enough to enable flow visualization at re-entry simulation pressures. Some of the systems explored, such as sub-fringe interferometry, high order interferometry, multi-pass interferometry, and double exposure schlieren are described.

Techniques for improving the usefulness of pulsed ruby lasers for front-lighted holography and interferometry have been developed. The production of pulsed ruby holographic contour maps has been achieved by two-frequency operation of the pulsed ruby laser and is briefly described.

INTRODUCTION

The first portion of this paper reviews a number of experiments which were performed in the quest for a system which would make visible aerodynamic flows in very low density gases, such as those used for re-entry simulation. The magnitude of the optical perturbations created by such flows is less than 1/100 of a wave. A system capable of such performance has not yet been found, but several systems will be described which have been explored in the attempt to find a system or combination of systems capable of such performance. Combinations of systems have not been experimentally explored, but the reader will observe that some of the techniques are compatible in principle with others, yielding the possibility that a combination system could yield a gain in sensitivity equal to the product of the sensitivity increases achieved by each individual system.

In addition to the quest for increased sensitivity, a number of experiments have been performed relating to the use of pulsed lasers for front lighted holography and holographic interferometry. One promising outcome of these experiments is a technique for producing contour maps via front lighted pulsed ruby laser holograms. A brief description of these experiments is given in the later portion of this paper.

---

* Contract NAS2-4992, Sponsored by NASA Ames Research Center.

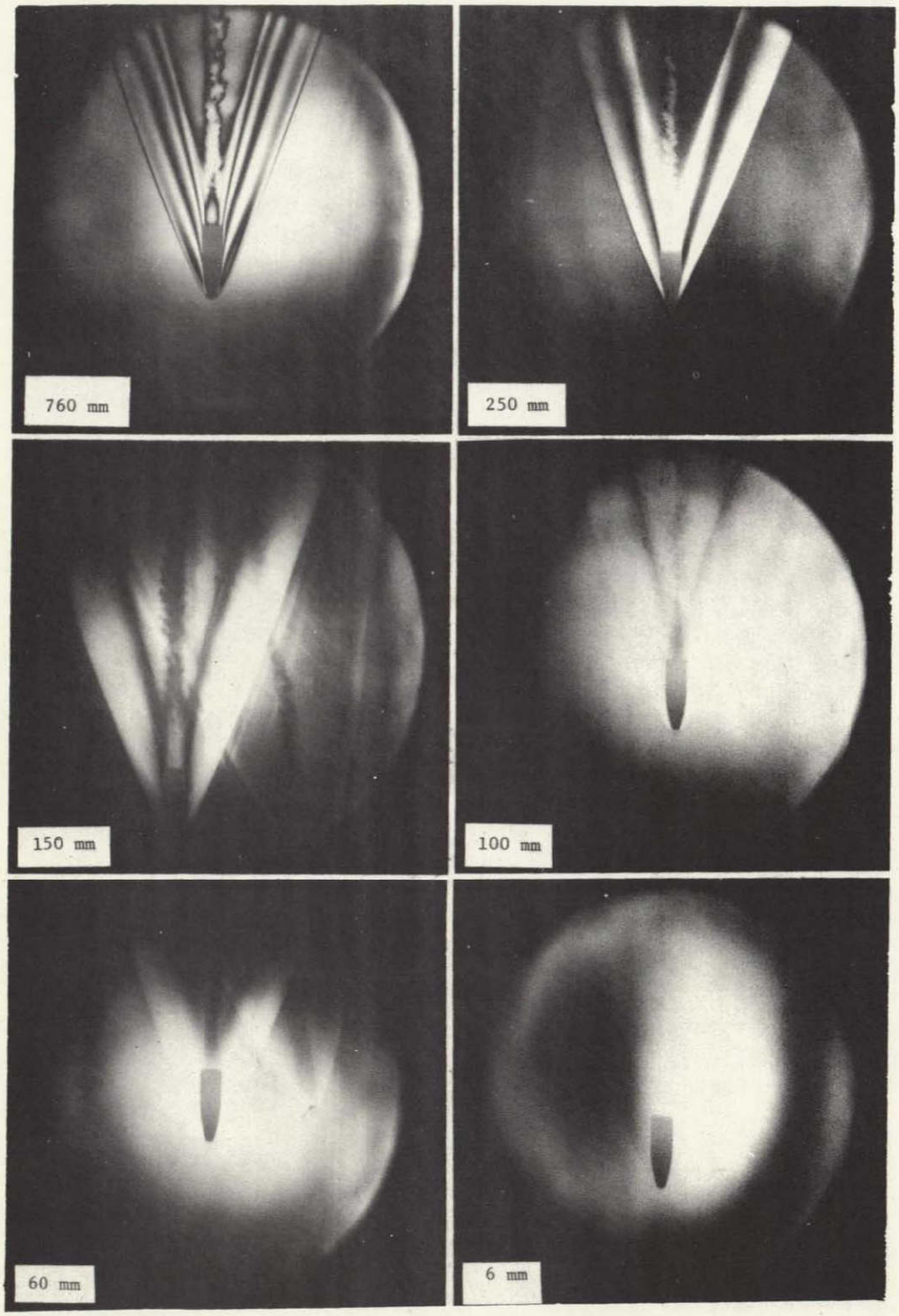

Figure 1 Double exposure holographic interferograms at various chamber pressures.

PART I. FLOW VISUALIZATION TECHNIQUES

Restrictions Set By The Intended Application

The goal of visualizing aerodynamic flows where the optical phase perturbation is less than 1/100 of a wave, together with the goal that a useful system be applicable to large test facilities, restricts the search to those systems which are self-compensating. By this it is meant that we shall ignore systems which require 1/100 wave flatness of the windows and optical components, and shall consider only systems which somehow have a built-in insensitivity to window imperfections, etc. However, this does not exclude systems which require conventional high quality optics such as 1/4 wave windows.

One of the most favorable applications for high sensitivity systems is the ballistic range. This application permits double exposures to be made with only 100 microseconds separation, thus eliminating many problems of stability and vibration. The addition of counterflow to the ballistic range complicates the problem with a turbulent boundary layer at the windows. A technique for circumventing this turbulence will be described. The most difficult application is to the steady state wind tunnels where vibration poses a major problem. To obtain full self-compensation in such applications probably requires the ability to make adjustments during the readout process which compensate for the vibrational displacements which occurred during the sampling exposures.

Figure 1 illustrates the need for high sensitivity systems as the operating pressures are reduced. In Figure 1 are shown straightforward double exposure holographic interferograms of a Mach 3 bullet in flight with various operating pressures in the flight chamber. The first picture shows operation at atmospheric pressure where an adequate number of fringes are available for even quantitative flow analysis. As the pressure is reduced, the number of fringes diminish until in the 6 mm Hg shot only a faint residual of a portion of the shock front is visible. The desired region of operation for certain simulations is nearly two orders of magnitude below the 6 mm shot. Thus, great gains in sensitivity over standard holographic interferometry are required.

Is Holography Capable of 1/100 Wave Fidelity?

A basic question is whether holography is capable of reproducing waves with 1/100 wave accuracy. It is obvious from stored beam or live fringe holographic interferometry that a hologram is capable of fractional wavelength accuracy. We describe next a simple experiment which illustrates local wave fidelity far in excess of 1/100 wave in the reproduction of optical waves by a hologram.

Consider as subject for a hologram two points A and B. Point B will be very dim compared to A and is displaced from A by a small angle. A reference beam is tacitly assumed.

If one represents the electric field at the hologram from the point A by the phasor a and that from B by b in the figure, then the total subject field at the hologram is represented by the vector sum of these. Because of the small angular difference between points A and B, the small phasor b rotates slowly relative to a as one moves across the hologram, the resultant oscillating slightly in phase and amplitude relative to a. The magnitude of this phase perturbation caused by the point B is $\sqrt{\frac{I_B}{I_A}}$ radians & the relative fluctuation in amplitude is $\sqrt{\frac{I_B}{I_A}}$

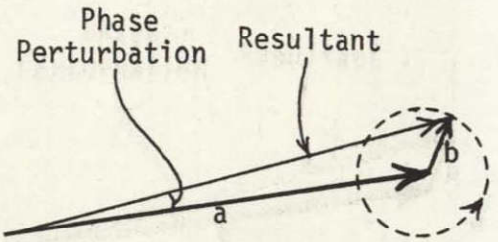

Detailed consideration of the experimental results leads to the conclusion that the phase perturbation is at least as significant as the amplitude perturbation in forming the reconstructed image. Thus the reconstructed image of point B is evidence of the holograms ability to detect phases of $\sqrt{\frac{I_B}{I_A}}$ radians. Holograms were made with various intensity ratios between the two subject points B and A. Upon reconstruction the point B was still visible when its intensity was 10^{-6} that of point A, for which the corresponding amplitude of the phase modulation was only 1/6000 of a wave. When the intensity of B was 10^{-7} that of A, its reconstruction was not visible to the unaided eye but could be made visible by the use of a telescope which increases the area of the hologram sampled.

We conclude from this simple experiment that holograms are easily capable of detecting 1/100 wave phase shift information when the information is appropriately presented, and when the sampling area is as large as the observer's eye pupil.*

---

* This experiment is also of interest in that it shows the dynamic range of hologram recording. The limit of 10^{-6} was the same whether subject A was a point source or a sizeable ground glass. Note that the reconstruction output is not necessarily linear over this entire range.

Sub-Fringe Interferometry

The principle of sub-fringe interferometry is simply to shift the phase of the subject beam 180 degrees between the exposures of a regular double exposed holographic interferogram.** Since the reconstruction reproduces the algebraic sum of the two exposing waves, the reconstruction should be a completely dark field except where the subject perturbation has upset the exact 180 degree relation. Thus, small subject perturbations make themselves visible as brightenings on the dark background.

The 6 mm shot of Figure 1 is a sort of accidental sub-fringe interferogram in that some extraneous air current or motion created a near 180 degree phase shift in the portion of the scene where the shock is faintly visible.

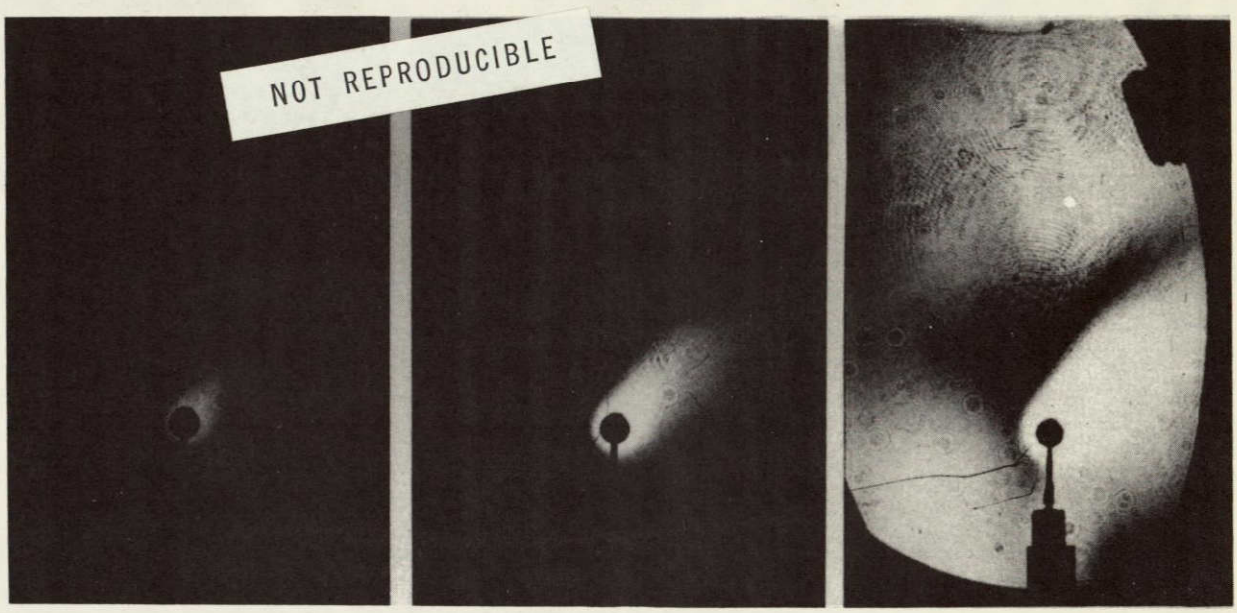

Figure 2 Sub-fringe interferogram of air surrounding a heated resistor. Path change at resistor is 1/3 wavelength and copy exposures of 1, 5, and 20 seconds show range of brightness of the holographic image.

Figure 2 is an example of sub-fringe interferometry. The subject is a heated resistor which creates a 1/3 wave change in optical path length in the air adjacent to the resistor. In the copy photographs, three different exposures were used to show the brightness range in the holographic reconstruction. It is estimated that perturbations at least as small as 1/10 wave are visible.

** Detailed analysis shows that a phase shift slightly different from 180 degrees produces maximum sensitivity, but this refinement will not be included here.

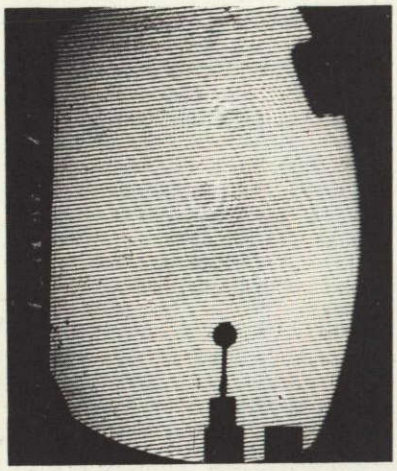

Figure 3 Finite fringe holographic interferogram of heated resistor.

Figure 4 Sub-fringe interferogram of same heated resistor with slightly different background phase shift. Copy exposures are in ratio 1:4.

For comparison, Figure 3 shows the same subject viewed by a finite fringe holographic interferogram. Examination shows 1/3 of a wave shift at the resistor.

Figure 4 shows another sub-fringe interferogram taken under nominally the same conditions. This photo shows two properties of sub-fringe interferometry of significance. The first is the sharpness in terms of phase of the black interference fringe. The phase shift required to move from one side of the fringe to the other is less than 1/6 of a wave. This narrowing of the dark null stems from the high contrast of the holographic recording medium. A truly linear film characteristic would exhibit a broader null. This is a desirable effect, for it increases the phase sensitivity of sub-fringe interferometry. This null sharpening effect is expected to occur only when no diffuser is used in the subject beam, as is the case in the above pictures.

The second property shown by Figure 4 is the experimental difficulty of obtaining precise 180 degree phase shifts. The ultimate sensitivity of the system can be no better than the precision of the 180 degree phase shift. Moreover, nearly precise equality of the two exposures is also required for high sensitivity. This later requirement is particularly difficult to satisfy with pulsed lasers. Figures 2, 3, and 4 were made with a gas laser where exposure equality is easy to achieve but vibration and air currents make the phase shift uncertain.

Figure 5 shows another instructive and useful property of sub-fringe interferograms made without a diffusing screen; in this case, subject and reference were both collimated beams. Such a sub-fringe interferogram is essentially a diffraction grating wherever the subject phase shift has upset the 180 degree conditions. Where the subject is absent, the exposure is a uniform grey and thus does not diffract. Thus, simply by holding the hologram so it diffracts light from the overhead white lights, as shown in Figure 5, one may observe the subject phase shifts.

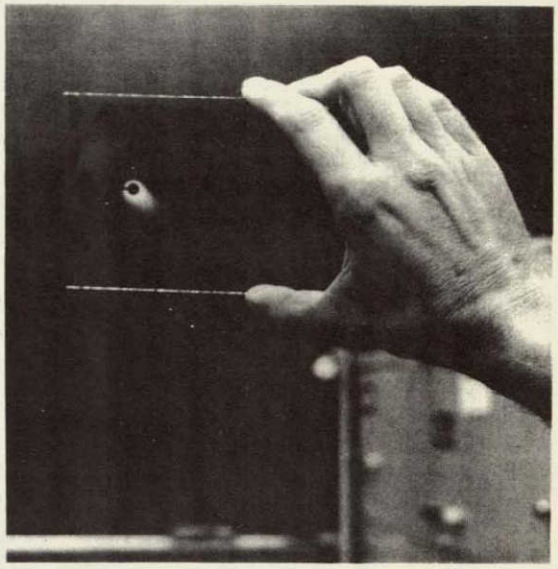

Figure 5 Readout of sub-fringe interferogram with overhead white lights.

Four-Beam Interferometry

An interferometer has been devised which theoretically reduces the 180 degree phase shift and exposure equality requirements to second order effects. By eliminating the precision required of these settings, the interferometer should be capable of more sensitive performance than the sub-fringe interferometer. The readout presentation appears similar to that of sub-fringe interferometry, namely, a dark field with brightening where subject phase shift exists.

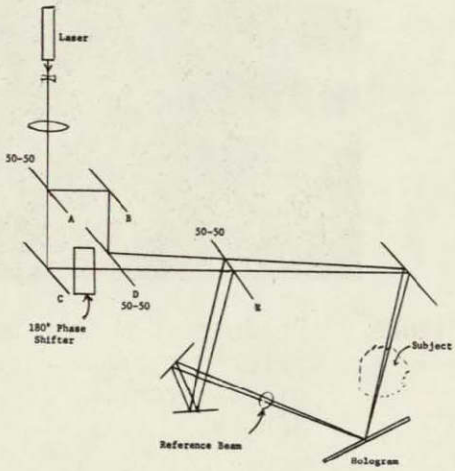

Figure 6 Four beam interferometer.

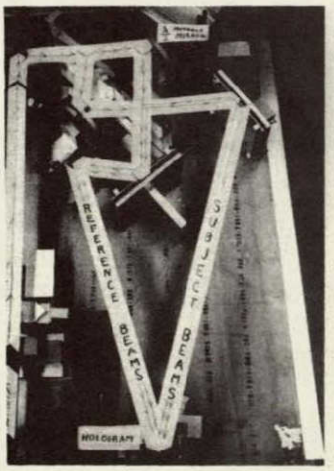

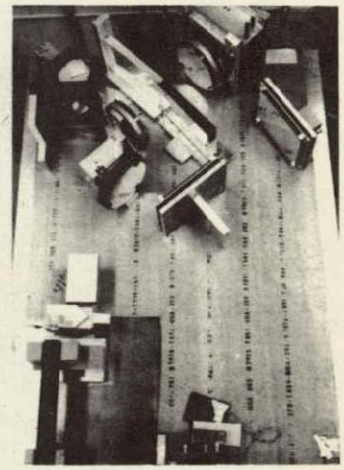

Figure 7 Test setup for four beam interferometer.

This four-beam interferometer is shown in Figure 6. It consists essentially of subject and reference beams separated by a large angle. Both subject and reference beams are each composed of two beams, separated by the same small angle. At the hologram on the first exposure, these four beams produce a grating of fine fringes, intensity-modulated at a low spatial frequency corresponding to the small angle. On the second exposure in absence of a subject perturbation, a similar pattern of fine fringes is produced, but due to the 180 degree phase shift, the low frequency intensity modulation is complementary to the intensity pattern of the first exposure in the sense that $\cos^2$ is complementary to $\sin^2$. Thus, in absence of a subject perturbation, the two exposures result in nothing more than a uniformly exposed ($\sin^2 + \cos^2 = 1$) high frequency grating.

However, in regions where the subject perturbation has disturbed the phase on the second exposure, the resulting high frequency grating produced by the two exposures will be phase-modulated at the low spatial frequency with the peak-to-peak amplitude of the phase modulation equal to the subject phase perturbation. The intensity of the grating is still uniform.

To readout the resulting hologram, it is illuminated with a single beam. The high frequency grating strongly diffracts light into what we shall call the primary order. Where the subject has introduced the phase modulation, side orders of diffracted light will appear at the small angle away from the primary order. The light of one of these side orders is selected by an aperture and constitutes the viewing light.

Figure 7 shows the experimental assembly with 6" diameter optics, used to test the concept and Figure 8 shows the readout of one of the holograms. The subject is again the heated resistor, but this time the perturbation at the surface of the resistor is only 1/6 of a wave. While the 1/6 wave is easily visible, this is far short of what we ultimately expect of the system.

Figure 8 Readout of a four-beam interferogram. Phase shift of resistor is 1/6 wavelength.

The reader will note the similarity between the structure of the hologram in this four-beam interferometer and the structure of the hologram in the tests used to see if holograms were basically capable of 1/100 wave sensitivity. Those tests were performed so as to bear a close relation to the four-beam interferometer and hence show the potential performance of the four-beam interferometer when all of the practical problems are conquered. Readout of the sensitivity test holograms in the configuration of the four-beam readout, yielded the same limits mentioned in the direct viewing tests above.

One practical problem evident in Firgure 8 is imperfect optics and alignment which create the horizontal banding. In the absence of alignment to

within 1/8 wave or so, it can be shown that the four-beam arrangement is not superior to the sub-fringe arrangement. Present optics do not permit such alignment.

Doubled Ruby Holographic Interferograms

A technique yielding a factor of two gain in sensitivity is simply to shorten the wavelength of light by running the output of the pulsed ruby laser through a doubling crystal.* Figure 9 shows an interferogram made in this way. An interesting property is that by letting both the direct and doubled light fall on the hologram, two interferograms are simultaneously obtained--one red and one in the near ultraviolet. These can be read out individually from the hologram. This technique may have applicability to the study of dispersive media.

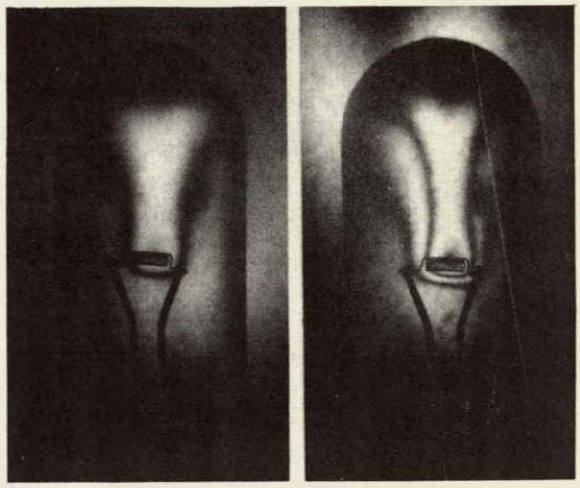

Figure 9 Simultaneous red and ultraviolet interferograms of heated filling gas of a lamp.

Multipass Holographic Interferometer

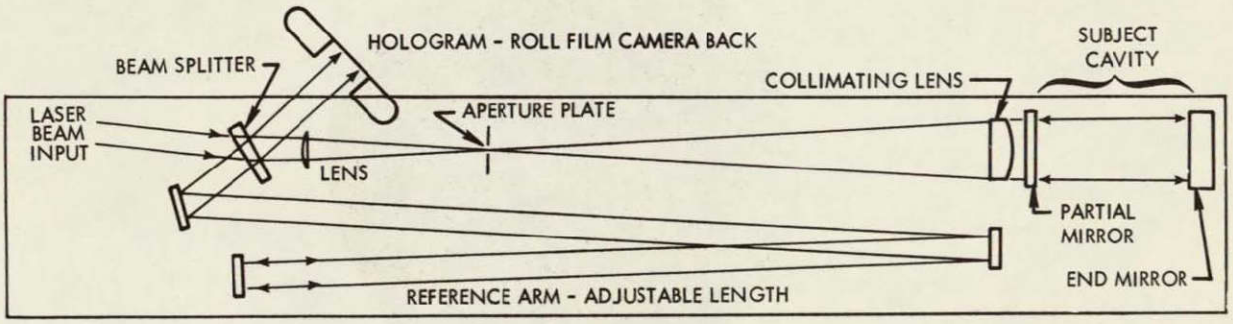

Figure 10 Multipass holographic interferometer.

---

* A more complete description has been published in: R. F. Wuerker, L. O. Heflinger, and R. A. Briones, "Holographic Interferometry with Ultraviolet Light," May 1, 1968, Applied Physics Letters, 12, No. 9 pp. 302-3.

Figure 10 shows a multipass holographic interferometer. To understand the operation of this interferometer begin with the subject light passing to the right through the small lens. This subject arm light is first brought to focus by the small lens, passes through the aperture and is recollimated by the larger lens. The light then passes into the subject cavity through the partial mirror where it undergoes many reflections and many passes through the subject. Upon each reflection at the partial mirror, a fraction exits the cavity and is brought to a focus by the larger lens at the aperture plate. However, because there is a small angle between the partial mirror and the end mirror these focus spots are displaced at the aperture plate. The arrangement is adjusted so that as the pass number increases the spots first move further away from the entrance aperture, then they turn around and move closer to the entrance aperture with a selected pass number, and only that one, falling back through the aperture. This selected pass is then recollimated by the small lens and used as the subject beam for a double exposure holographic interferogram. In the arrangement shown the reference beam for the hologram is displaced at a very small angle from the subject beam which permits the use of high speed films to compensate for the small fraction of light returning from the selected pass. The beam splitter and reference arm mirrors achieve this small reference angle conveniently.

Note that because this is really a double exposure holographic interferometer it has self compensation for imperfect optics. The optical quality is dictated by the requirement that only the desired pass fall through the aperture which still sets fair demands on quality. Figure 11 shows the quality of the optics used in the experiment. The photograph was made with 20 passes by adjusting the reference arm for zero offset.

Figure 11 Interferogram showing optical quality of multipass interferometer.

Figure 12 shows the heated resistor at different temperature rises with 10 passes. A finger is shown in (f) and finite fringe presentations at 10 passes are shown in (g) and (h).

The ultimate sensitivity of this technique is related to the required resolution at the subject because the beam walks sideways as it passes back and forth between the mirrors.

Another scheme utilizing coherence sorting rather than spatial sorting of the desired pass has been devised which does not suffer this resolution restriction. This later scheme has not been tested.

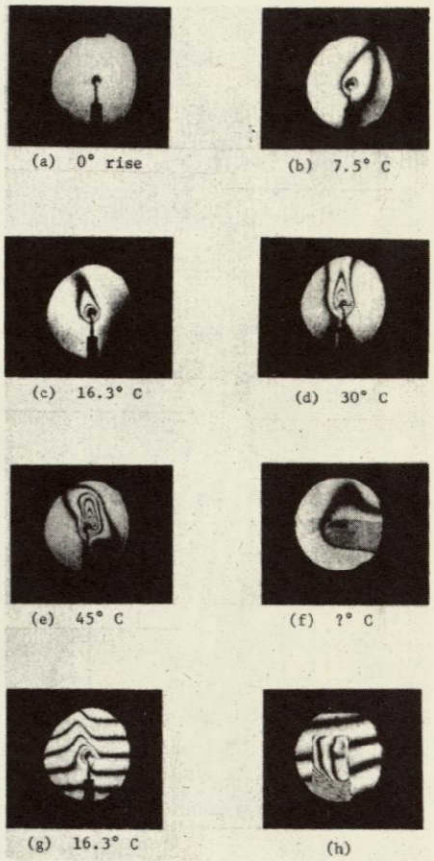

Figure 12 Examples of 10 pass operation of multipass interferometer.

High Order Interferometry

Still another approach to increased phase sensitivity utilizes the fact that readout of a hologram in the nth order yields n times the phase sensitivity of first order readout.

Figure 13 illustrates the basic principle. For example if a 1/10 wave phase shift occured during exposure the position of the fringe lines will be shifted by 1/10 d. Readout in the first order shown in (a) will yield just a 1/10 wave shift in the readout wave whereas readout in the nth order shown in (b) will have a phase shift of n · 1/10 wave.

In order to use this principle in a self compensating system so that perfect optics are not required, the following scheme has been devised and tried. The arrangement

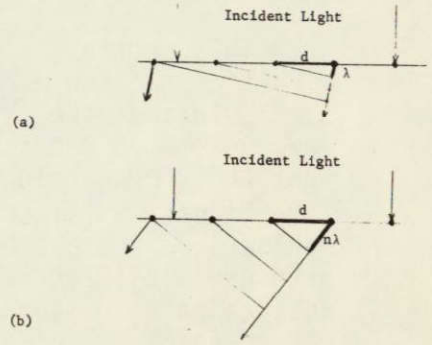

Figure 13 Principle of high order interferometry.

consists of equal strength collimated subject and reference beams impinging on the hologram at a very small angle. A first hologram is made of the empty scene with a very heavy exposure. Thus the developed hologram consists of a grating of very narrow clear lines at the nulls of the interference pattern. A second hologram is made on a second photographic plate with the subject present. A kinematic jig is used to secure reproducibility of plate positions. A double exposed contact print is made with one exposure from each of the developed holograms. The contact print is then illuminated with a collimated beam and read out in the nth order.

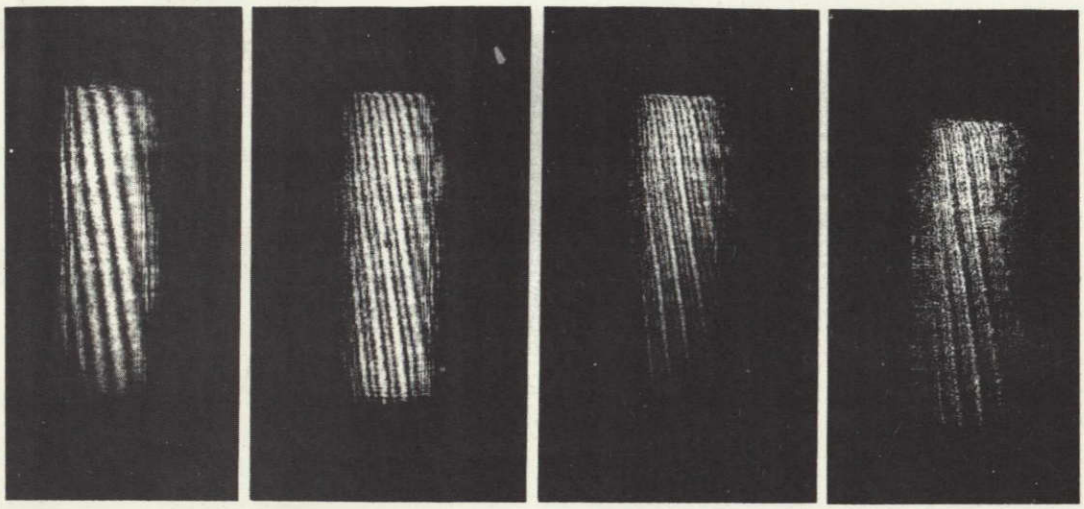

Figure 14 Readout of high order interferogram in orders one through four.

Figure 14 shows the result in which the subject is a wedge that entirely fills the scene. Readouts of first through fourth order show the expected increase in the number of fringe lines.

The results are not particularly encouraging. While in accompanying experiments light has been detected at the 100th order of special holographic gratings, the complexities of the process and the strong dependence on non linear emulsion properties (Kodalith plate was used) have been discouraging in the attempt to actually use very high orders.

Double Exposure Holographic Schlieren

This section, together with the following two sections, have a less direct connection with the quest for high sensitivity than the foregoing sections, in that they struggle with some of the practical instrumentation problems. Some of the concepts described here have direct applicability aside from their connection to the sensitivity problem.

Figure 15 illustrates a technique for double exposure holographic schlieren which has been devised and given a cursory test. This double exposure schlieren is self compensating for optical imperfections in the subject path in contrast to the more familiar single exposure holographic recording of a schlieren output beam. Like the latter, the double exposure

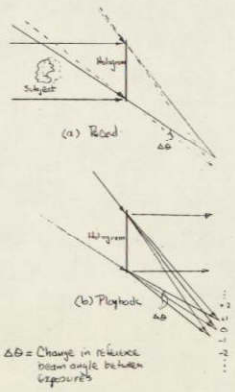

Figure 15 Process of double exposure schlieren.

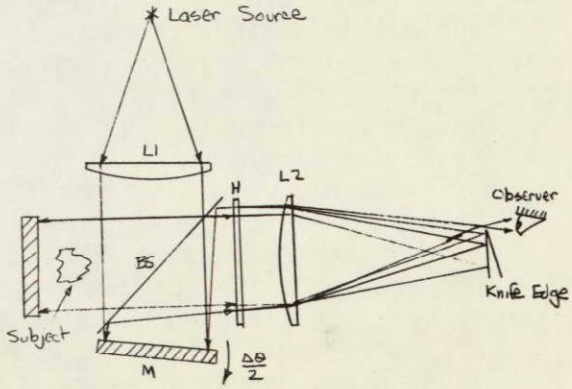

Figure 16 Configuration used for low angle double exposure schlieren tests.

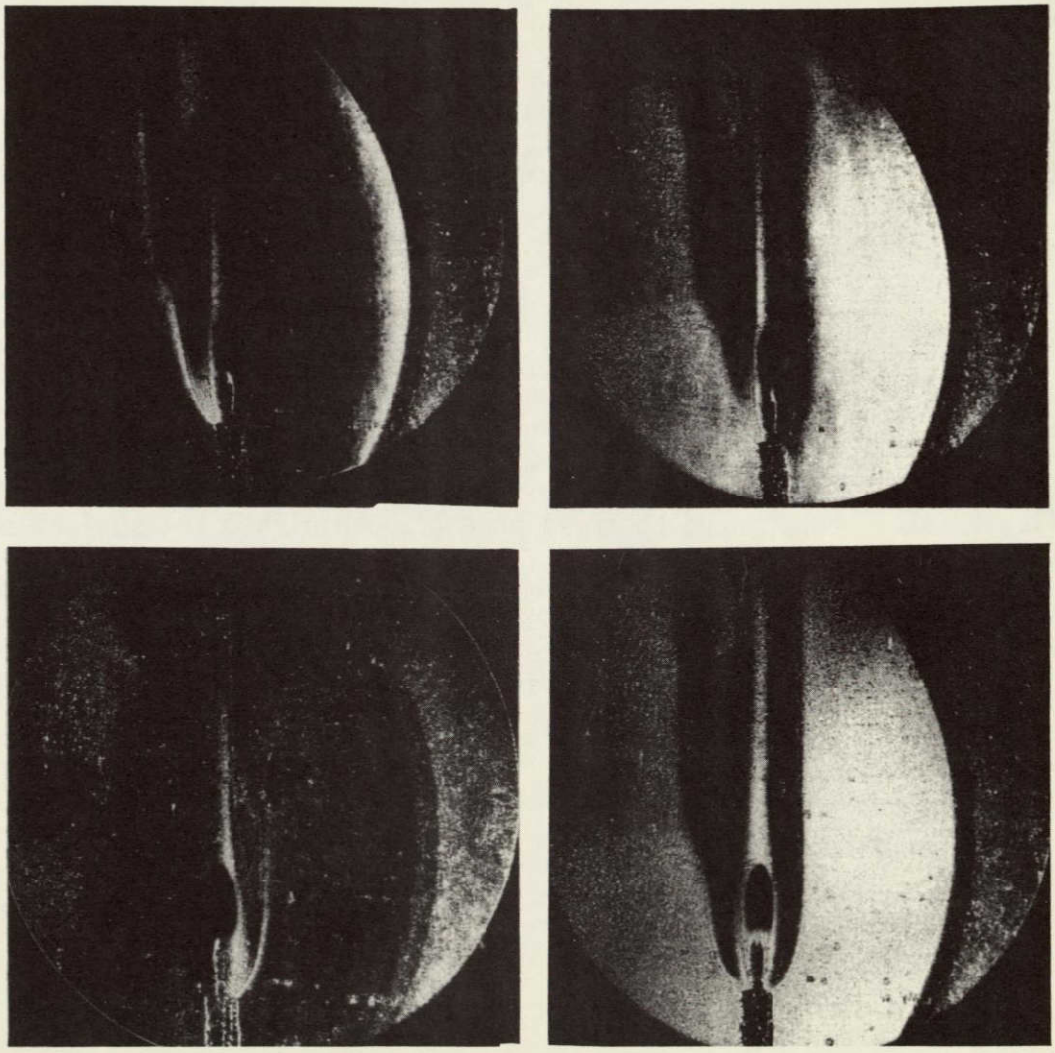

Figure 17 Double exposure schlieren readout.

technique also permits adjustment of the knife edge during readout.

The recording steps are shown in (a) of Figure 15. Shown there are the subject and reference beams incident on the hologram. Note that the reference beam would converge to a point were it to pass on through the hologram. The first exposure is shown by the solid lines. For the second exposure the subject perturbation is introduced and the reference beam direction is changed by a small angle as shown by the dotted lines.

After development the plate is readout as shown in (b). The readout light source is focused to a point at O duplicating the reference beam. This of course reconstructs the subject beam but the reconstructed subject beam is not used. At the reference beam offset angle from the reconstruction beam appear reconstructed beams as shown. These beams arise from non linearities of the recording plate and carry the information about the subject perturbation in the manner of a conventional schlieren beam. One of these beams is used for schlieren viewing by inserting a knife edge at its focus.

Analysis indicates that it is only the subject perturbation which effects the readout beam. Thus even the recording reference beams need not be perfect as long as the imperfections are the same for the two exposures. This suggests the technique may be useful where recordings are made with imperfect pulsed lasers.

Because the technique depends on the non linear behavior of the emulsion it was first tried in the narrow angle configuration shown in Figure 16. The readout result is shown in Figure 17 for different knife edge settings. The upper and lower left hand pictures show the expected schlieren asymmetry for the knife edge on opposite sides of the beam. However, there is much extraneous darkening of unknown origin in these pictures. It may be due to motion of the candle flame during exposure. This cursory test should not be regarded as an evaluation of the techniques potential.

Finite Fringes in Three-Dimensional Interferometry

One of the most useful techniques in classical interferometry for the detection of small phase shifts is the finite fringe technique wherein the subject causes a displacement of the background fringe grid. Because of the three-dimensional nature of holographic interferograms in which a ground glass is used behind the object, simple attempts to produce finite fringes usually result in the fringe grid appearing in some plane other than that of the subject. Thus when the hologram is photographed either the subject or fringe grid are out of focus.

To overcome this problem a formula was derived which describes how the ground glass itself may be given a slight rotation about a specified point in order to make the finite fringe grid appear in the same plane as the subject. To verify the concept a gas laser was used to make a hologram of three vertical wires spaced one inch apart in depth. Figure 18 shows three photographs

of the holographic image with the camera focused successively on each wire. The fringes are located in the plane of the closest wire (c) and are progressively out of focus in (b) and (a).

An interesting possibility stemming from the three-dimensional nature of diffuse holographic interferograms is to develop a precision fringe position measuring system operating directly on the holographic image. Because both the diffuser and the hologram are not in the plane of the subject the quality of the fringes at the subject should be very high and free from imperfections arising from dust etc. Moreover because the background fringes arise from the rotation of a rigid body and not from optical perfection, they can be extremely straight, permitting the detection of minute departures due to subject perturbations. The sensitivity possible should be set by the well behaved statistics of laser granularity, the resolution, which sets the area over which one can average, and the permitted angular viewing aperture, which is set by the nature of the subject itself.

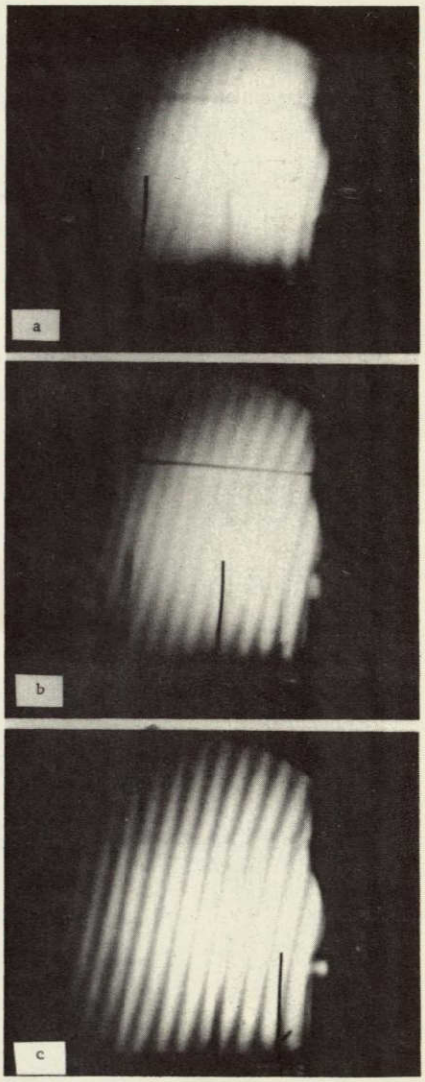

Figure 18 Test of placement of finite fringes.

Viewing Through Turbulent Boundary Layers

Another example where diffusely illuminated three-dimensional holographic interferograms open new possibilities is in viewing through turbulent boundary layers which occur on the windows of tunnels. Essentially the ground glass used to illuminate the subject provides light traversing the subject from many different directions. If the subject posseses sufficient symmetry (e.g. rotational) so that the interference patterns for different directions are effectively the same, then the interference patterns appears to focus at the center plane of the subject when viewed with a large aperture lens. However, contributions from the boundary layer turbulence affect each direction of view in a different way. By using a sufficiently large aperture so that a large sample of the random boundary layer is averaged, a true view of the subject interferogram is obtained. The effect of the turbulence is to reduce the contrast of the subject fringes but it does not displace them.

For a boundary layer giving a gaussian variation in boundary layer optical phase shift, the subject fringe visibility, (Imax - Imin)/(Imax + Imin), is given by $e^{-\sigma^2/2}$ where σ is the RMS fluctuation of the boundary layer optical path in radians. The interpretation of this formula is that the technique is useful when the boundary fluctuations create less than one wave of optical path excursion while for greater excursions the fringe contrast is too low to be useful.

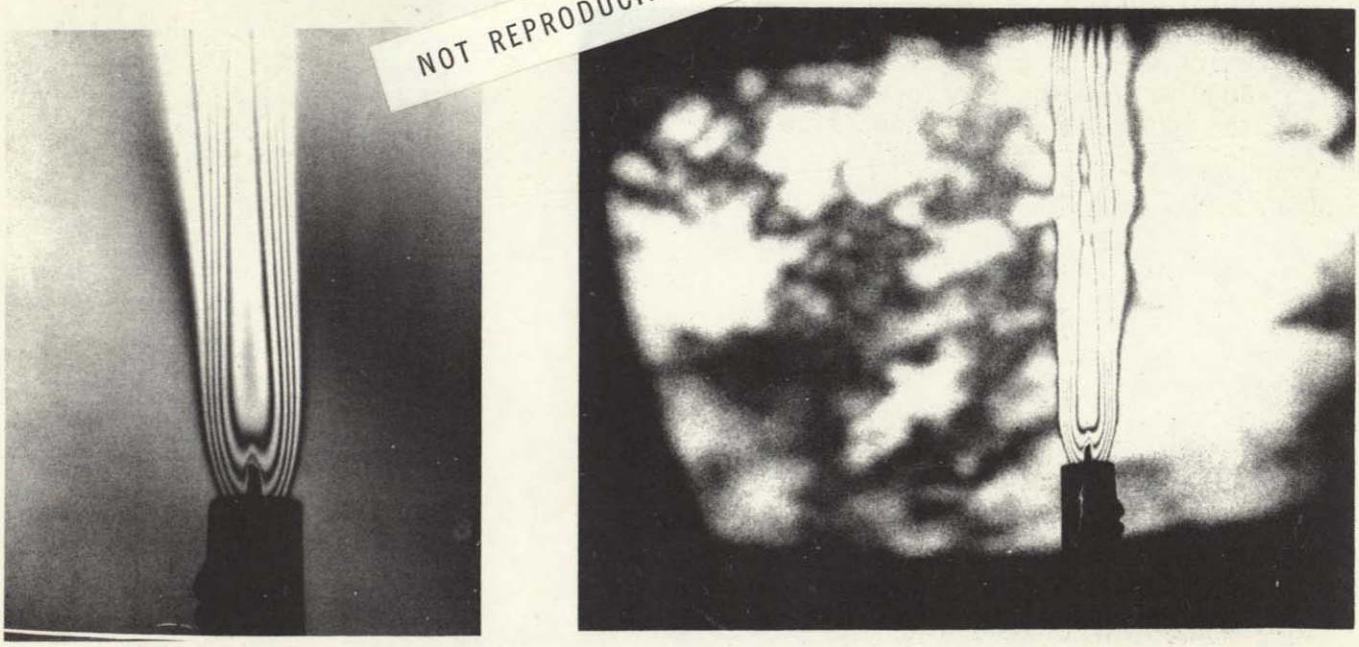

a b

Figure 19 Interferogram of candle flame through turbulent boundary layer. Left, viewed with wide aperture. Right viewed with narrow aperture showing boundary layer.

Figure 19a shows an interferogram of a candle flame copied with a large angular aperture ($\sim$ f/4) so the boundary layer is averaged out and copied at a small aperture, Figure 19b, f/45, so the boundary layer shows. For this hologram the boundary layer was created by a heat gun blowing through a plexiglass channel in front of the hologram.

PART II. FRONT LIGHTED PULSED LASER HOLOGRAPHY AND HOLOGRAPHIC INTERFEROMETRY

Pulsed Laser Two Frequency Contour Mapping*

It was discovered in the course of making front lighted holograms that the ruby laser readily operates at two frequencies simultaneously. By operating with an output reflector consisting of a dielectric slab of proper thickness this effect can be controlled and rendered useful for making range contour pictures.

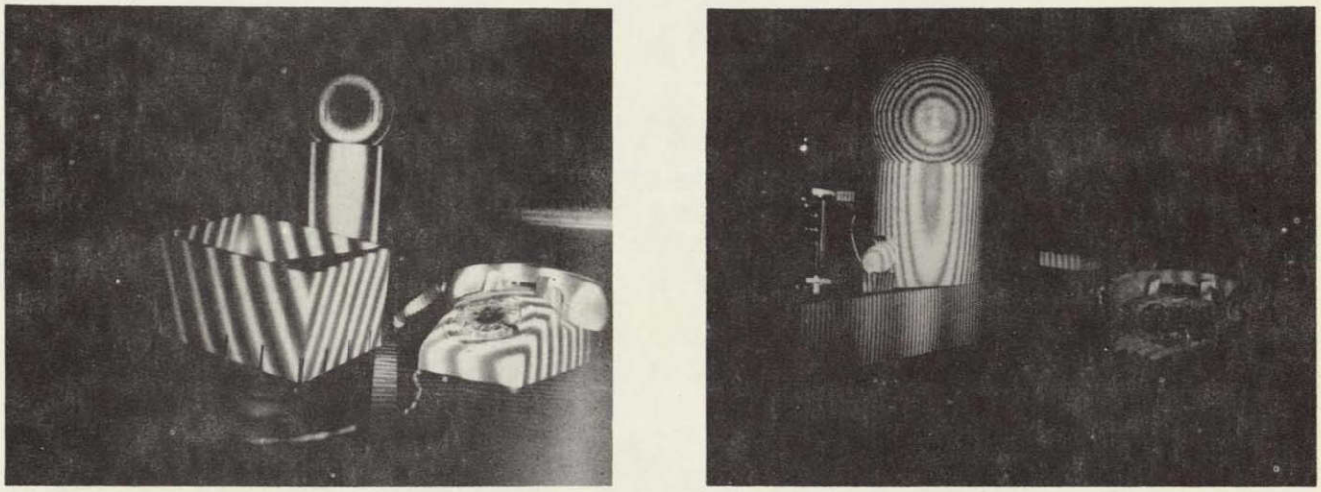

Figure 20 Two frequency pulsed ruby contour maps.

Figure 20 (left) shows a range contour picture made from a single pulse of the ruby laser. The contour spacing of 23 mm is equal to the optical thickness of the resonant reflector. By decreasing the thickness of the reflector the contour interval is shortened as is shown in Figure 20 (right) where the contours are 8 mm.

This technique appears to have application to such problems as the testing of large paraboloid antennas. As developed thus far contours of about 1/2 cm and larger are producible.

---

* A more detailed description of this technique has been published in: Holographic Contouring Via Multifrequency Lasers, L. O. Heflinger, and R. F. Wuerker. Applied Physics Letters, 15, No. 1, 1 July 1969, pp. 28-30.

One interpretation of the holographic image is that its intensity vs. range is a pictorial presentation of the classical Michelson fringe visibility function and as such is useful in the study of the lasers spectral composition. Figure 21 illustrates a case in which more than two spectral components were operating as revealed by the more complex intensity pattern.

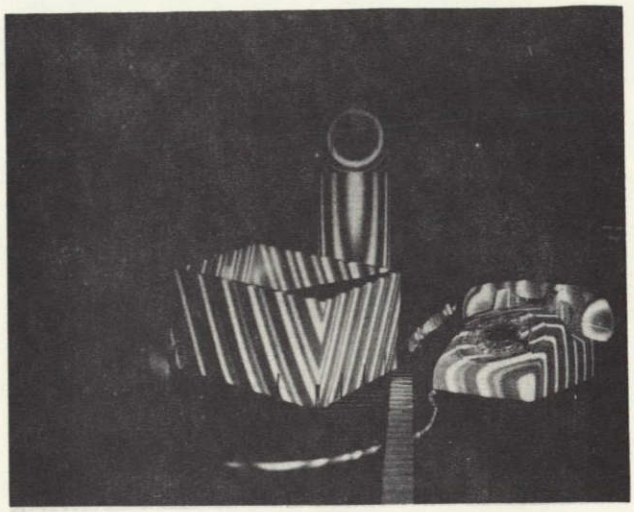

Figure 21 Multifrequency laser operation.

Front Lighted Pulsed Laser Interferometry

For unambiguous interpretation of holographic interferograms, the laser must operate at the same (single) frequency for each pulse. Otherwise, where optical path variations occur over the subject, the fringe pattern is created by both physical changes between pulses and optical path contours, inasmuch as the production of two frequency contours is independent of whether the frequencies occur simultaneously or sequentially. This is a particularly severe requirement for front illuminated subjects because of the large possible optical path variations.

Figure 22 shows single frequency operation produced by the well-known dye cell Q-switching technique. The sloping 1 1/2 by 2 ft. card would readily show up multi-frequency operation as contouring. Figure 23 shows double exposure interferograms made with the same laser conditions as Figure 22. In Figure 23a one observes a basic 8 mm contour pattern distorted by the sagging of the cardboard between the two exposures. In Figure 23b the two frequencies produced on the successive exposures are much closer together but not necessarily identical, resulting in coarse contours distorted by the card sag. From such a picture it is not possible to quantitatively unravel how the displacement fringes have been altered by

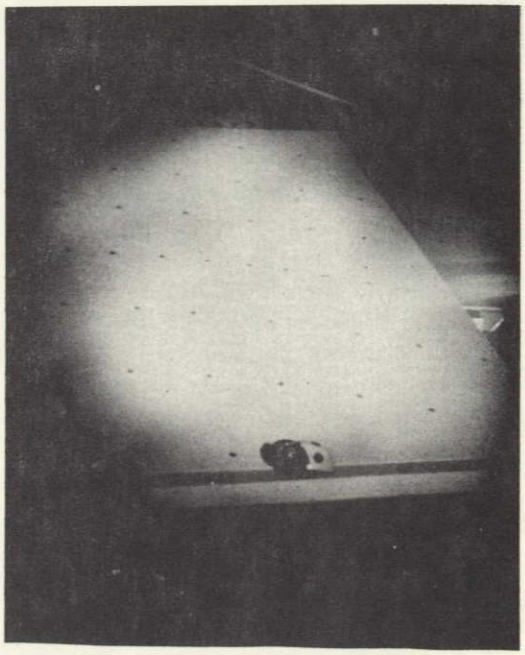

Figure 22 Single frequency laser operation.

the unknown frequency shift. The point to be emphasized here is that one should use care in the interpretation of front lighted pulsed interferograms.

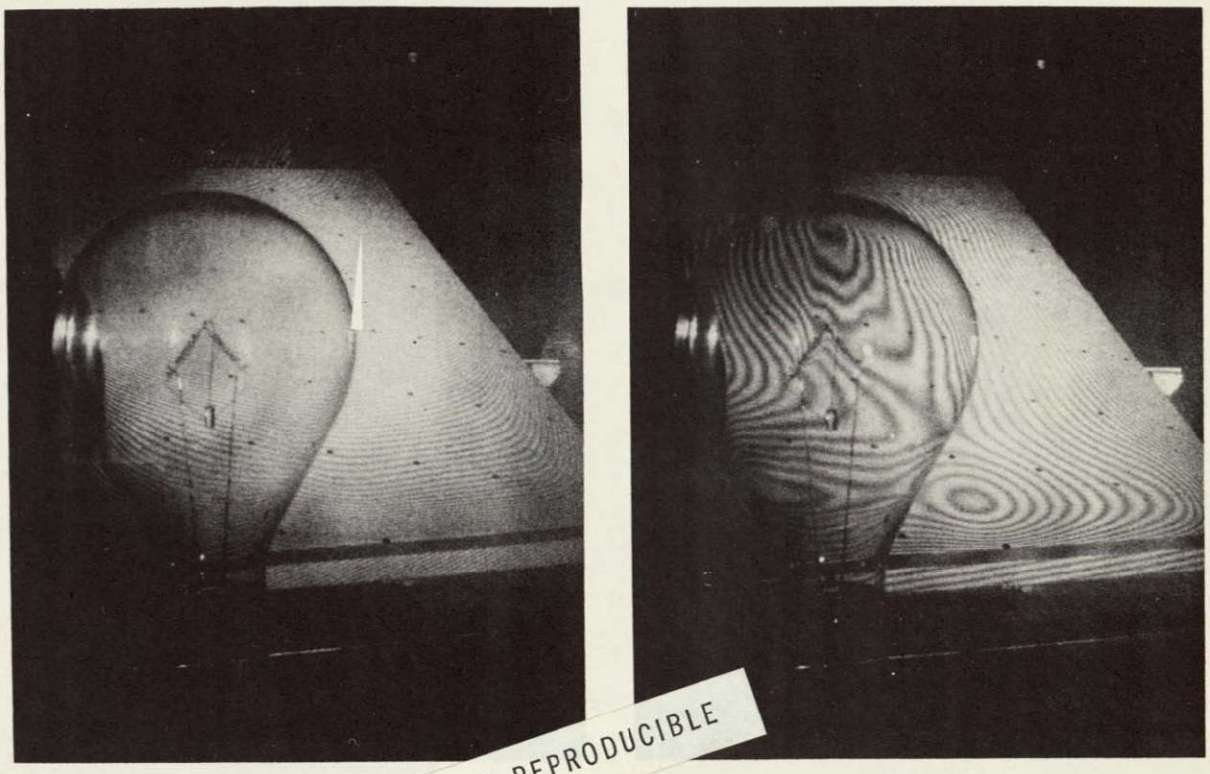

a b

Figure 23 Combination contour-displacement interferograms.

Acknowledgement

R. F. Wuerker has been co-investigator on several of the experiments described in this report. In particular he is largely responsible for the success of the techniques of Doubled Ruby Interferometry, Viewing Through Turbulent Boundary Layers, and Pulsed Laser Contouring. Moreover, he has made valuable contributions in discussions of many of the other techniques. He should have been a co-author but he was busy writing another paper for this same volume.

Reprinted from **APPLIED OPTICS**, Vol. 8, page 2351, November 1969

Phase Visualization Using a Reconstructed Reference Beam

Robert E. Brooks

TRW Systems, Redondo Beach, California 90278.
Received 9 May 1969.

It is well known that one can perform interferometry by recording on a hologram the coherent light waves from a subject to be studied, and then comparing the reconstructed waves with those from the perturbed subject. This technique is known as real time, stored beam, or live fringe holographic interferometry.[1-3] When a specular or transparent subject is to be studied, it may be desirable, for reasons of increased luminous efficiency or freedom from laser granularity, to illuminate the subject with nondiffuse light. However, if the subject is too irregular, the reflected or refracted rays cannot ordinarily be focused through the iris of the observer's eye or recording camera to allow simultaneous viewing of the entire subject. This letter describes a holographic technique which transfers the phase perturbation of the subject waves onto spherical waves which can be focused through a small aperture and examined by interferometric and schlieren methods. The technique is useful for applications such as the thermal testing of cast mirror blanks, phase measurements through distorted and striated glassware, or measurements involving optical components with gross aberrations (e.g., condenser lenses).

If a hologram of the subject is accurately replaced in the recording apparatus and is illuminated with the waves from the *subject*, the *reference* beam is reconstructed (spatially modulated in amplitude by intensity variations of the subject beam). When the subject is perturbed, the reconstructed reference waves will be phase aberrated in accordance with the phase perturbation of the subject waves at the hologram plane. By imaging the subject onto the hologram, phase perturbations at the subject are transferred to the hologram plane and then to the reconstructed reference beam.

If the perturbed reconstructed reference is superimposed on the original reference beam, a fringe pattern is created which corresponds exactly to the subject perturbation, as in the case of conventional holographic interferometry. If spherical reference waves are used, they can be readily focused through a small aperture. Similarly the reconstructed reference waves can be focused through the same aperture, where the aperture size is limited only by the severity of the phase perturbation of the subject waves and not their absolute phase shape.

If the reference beam is blocked and only the reconstructed reference beam is viewed, schlieren viewing of the subject *perturbation* can be easily carried out by introducing a knife edge at the focus of the reconstructed reference beam.[4] Unlike the interferogram, the accuracy of the schlieren observations depends on the degree to which the (unperturbed) reference beam can be brought to a sharp focus. The accuracy and sensitivity of the measurements are commensurate with the quality of the optical components through which the reference beam passes, but do not depend on the subject or optical components (e.g., windows) which affect only the subject waves. Thus, the reconstructed reference beam technique has endowed schlieren viewing with a property found most valuable in holographic interferometry, the ability to view subtle changes in a complex subject or environment.

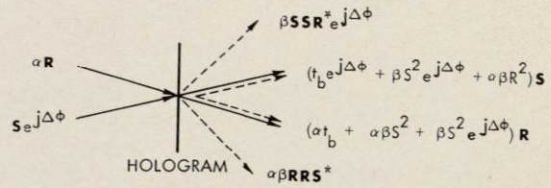

Figure 1. Angular distribution of light transmitted by the hologram when illuminated by the reference and perturbed subject beams.

To verify the contentions stated thus far, we shall examine the waves transmitted by the reconstructed hologram.[5] Let the recording subject and reference waves be represented by the complex fields,

$$\mathbf{S}(x,y) = S(x,y)\exp j\phi(x,y)$$

and

$$\mathbf{R}(x,y) = R(x,y)\exp j\psi(x,y),$$

respectively, where the optical frequency term $\exp j2\pi\nu t$ has been suppressed. The intensity of the waves forming the hologram recording is thus given as,

$$g(x,y) = |\mathbf{R}+\mathbf{S}|^2 = R^2 + S^2 + \bar{S}\bar{R}^* + \bar{R}\bar{S}^*.$$

Assume a linear amplitude-transmittance vs exposure (t vs E) characteristic for the photographic plate which records the hologram, and for simplicity let the exposure time be 1 sec (so that exposure equals intensity). Then the transmittance of he developed hologram can be written,

$$t(x,y) = t_b + \beta(S^2 + \mathbf{SR}^* + \mathbf{SR}^*)$$

where t_b is the bias transmittance established by the reference beam intensity and β is the slope of the t vs E characteristic at the bias point. Placing the hologram back into the recording apparatus, the reconstructing beams consist of the original reference

beam attenuated by a factor α and the perturbed subject beam. We shall assume that the subject perturbation simply alters the phase of the subject waves at the hologram by the amount $\Delta\phi(x,y)$ without changing its amplitude. The reconstructing waves at the hologram can be written,

$$\alpha\mathbf{R}(x,y) + \mathbf{S}(x,y)\exp j\Delta\phi(x,y).$$

The waves transmitted by the hologram are given by the product of the hologram transmittance and the reconstructing waves. The angular distribution of the transmitted terms are shown in Fig. 1.

The perturbed and unperturbed reference waves, which give rise to the expected interference pattern, are,

$$(\alpha t_b + \alpha\beta S^2 + \beta S^2 \exp j\Delta\phi)\mathbf{R},$$

where the phase term $\exp j\Delta\phi$ is responsible for the interference pattern. The fringe visibility is unity (a maximum) when the attenuation α is chosen to be

$$\alpha = \beta S^2/(t_b + \beta S^2),$$

where it has been assumed that negligible light is diffracted by the amplitude variations of S^2. For subjects which have reasonably uniform reflectivity or transmissivity and which can be adequately imaged onto the hologram, the variations of S^2 are small and the fringe visibility is approximately constant.

For schlieren viewing, the reference beam is blocked, ($\alpha = 0$), so that the only wave transmitted by the hologram in the direction of the reference beam is the reconstructed reference,

$$\beta S^2\,\mathbf{R}\exp j\Delta\phi.$$

Because $\mathbf{R}$ can be chosen to have a spherical (or plane) phase, the only phase term responsible for ray deviation at the focus of the reconstructed reference wave is $\exp j\Delta\phi$, the phase of the perturbation.

The techniques have been experimentally verified using the basic Twyman-Green holographic interferometer shown in Fig. 2. A 3-mW He–Ne laser beam was expanded to form a collimated beam 12 cm in diameter. The plane reference mirror was adjusted to form a small angle between the subject and reference beams. The small angle results in a low spatial carrier frequency on the hologram which greatly eases the problem of accurately replacing the hologram plate after its development. Although the arrangement is shown with a reflecting subject, the same apparatus has been used for transillumination of a transparent subject by terminating the subject arm with a plane mirror and placing the subject between the mirror and the beam splitter.

The subject and hologram are placed at the conjugate planes of an imaging lens in order to transfer phase perturbation and detail at the subject to the hologram and to provide uniform illumination of the hologram. The subject of the experimental investigation is an imperfect reflecting cylinder transformed into

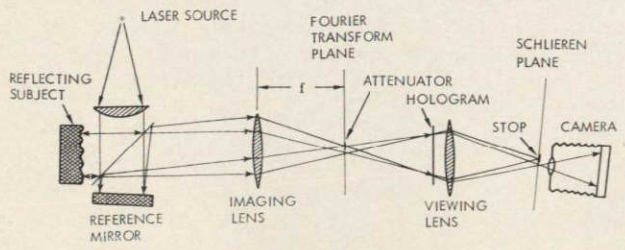

Figure 2. Twyman-Green holographic interferometer.

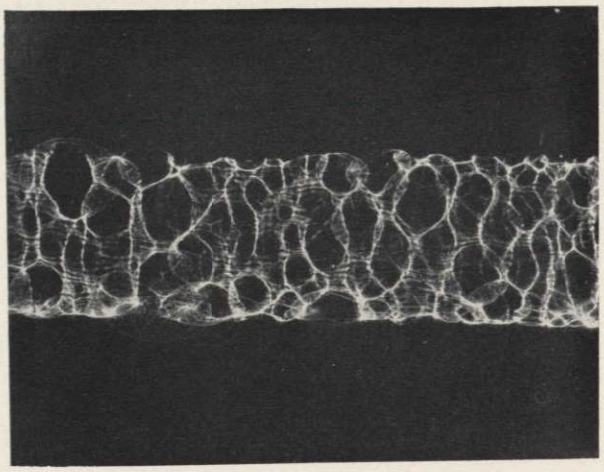

Figure 3. Photograph (type 649F plate) of the distorted light intensity pattern from the subject when the imaging lens is not used.

an irregular plane by means of a simple plano-convex cylinder lens (not shown). Figure 3 shows the intensity pattern at the hologram when the subject is evenly illuminated but when the imaging lens is not used.

The imaging lens also enables the subject to be conveniently scaled to fit the hologram plate and provides a convenient means (in the Fourier transform plane of the subject) for spatially filtering to discriminate against stray light and incoherent light from a luminous subject. Because the reference beam is brought to a sharp focus and is spatially separated from the subject beam, it can be easily attenuated to achieve good fringe contrast without introducing wavefront aberrations by placing an attenuator at its focus. The imaging lens also provides wavefront matching at the hologram to compensate for imperfect laser coherence.[5,7]

Figure 4(a) shows an interferogram of the subject after it has been deformed. The recording camera is focused on the hologram. Because the subject rays are approximately normal to the surface, the interferogram can be directly interpreted as a contour map of deformation with a contour interval equal to one-half the optical wavelength. The vertical lines (6-mm spacing) are from a calibration grid placed in front of the subject.

Figure 4(b) shows the schlieren pattern of the same subject with the same deformation for a vertical knife edge. Areas of the surface which have a sufficiently large gradient of deformation, increasing from right to left, cause the rays to be deflected so they strike the knife and appear dark in the schlierien pattern.

For the particular knife position used, these areas correspond to deformation slopes greater than a given value on the "west side of the mountains or the east side of the valleys." Even though the beam splitter used in this experiment deviated from flatness by approximately fifty waves, the schlieren pattern is sufficiently accurate to determine the sense of the infinite fringe interferogram in Fig. 4(a), and examples of a relative hill and depression have been marked by + and − signs for two points.

Valuable discussions with L. O. Heflinger are gratefully acknowledged. This work was supported by NASA contract NAS2-4992 and by the TRW independent research program.

Note added in proof: The author has recently learned that the technique has been employed for schlieren and phase contrast measurement of diffusely lighted subjects by Tsuruta and Itoh.[8]

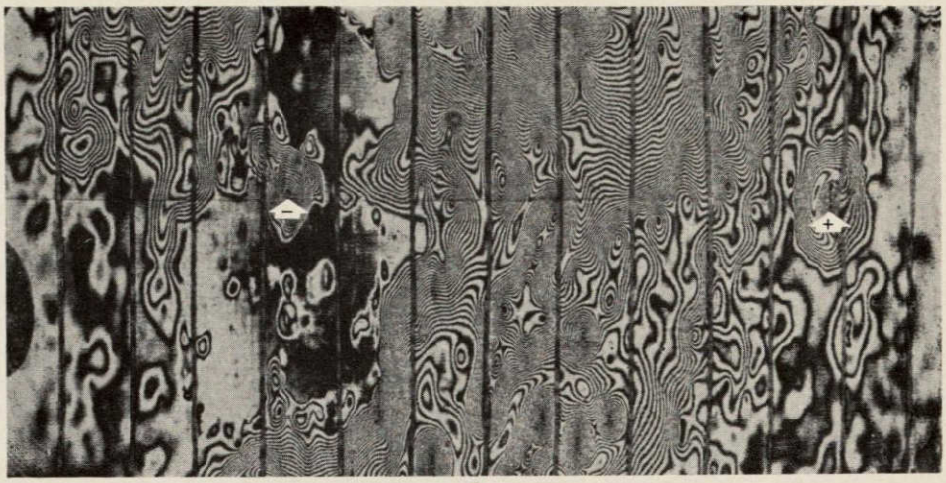

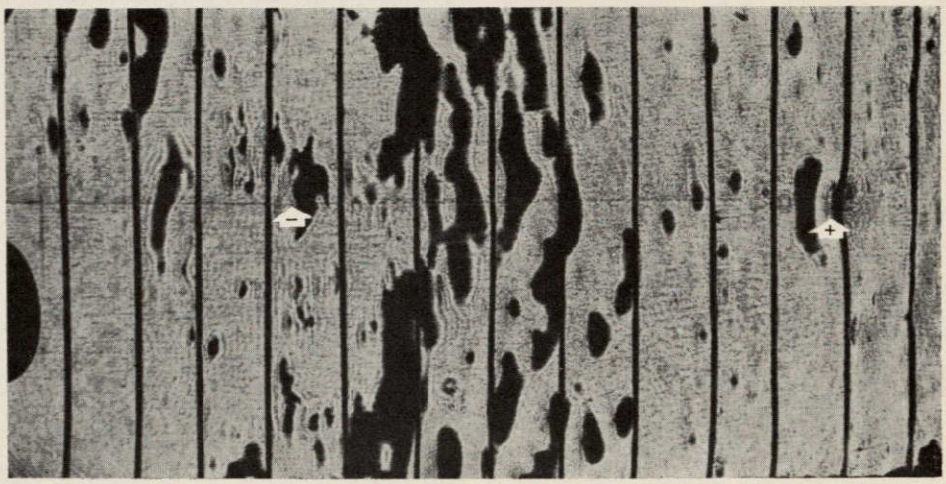

Figure 4. (a) Interferogram of the subject deformation. (b) Corresponding schlerien photograph.

References

1. R. J. Collier, E. T. Doherty, and K. S. Pennington, Appl. Phys. Lett. **7,** 223 (1965).
2. R. E. Brooks, L. O. Heflinger, and R. F. Wuerker, Appl. Phys. Lett. **7,** 248 (1965).
3. K. A. Haines and B. P. Hildebrand, Appl. Opt. **5,** 595 (1966).
4. R. Ladenburg, Ed., *Physical Measurement in Gas Dynamics and Combustion* (Princeton University Press, Princeton, 1954).
5. J. W. Goodman, *Introduction to Fourier Optics* (McGraw-Hill, Book Co., New York, 1968), p. 82.
6. R. E. Brooks, L. O. Heflinger, and R. F. Wuerker, IEEE J. Quantum Electron. **QE-2,** 275 (1966).
7. E. Leith and J. Upatnieks, J. Opt. Soc. Amer. **57,** 975 (1967).
8. T. Tsuruta and Y. Itoh, Japan. J. Appl. Phys. **8,** 96 (1969).

Reprinted from

Volume 15, Number 1 APPLIED PHYSICS LETTERS 1 July 1969

HOLOGRAPHIC CONTOURING VIA MULTIFREQUENCY LASERS*

L. O. Heflinger and *R. F. Wuerker*
TRW/Systems
Redondo Beach, California 90278
(Received 21 April 1969; in final form 19 May 1969)

Holographic images covered with range contours were produced by the multifrequency emission of a pulsed ruby. The multifrequency emission arises from the use of a resonant output reflector in the laser cavity, producing contour intervals equal to the optical thickness of the resonator. Intervals of about 1 cm and greater are attainable.

Holographic contour maps made with two-frequency gas lasers have been reported.[1,2] We report here on holographic contour maps made with a single pulse from a ruby laser.

Aleksoff has shown that the intensity I_{app} of each point of the reconstructed image of a hologram is

$$I_{app} = [V(l)]^2 I_{mono} , \tag{1}$$

where I_{mono} is the reconstructed intensity of the point had the hologram been produced with truly monochromatic light.[3] $V(l)$ is the Michelson fringe visibility function,[4] which depends on the path mismatch l between the reference beam and scene point in question. The Michelson fringe visibility function $V(l)$ is determined by the spectral intensity $j(k)$ of the exposing light via the formula

$$[V(l)]^2 = \{\int j(k)[\cos(k - k_0)l]\,dk\}^2 + \{\int j(k)[\sin(k - k_0)l]\,dk\}^2 , \tag{2}$$

where k_0 is the mean wave number and the spectral intensity has been normalized so that $\int j(k)dk = 1$. The holograph image thus constitutes a pictorial presentation of the Michelson fringe visibility function.

When only two optical frequencies are used, the above formulas give $[V(l)]^2 = \cos^2[\frac{1}{2}(k_1 - k_2)l]$ which, as described by Hildebrand and Haines[1], fills the object space with ellipsoidal surfaces with foci at the illumination point source and on that point on the hologram which is on the axis of view. This gives a range contour interval of $\lambda^2/(2\Delta\lambda \cos\theta/2)$, where θ is the angle between the direction of viewing and the direction of the incident light for each point of the scene; the range contour interval is measured along the bisector of the viewing and incidence directions.

Figures 1 and 2 show range contour maps each made with a single pulse from a ruby laser which operated essentially at two optical frequencies. The double frequency operation was produced by use of a resonant reflector of selected thickness as the output reflector of the laser cavity. The reflectivity of a simple two-surface reflector is periodic with frequency, a maximum of reflectivity occurring whenever the optical thickness is a multiple of a half-wave. Using the above formulas, one can show that the range contour interval (for $\theta \cong 0$) is equal to the optical path length between the two surfaces of such a reflector.

The number of peaks of reflectivity at which lasing occurs depends on the lasing linewidth and the spacing of the reflectivity peaks. The holographic image obtained when using a single surface dielectric reflector shows a bright reconstruction for $\pm\frac{1}{2}$ cm about the path match position with only a residue of low visibility throughout the remainder of the scene. From formulas (1) and (2) and the assumption of an approximate Gaussian spectral intensity profile,[5] the lasing linewidth of a 5°C ruby was found to be $\frac{1}{4}$ Å. Resonant reflectors which are optically thicker than $\frac{1}{2}$ cm have two or more peaks within this lasing width and hence produce holographic images with contours. Thus, this simple technique is useful for producing contour maps with intervals on the order of 1 cm and longer. Figure 2 is an example with contour intervals near the minimum value. In this case the observed contours are 35% longer than the optical thickness of the resonator, presumably due to "pulling" due to the lasing linewidth.

The laser configuration used is the same as that described earlier.[6,7] The non-Q-switched mode of operation was used for Fig. 1 and 2. Contours of slightly inferior quality have also been made with both cryptocyanine dye and Kerr cell Q-switched operation. We have found that adjustment of the total cavity length to (presumably) a multiple of the resonator spacing increases the contrast and clarity of the contour fringes.

A tempting thought is that the holographic contours may be a pictorial representation of the pulse train from the exposing laser, stemming from the coincident arrival of scene and reference pulses at the hologram. Examination of formulas (1) and (2) shows that the image is determined only by the spectral intensity; the phase relations among the spectral components play no role. Thus it is not possible to use the holographic image as a pictorial representation of the laser pulse train in the general case.

*Work for this research was jointly sponsored by National Aeronautics and Space Administration and the U.S. Air Force Avionics Laboratory.

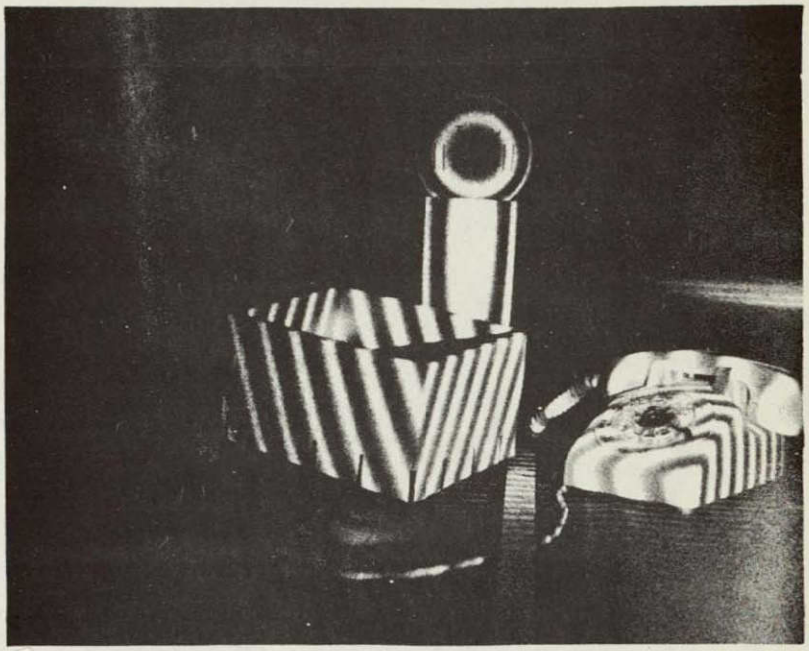

Fig. 1. Photograph of a holographic image showing 23-mm contours. Contour spacing was equal to the optical thickness of the resonant reflector in the ruby laser illuminator.

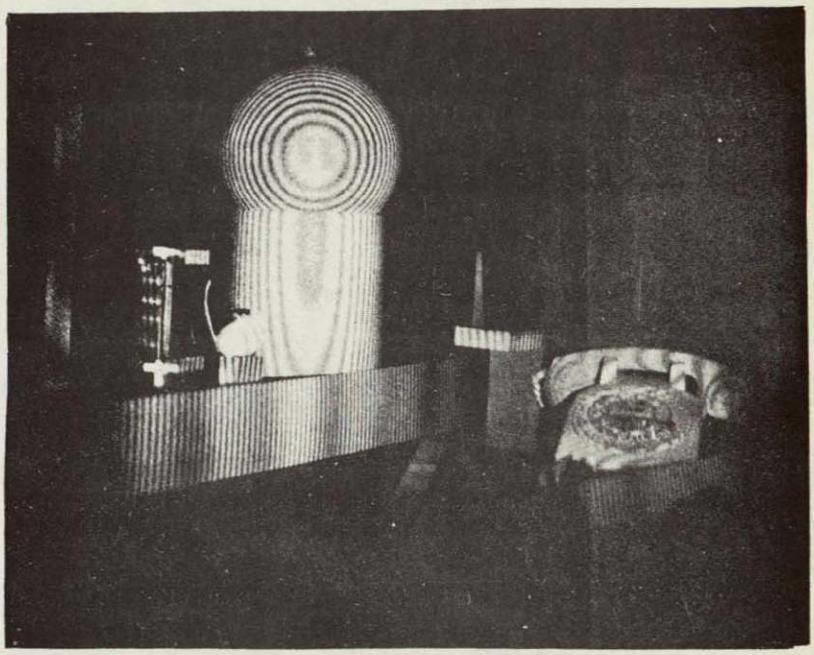

Fig. 2. Photograph of a holographic image showing 7.7-mm contours.

In general the ruby laser emits at more than two frequencies. Figures 1 and 2 were selected as examples of nearly pure two-frequency operation. Figure 3 shows a more typical example in which more than two frequencies were present. In other holograms the interperiod contour fringes were symmetrical, and appeared like the fringe visibility functions theoretically calculated by Erickson and Brown for three-frequency laser operations.[8]

[1] B. P. Hildebrand and K. A. Haines, J. Opt. Soc. Am. 57, 155 (1967).

[2] J. S. Zelenka and J. R. Varner, Appl. Opt. 7, 2107 (1968).

[3] C. Aleksoff, Appl. Opt. 6, 2192 (1967).

[4] M. Born and Emil Wolf, *Principles of Optics* (Macmillan Company, New York, 1964), [2nd Rev. ed.], p. 320.

[5] Reference 4, p. 322.

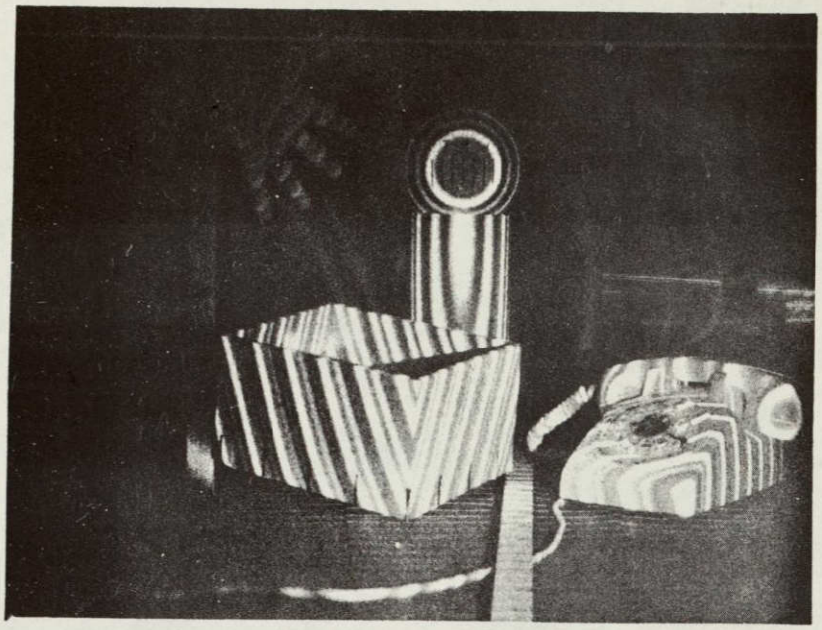

Fig. 3. Photograph of a holographic image in which the Kerr cell Q-switched ruby laser emitted at more than two wavelengths. The conditions were nominally identical to Fig. 1.

[6] R. E. Brooks, L. O. Heflinger, R. F. Wuerker, and R. A. Briones, Appl. Phys. Letters 7, 92 (1965).

[7] The reader will note that many lasers in common use have resonant reflectors. The thickness of these reflectors is frequently chosen just near the threshold for two-frequency operation, which results in occasional contours, depending on the exact temperature of the ruby.

[8] E. F. Erickson and R. M. Brown, J. Opt. Soc. Am. 57. 367 (1967).

Appendix D

DERIVATION OF THE RELATION BETWEEN RECONSTRUCTED INTENSITY AND THE EXPOSING SPECTRA OF HOLOGRAMS

The relation,

$$I_{app} = [V(\ell)]^2 I_{mono} \quad ,$$

relating the apparent image intensity and the Michelson fringe visibility function, was first pointed out by Aleksoff.* Because of its importance, we give here a somewhat detailed derivation of this relation.

In Fig. 4-1 is sketched a configuration for making a hologram when the illumination source is a point. The coordinate system x,y lies on the plane of the hologram, and the coordinate system u,v covers the object. By means of the Huygens' wavelet principle and the Kirchoff diffraction integral, the electric field of the light wave E(x,y) at the hologram plate due to the object can be written as

$$E(x,y) = E_s \iint e^{ikL(x,y,u,v)} \rho(x,y,u,v) du dv. \qquad (1)$$

Here $k = 2\pi/\lambda$ is the wavenumber, $L(x,y,u,v)$ is the total pathlength from the point source S to the point (x,y) via the point (u,v). The function $\rho(x,y,u,v)$ contains the reflectivity of each point (u,v) of the object, and also the phase, length, and obliquity factors of the Kirchoff diffraction integral. Because we are only concerned with a narrow spectral region the function ρ can be considered to be independent of the wavenumber.

---

* C. Aleksoff, Appl. Opt. 6, 2192 (1967).

As in the usual analysis, to maintain simplicity, the amplitude transmittance of the developed hologram is assumed to be proportional to the exposing intensity. Upon multiplying the reconstructing beam

$$R_o = E_s \alpha(x,y) e^{ik_o \mathcal{L}(x,y)} \tag{4}$$

of wavenumber k_o, by the amplitude transmittance (proportional to (3)) we have that the fourth term on the right hand side of (3), yields an electric field at the output side of the hologram of

$$\sigma R_o \int j(k)\ R^* E dk \quad .$$

Substituting expressions from (1), (2), and (4) in this true reconstructed image term, we have

$$\sigma E_s\ \alpha e^{ik_o \mathcal{L}} \int j(k)\ E_s{}^* \alpha^* e^{-ik\mathcal{L}} \left(E_s \iint e^{ikL} \rho du dv \right) dk$$

Changing the order of integration and rearranging the order of factors yields

$$= \sigma E_s E_s{}^*\ \alpha\alpha^* \left[E_s \iint e^{ik_o L} \left(\int j(k) e^{i(k-k_o)(L-\mathcal{L})} dk \right) \rho du dv \right] \quad .$$

The factor $E_s E_s{}^*\ \alpha\alpha^*$ is the intensity of the reference wave at the holographic plate, and is approximately a constant. The factor in square brackets thus represents the reconstructed wave of the true holographic image. Comparison of the term in square brackets with the object wave given by (1), for wavenumber k_o, shows that the effect on the reconstructed image is that each point on the object apparently has had its amplitude reflectivity modified by the factor

$$\int j(k) e^{i(k-k_o)(L-\mathcal{L})} dk.$$

Note that $L - \mathcal{L}$ is the path length mismatch between the reference beam and each point of the scene. By writing the exponential function in terms of cos and sin, this factor can be written as $C + iS$ which in turn can be written as

$$V(\Delta\ell) e^{i \arctan\frac{S}{C}} \tag{5}$$

where

$$\left.\begin{aligned} V(\Delta\ell) &= \sqrt{C^2 + S^2} \quad , \\ C(\Delta\ell) &= \int j(k) \cos\left((k-k_o)\Delta\ell\right) dk \quad , \\ S(\Delta\ell) &= \int j(k) \sin\left((k-k_o)\Delta\ell\right) dk \quad , \end{aligned}\right\} \tag{6}$$

and

$$\Delta\ell = L - \mathcal{L} \quad .$$

When the reconstructing wavenumber k_o is the mean wavenumber of the exposing spectrum, and the exposing spectrum is narrow, the real functions C and S are slowly varying functions of the path length mismatch $\Delta\ell$. The exponential factor of (5) gives the phase shift which ordinarily will not make any change in the appearance of the image. The factor $V(\Delta\ell)$, however, modifies the object's apparent amplitude reflectivity. Thus the apparent intensity I_{app} of each point of the object is given by

$$I_{app} \propto [V(\Delta\ell)]^2 I_{mono} \quad . \tag{7}$$

where I_{mono} is the intensity of the object's reconstruction, had the hologram been made with purely monochromatic light.

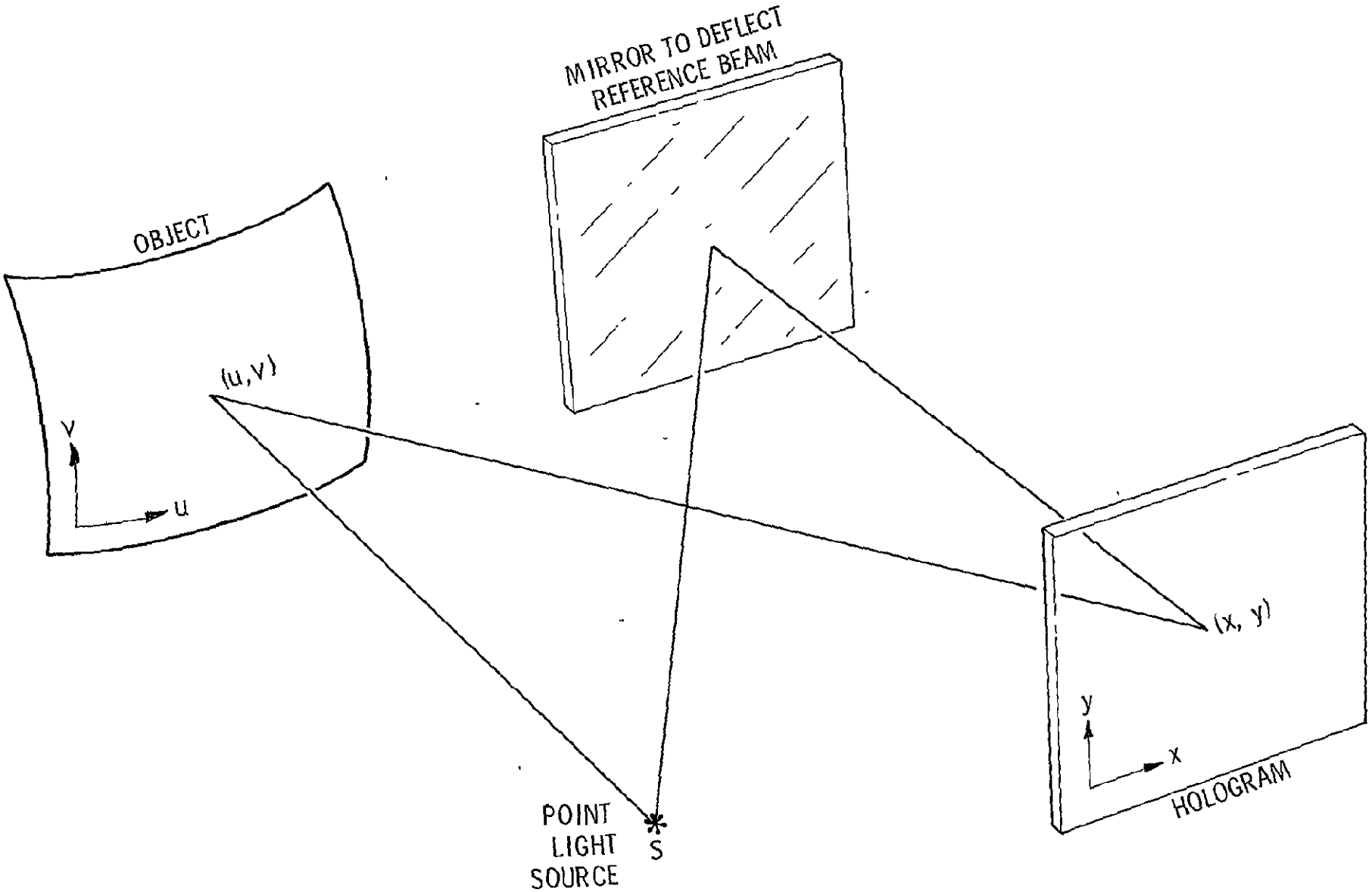
MIRROR TO DEFLECT
REFERENCE BEAM
OBJECT
(u,v)
v
u
(x, y)
y
x
HOLOGRAM
POINT
LIGHT
SOURCE
S

Figure 4-1

The other source of light at the hologram is the reference beam, the electric field of which may be written

$$R(x,y) = E_s \alpha(x,y) e^{ik\mathcal{L}(x,y)} \tag{2}$$

where $\mathcal{L}(x,y)$ is the length from the source to the point (x,y) along the reference path. The factor $\alpha(x,y)$ depends on the beam profile, but not on the wavenumber. For a uniform beam $\alpha = 1$.

E_s in both of the above formulas is the source strength and contains the optical frequency factor $e^{i\omega t}$.

Proceeding as with the usual holographic analysis, the total electric field at the hologram for each wavenumber is $R + E$, and the intensity at the hologram is

$$\mathcal{I}(x,y,k) = (R+E)(R+E)^* = RR^* + EE^* + RE^* + R^*E \quad .$$

Now let $j(k)$ denote the spectral intensity of the light, normalized so that $\int j(k)dk = 1$. The intensities due to light of different wavenumbers add incoherently. Thus the intensity at the hologram due to all the wavenumbers is

$$\begin{aligned} I(x,y) &= \int j(k)\, \mathcal{I}(x,y,k)dk \\ &= \int j(k)\, RR^* dk + \int j(k) EE^* dk \\ &\quad + \int j(k)\, RE^* dk + \int j(k) R^* E dk \quad . \end{aligned} \tag{3}$$

The four terms as usual give rise to the zero order, the scene-scene noise, the conjugate holographic image and the true holographic image respectively.

The factor $V(\Delta\ell)$ has a simple classical meaning. Analysis of a Michelson interferometer operating with light of spectral intensity $j(k)$ leads to the conclusion that $V(\Delta\ell)$ is the visibility

$$V(\Delta\ell) = \frac{I_{max} - I_{min}}{I_{max} + I_{min}}$$

of the observed fringes, with arm length inequality of $\Delta\ell$ and equal beam intensities.* Thus the holographic image of the object is a pictorial representation of the Michelson fringe visibility function!

If the hologram is reconstructed with light of wavenumber different from the mean exposing wavenumber, an extension of the above analysis shows that the basic image is not changed except for the usual magnifications that accompany a change in wavelength.

The foregoing derivation, which deals with all the subject light simultaneously, makes it somewhat unintuitive as to why the Michelson fringe visibility function suddenly appears as the modifier of the reconstructed intensity. The following simple argument presents an intuitive picture of why the fringe visibility function appears and is presented only as an aid to memory, and the intuitive understanding of holograms. The weakness of the following argument is that it deals with one scene point at a time and ignores interaction with light from other scene points.

Recall first that the Michelson fringe visibility function represents the visibility or contrast of the fringes seen in a Michelson

---

* M. Born and Emil Wolf, Principles of Optics, (MacMillan Company, 1964), 2nd (Rev.) Ed., p. 320.

interferometer as arm length inequality is varied. Next consider a small region of the hologram and the light reflected from one point only of the subject. When this light interferes with the reference beam light, it will produce fringes. The visibility of these hologram fringes will be the same as the visibility of fringes in a Michelson interferometer whose arm length inequality is equal to the difference between the subject path and the reference path. If the fringe visibility is high, then high contrast holographic fringes will be recorded, which in turn will give rise to a bright image of the subject point upon reconstruction. If the fringe visibility is low, a dim or absent reconstruction will be produced. Thus, it is intuitively plausible that the reconstruction brightness of each subject point should correspond to the visibility of fringes in a Michelson interferometer with arm length inequality equal to the difference in subject and reference paths. In other words, the reconstructed image is a pictorial presentation of the Michelson fringe visibility function.

Appendix E

FILM SENSITIVITY DATA PLOT

The following plot of film sensitivity was made to facilitate exposure considerations in holography. It has been found useful within our group and numerous visitors have requested copies, so we are including it here because of likely NASA interest. We emphasize here that this is simply a replotting of manufacturers data on a common scale; these curves have not been verified by us.

EXPOSURE NOMOGRAM FOR LASER PHOTOGRAPHY AND HOLOGRAPHY

The simple nomogram relates the emulsion sensitivity, plate size, and exposure energy. In addition, the spectral sensitivity of a number of useful emulsions is given. The following precautions must be observed:

- Exposure refers to the total energy uniformly deposited over a plate with area (cm^2) equal to the square of the plate size (cm).
- Unless otherwise noted, all exposure and development is to a density of 0.5 - 0.6, generally recognized as the optimum hologram density.
- No account has been made for reciprocity failure.
- Manufacturers can change their emulsion characteristics without notice.

Eastman Kodak

2485	Kodak Developer MX642-1, 4 min at 90F - Kodak Pub. P-94
2475	Kodak DK-50, 8 min at 68F - Kodak Pamp. P-95
103F	Kodak D-19, 4 min at 68F
Tri-X Pan Plate	Kodak D-19, 4 min at 68F
649F	Kodak D-19, 5 min at 68F
649GH	Kodak D-19, 5 min at 68F
Microfile AHU	Recordak Microfile Developer (as recommended) - Pamp. P-151
6451	Kodak D-19, 4 min at 68F - Kodak Pamp. No. P-163
SO-243	Kodak Pub. No. M-118-0

Kodak Plates and Films for Science and Industry, No. P-9

Polaroid

47, 107, 57 — Reflected density = 0.5 - G. R. Bird, et al.,"High Speed Oscillography," Image Technology, 11, No. 5 (Oct.-Nov. 1968), p. 31

Agfa-Gevaert

8E70, 8E75, 10E56 — D. Schultze,"Red-Sensitized, High-Resolution Emulsions for Laser Photography," Laser Focus, 4, June 1968, pp. 23-25.

10E70, 10E75, 14C70 — H. Nassenstein, et al., "An Investigation of the Properties of Photographic Materials for Holography," Symposium on Engineering Uses of Holography, Sept., 1968, Glasgow; Proceedings to be published.

14C75 — Agfa-Gevaert Technical Information, Scientific Photography, Oct. 1967.

Photoresist — J. Kosar, Light-Sensitive Systems, John Wiley, 1965, p. 71.

B. O'Brien, Jr., Spectral Sensitivity of Photosensitive Acid Resists

Dichromated Gelatin — Exposure for 90% diffraction efficiency - L. H. Lin and H. L. Beauchamp, "Hologram Formation in Hardened Dichromated Gelatin," Talk given at OSA meeting, 9 Oct. 1968, Pittsburgh.

REB/bj

11/68

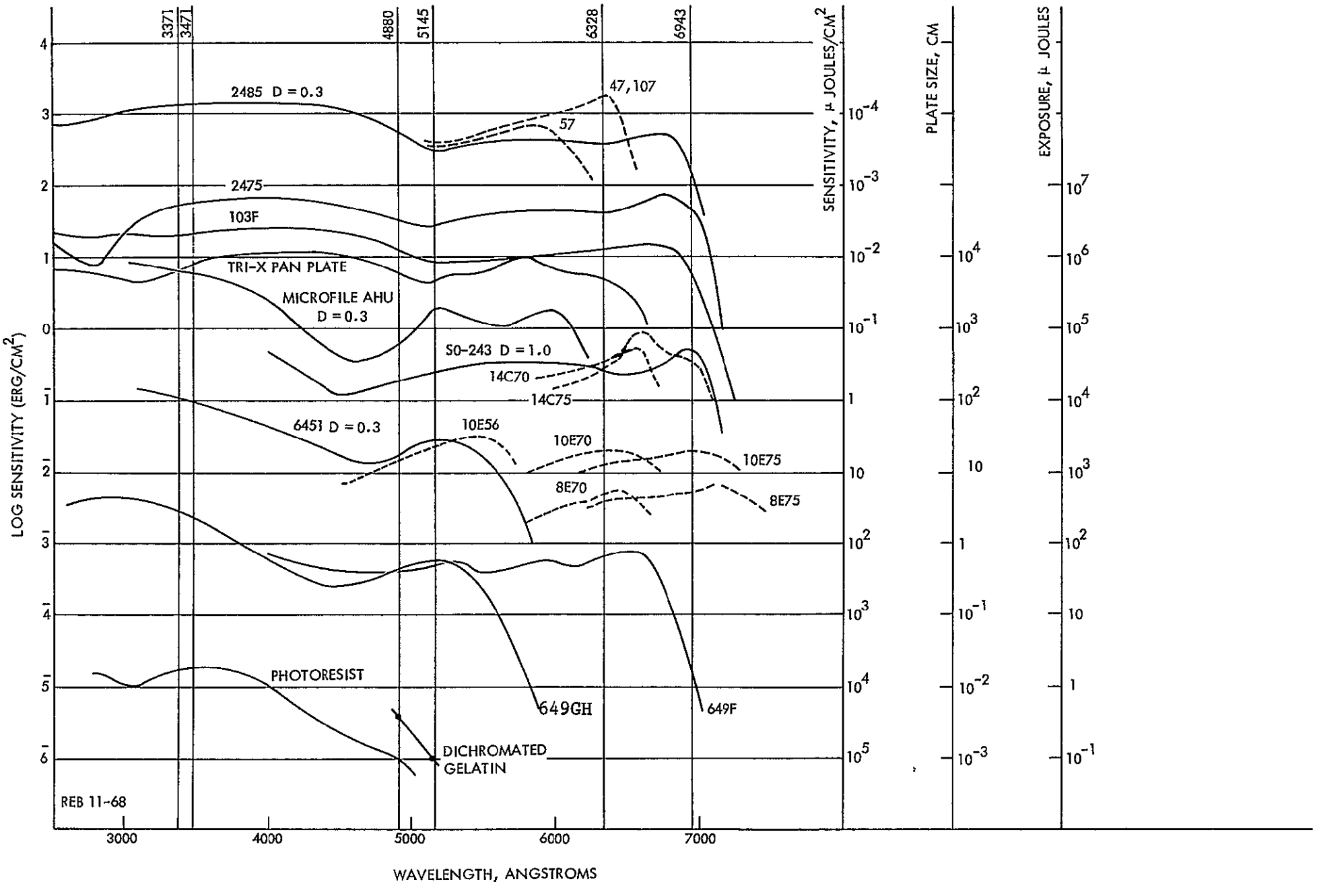
3371
3471
4880
5145
6328
6943
2485 D = 0.3
47,107
57
2475
103F
TRI-X PAN PLATE
MICROFILE AHU
D = 0.3
S0-243 D = 1.0
14C70
14C75
6451 D = 0.3
10E56
10E70
10E75
8E70
8E75
PHOTORESIST
649GH
649F
DICHROMATED
GELATIN
REB 11-68
LOG SENSITIVITY (ERG/CM2)
SENSITIVITY, μ JOULES/CM2
PLATE SIZE, CM
EXPOSURE, μ JOULES
WAVELENGTH, ANGSTROMS